ผลของตัวรองรับเซอร์โคเนียที่มีความบกพร่องต่อความว่องไวในเชิงปฏิกิริยาของ
ปฏิกิริยาคาร์บอนมอนอกไซด์ไฮโดรจิเนชัน

นางสาวสร้อยพัทธา สร้อยสุวรรณ
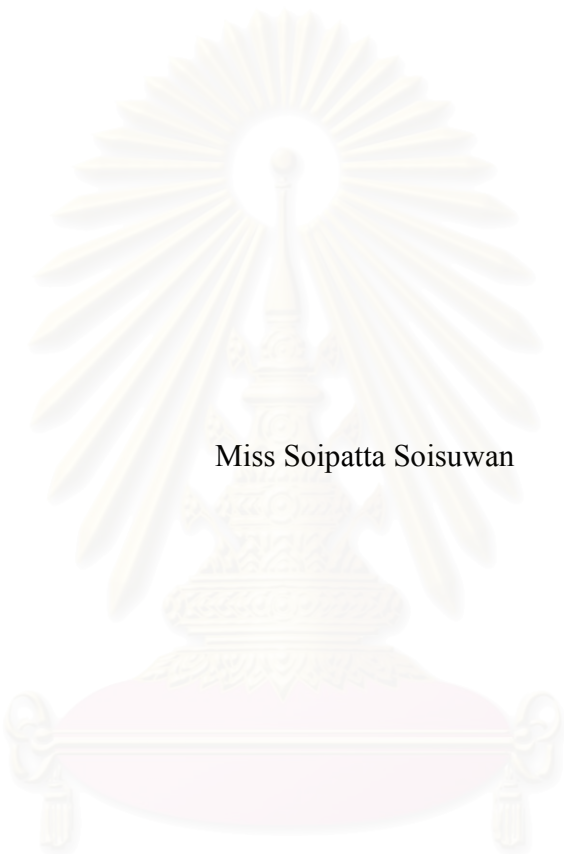
EFFECT OF DEFECTED ZIRCONIA SUPPORT ON CATALYTIC ACTIVITY OF
CARBONMONOXIDE HYDROGENATION

Miss Soipatta Soisuwan

A Dissertation Submitted in Partial Fulfillment of the Requirements
for the Degree of Doctor of Engineering Program in Chemical Engineering
Department of Chemical Engineering
Faculty of Engineering
Chulalongkorn University
Academic Year 2005
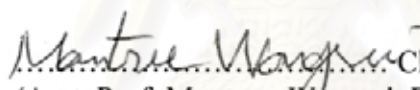
Thesis Title   EFFECT OF DEFECTED ZIRCONIA SUPPORT ON CATALYTIC
               ACTIVITY OF CARBONMONOXIDE HYDROGENATION
By   Miss Soipatta Soisuwan
Field of Study Chemical Engineering
Thesis Advisor Professor Piyasan Praserthdam, Dr.Ing.
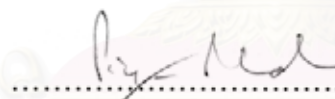Thesis Co-advisor   Professor David L. Trimm, Ph.D.

_____
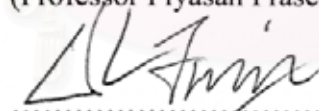
Accepted by the Faculty of Engineering, Chulalongkorn University in Partial
Fulfillment of the Requirements for the Doctor's Degree
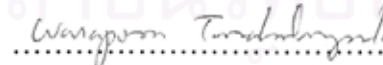
.... Dean of the Faculty of Engineering
(Professor Direk Lavansiri, Ph.D.)
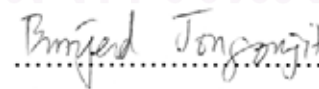
THESIS COMMITTEE
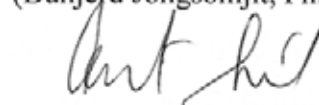
.... Chairman
(Asst. Prof. Montree Wongsri, D.Sc.)

.... Thesis Advisor
(Professor Piyasan Praserthdam, Dr.Ing.)

.... Thesis Co-advisor
(Professor David L. Trimm, Ph.D.)

.... Member
(Waraporn Tanakulrungsank, D.Eng.)

.... Member
(Bunjerd Jongsomjit, Ph.D.)

.... Member
(Akawat Sirisuk, Ph.D.)

สร้อยพัทธา สร้อยสุวรรณ: ผลของตัวรองรับเซอร์โคเนียที่มีความบกพร่องต่อความว่องไวในเชิง
ปฏิกิริยาของปฏิกิริยาคาร์บอนมอนอกไซด์ไฮโดรจิเนชัน (EFFECT OF DEFECTED ZIRCONIA
SUPPORT ON CATALYTIC ACTIVITY OF CARBONMONOXIDE HYDROGENATION)
อ.ที่ปรึกษา: ศ.ดร.ปิยะสาร ประเสริฐธรรม, อ.ปรึกษาร่วม: PROF. DAVID L. TRIMM119 หน้า.
ISBN 974-17-5621-6

ในการศึกษาครั้งนี้ได้มีการนำวิธีการของพิชีนีปรับปรุงใหม่มาใช้ในการเตรียมออกไซด์
ผสมของอะลูมินาและเซอร์โคเนียในช่วง 25-75 โมล% ของอะลูมินา ทั้งนี้อะลูมินาและเซอร์โคเนีย
บริสุทธิ์ได้ถูกเตรียมขึ้นโดยวิธีการเดียวกัน เพื่อเปรียบเทียบกับออกไซด์ผสมโดยการวิเคราะห์
คุณสมบัติทางกายภาพและทางเคมี อีกทั้งใช้เป็นตัวเร่งปฏิกิริยาการอิลิมิเนชันของ 2-โพรพานอล
พบว่าอะลูมินาจากการเตรียมแบบพิชีนีความเป็นกรดและเบสที่ผิวต่ำ ส่งผลให้เกิดการเลือกเกิด
ของอะซิโตนในปฏิกิริยาอิลิมิเนชันของ 2-โพรพานอน ในขณะที่โครงสร้างที่บกพร่องของเตตระ
โกนอลเซอร์โคเนียเลือกเกิดโพไพลีนที่ 200 องศาเซลเซียส นอกจากนี้สารตัวอย่างได้ถูกนำไป
ประยุกต์ใช้เป็นตัวรองรับตัวเร่งปฏิกิริยาสำหรับปฏิกิริยาคาร์บอนมอนอกไซด์ไฮโดรจีเนชัน และ
เซอร์โคเนียที่ปรับปรุงด้วยอะลูมินาปริมาณต่ำ (0.5-1โมล%) ได้ถูกเตรียมและใช้เป็นตัวรองรับโลหะ
โคบอลต์ พบว่าความว่องไวสำหรับปฏิกิริยาคาร์บอนมอนอกไซด์ไฮโดรจิเนชันสูงกว่าตัว
รองรับอะลูมินาบริสุทธิ์และเซอร์โคเนียบริสุทธิ์ 30% ทั้งนี้สันนิษฐานว่าการปรับปรุงเซอร์โคเนียโดย
อะลูมินาปริมาณต่ำส่งเสริมให้เกิดการกระจายตัวของโลหะโคบอลต์ อย่างไรก็ตามเมื่อใช้ตัวรองรับที่
มีปริมาณอะลูมินาสูง 40-75โมล% พบว่าการกระจายตัวของโลหะโคบอลต์ต่ำและส่งผลให้ความ
ว่องไวในเชิงปฏิกิริยาต่ำ ซึ่งอาจเกิดจากการเกิดสารประกอบระหว่างโคบอลต์ออกไซด์และตัวรองรับ
ที่มีโครงสร้างอสัณฐานในขณะเกิดปฏิกิริยารีดักชันโดยไฮโดรเจน นอกจากนี้เตตระโกนอลเซอร์
โคเนียปรับปรุงด้วยธาตุชนิดอื่นในปริมาณต่ำ (0.5-1โมล%) ได้แก่ ยิเทรีย หรือ ซิลิกา ถูกนำมาใช้เป็น
ตัวรองรับสำหรับโลหะโคบอลต์ พบว่าความว่องไวในการเกิดปฏิกิริยาและเสถียรภาพของตัวเร่ง
ปฏิกิริยามีค่าต่ำกว่าการใช้ตัวรองรับเซอร์โคเนียปรับปรุงด้วยอะลูมินาปริมาณต่ำ

ภาควิชา........วิศวกรรมเคมี..........	ลายมือชื่อนิสิต.........................	
สาขาวิชา.......วิศวกรรมเคมี..........	ลายมือชื่ออาจารย์ที่ปรึกษา............	
ปีการศึกษา......2548.................	ลายมือชื่ออาจารย์ที่ปรึกษาร่วม........	

4670255921: MAJOR CHEMICAL ENGINEERING

KEY WORD: ZIRCONIA / PECHINI METHOD/CO HYDROGENATION

SOIPATTA SOISUWAN: EFFECT OF DEFECTED ZIRCONIA SUPPORT ON CATALYTIC ACTIVITY CARBONMONOXIDE HYDROGENATION. THESIS ADVISOR: PROF. PIYASAN PRASERTHDAM, Dr.Ing. THESIS CO-ADVISOR: PROF. DAVID L. TRIMM, Ph.D 119pp. ISBN 974-17-5621-6

In this study, the modified Pechini method has been used to prepare alumina-zirconia mixed oxides varied in a range of 25-75% by mole of alumina in zirconia. To compare with the mixed oxides, pure alumina and pure zirconia were also prepared by the same method. Physicochemical properties of all samples were investigated and elimination of 2-propanol was used to evaluate the catalytic performance of solid surface. The modified Pechini preparation resulted in poor acid-base strength of alumina surface resulting in high acetone selectivity where imperfect crystal structure of the tetragonal zirconia favoured high propylene production in 2-propanol elimination at 200°C. In order to apply these solid samples in an alternative way, all samples were employed as cobalt catalyst support for CO hydrogenation. Moreover, zirconia with low alumina content (0.5-1 mole% Al) were also prepared and tested as support. When employed as supports for Co catalyst for CO hydrogenation, it was found that of zirconia with low Al content supported Co catalysts increased 30% compared to the ones supported on pure zirconia or pure alumina suggesting the modification of zirconia by alumina resulting in higher Co dispersion. However, when supports with high alumina contents (40-75 mole% Al) were used, low Co dispersion and poor catalytic performance were found. It is likely that cobalt formed metal-support compounds with amorphous phase of these mixed oxides. Finally, tetragonal zirconia with low content of another elements (0.5-1 mole%), i.e. Y or Si was introduced to be Co catalyst support, however the catalytic performances and stabilities of these supports exhibited fairly lower than that of zirconia with low Al content.

Department ... Chemical Engineering...   Student's signature..........................

Field of study...Chemical Engineering...   Advisor's signature.............................

Academic year..........2005...............   Co-advisor's signature.........................

ACKNOWLEDGEMENTS

CONTENTS

CONTENTS (CONT.)

LIST OF TABLES

LIST OF FIGURES

CHAPTER I

INTRODUCTION

1.1 Rationale

In recent years, zirconia has received much attention from researchers in the field of heterogeneous catalysis as a support material as well as a catalyst because it is more chemically inert than the classical supports (e.g., γ-alumina and silica) and it may possess different chemical properties such as acidity, basicity, reducing, or oxidizing ability [1]. It was categorized as an acid-base concerted bifunctional catalyst due to the presence of weakly acid sites and weakly base sites suitably oriented on zirconia surface [2]. Due to its acid-base bifunctional surface, zirconia exhibited remarkably high catalytic activity, selectivity, and long catalytic life for particular reactions [3-5]. In spite of its almost neutral surface properties, it also has been applied for the synthesis of ketones [6], methanol [7] and other organic chemicals [8,9], for hydrogenation of carbon monoxide [10,11] and olefins [12], for photocatalysis [13], and for hydrolysis [14]. Moreover, it has been reported that zirconia exhibited a pronounced catalytic behaviour for dehydration superior to other oxides i.e. alumina, titania, yttria, silica, magnesia and ceria [15,16], though it possesses fairly low surface area (typically less than 50 m^2/g). Moreover, the catalytic activity over zirconia catalyst can be improved by increasing the zirconia surface or by modifying with NaOH [17] or sulphate groups [18].

As can be seen, zirconia is a versatile material in catalysis. Not only as a catalyst, but also as a catalyst support because it has shown promising results in many environmental catalysis reactions such as CO_2 hydrogenation [19], CO oxidation [20], and the Fischer-Tropsch reaction [21-24].

However, zirconia can cause a drawback of being used as a catalyst or catalyst support. This is because the zirconia surface area decreases rapidly when the material is heated above 500°C [25]. One of the reasons cited for the instability of zirconia materials is the polymorphism, which gives rise to phase transitions. It was reported

that the stability of the tetragonal phase of zirconia is important for applications as a catalyst or catalyst support. A few researchers have recently reported methods to overcome these problems using special synthesis such as citric gel [26], sol-gel (55-205 m^2/g) [27], and solvothermal methods (~200 m^2/g) [28]. In addition, dispersion of impregnated zirconia over common supports (e.g. silica or alumina) is an alternative route and the presence of zirconia was also found to be a promoter of reactions [29,30]. Thus, the preparation of zirconia mixed oxides is of interest in order to maintain surface area and thermal stability.

There are a number of reports in the literature on modification of zirconia surface area and thermal stability with the other oxides such as aluminium [31-33], silicon [28,34], yttrium [35-37], lanthanum [38], and silicotungstate [39]. It has been reported that addition of small amounts of second metals can improve the thermal stability of tetragonal phase zirconia. For examples, silica-modified zirconia obtained by the reaction of mixture of zirconium *n*-propoxide and tetraethyl orthosilicate in 1,4-butanediol at $300^{\circ}C$ had large surface area and high stability of tetragonal phase even after calcination at high temperatures [28].

To our knowledge, the effect of Al-, Si- or Y-modified zirconia on the properties of zirconia supported catalysts, i.e. Co/ZrO_2 has never been studied. In this study, we report the synthesis of nanocrystalline zirconia by modified Pechini's method and their applications as catalysts and cobalt catalyst supports for dehydration of 2-propanol and CO hydrogenation, respectively. The modified Pechini's method is known to be a successful method for production of solid powders by polymerization of citric acid and ethylene glycol around metal ions [40]. Due to high surface areas, the obtained materials could bring about high dispersion of metal loading and consequently high active sites for catalytic reactions. The catalysts were characterized by N_2 physisorption, XRD, H_2 chemisorption, TPR, TEM, SEM, and tested for catalytic activity in CO hydrogenation reaction and elimination of 2-propanol.

1.2 Objectives

The objectives of this research are

1. to investigate effect of Al added in a range of 25-75mole% on the characteristics of alumina-zirconia mixed oxide and the catalytic activity for reactant of 2-propanol

2. to investigate effect of Al addition in 2 different ranges (1) 0.5-1mole% Al and (2) 25-75mole% Al on the characteristics of alumina-zirconia supported catalysts and then catalytic activity for CO hydrogenation

3. to investigate the characteristics and the catalytic properties of the Si- and Y-modified ZrO_2 supported cobalt catalyst in CO hydrogenation.

1.3   Scope of works

1. Preparation of zirconia, alumina and alumina-zirconia mixed oxides using the modified Pechini's method

2. Preparation of cobalt catalysts supported by zirconia, alumina and alumina-zirconia mixed oxides by incipient wetness impregnation

3. Preparation of Si- and Y- modified zirconia with small amounts of the second metal (0.5-1mole%) using the modified Pechini's method

4. Preparation of cobalt catalysts supported on Si- and Y- modified zirconia

5. Characterization of zirconia, alumina and alumina-zirconia mixed oxides using X-ray diffraction (XRD), BET surface area, CO_2 temperature programmed desorption (CO_2-TPD), NH_3 temperature programmed desorption (NH_3-TPD) and scanning electron microscopy (SEM)

6. Characterization of the supported cobalt catalyst samples using X-ray diffraction (XRD), BET surface area, temperature-programmed reduction (TPR), hydrogen chemisorption, scanning electron microscopy (SEM) and transmission electron microscopy (TEM)

7. Catalytic testing for zirconia, alumina, alumina-zirconia mixed oxides by the of 2-propanol at 150, 200, and 250°C and 1 atm

8. Reaction study of the catalyst samples for CO hydrogenation at 220°C and 1 atm and a H_2/CO ratio of 9:1.

This thesis is intended to give an understanding of behaviour of zirconia modified by three metals i.e. aluminium, silicon or yttrium, which were employed as catalysts and catalyst supports for dehydration of 2-propanol and CO hydrogenation, respectively. The content of this thesis is divided into two parts: the first three chapters describe general information about the study, while the following chapters emphasize the results and discussion observed from a present study. The background and scope of this study are described in Chapter I. Review of zirconia application in catalysis, especially used in alcohol dehydration and CO hydrogenation in the past and comment on previous work are in chapter II. The following Chapter III gives fundamental aspects of dehydration of alcohol and CO hydrogenation including theoretical content of zirconia and its preparation. The experimental in Chapter IV consists of catalyst preparation method, catalyst characterization and catalyst evaluation whereas results and expanded discussion are described in Chapter V. The last chapter, overall conclusion from this work and some recommendation for future are presented.

CHAPTER II

LITERATURE REVIEWS

Modification of zirconia by the second oxides has been widely prepared for many reasons. From the literatures, it is possibly concluded that amount of second-oxide addition may be classified into 2 groups, i.e. (i) adding as dopant and (ii) adding to form mixed oxide with zirconia.

Being as dopant, it was employed by small amount of the second metal and had an effect on physical properties of zirconia reported in most of ceramic literatures. The crystal structure of zirconia was found to be different due to extension of c lattice parameters caused by doped zirconia with oversized rare earth R^{3+} (Sc, Yb, Y, Gd, and Sm) [41,42], thereby suggesting that zirconia and these rare-earth oxides completely formed solid solution. It was found that tensile strength of zirconia was improved by increasing amount of dopant and ionic radian size.

Moreover, it has been reported that addition of dopant in zirconia exhibited an influence on phase stability contributing to maintain zirconia surface area. Due to its polymorphism, phase transformation can occur easily by heating up to $500^{o}C$ [25]. It was reported that stability of tetragonal phase is important for applications as catalyst or catalyst support. The elements were frequently used as dopant for zirconia, i.e. yttria, lanthania, silica and alumina.

There have been a number of researchers studying the effect of ZrO_2 as a promoter, a support modifier, and a catalyst support in the Fischer-Tropsch synthesis. Most studies show significant improvement in catalyst actives and selectivities. Followings are some recent studies in application of ZrO_2 in FTS.

2.1 Application of ZrO$_2$ in FTS

2.1.1 As a promoter

Feller et al. [43] studied the addition of zirconium oxide chloride to the catalyst formulation of Co/SiO$_2$. It leads to a higher reducibility of cobalt, due to the formation of a cobalt zirconium species, which can be reduced at lower temperatures than cobalt silicate. Furthermore, the metal particle size of cobalt is increased, but the size of cobalt clusters is reduced. The Co–Zr/SiO$_2$ catalysts were tested for their activity in the Fischer–Tropsch synthesis. The steady-state activity increased with increasing zirconium loading, which was attributed to the resistance against reoxidation of the larger cobalt particles and thus to the larger amount of surface cobalt metal present at steady-state in the zirconium promote catalysts. Based on the assumption that the intrinsic activity of cobalt in these catalysts remains unchanged, the observed changes in selectivity could be explained on the basis of secondary reactions in the Fischer–Tropsch system. With increasing zirconium content the number of surface metal atoms at steady-state conditions increases, leading to a higher extent of secondary reactions, but the size of the cobalt clusters decreases, leading to a decrease in the extent of secondary reactions. With increasing zirconium content the extent of secondary hydrogenation of olefins (e.g., ethene) passes a minimum, and the C$_{5+}$-selectivity passes a maximum due to re-adsorption of small, reactive organic product compounds, which can be incorporated in larger product compounds. Double bond isomerization increases with increasing zirconium content. This might be attributed to the catalytic activity of zirconia.

Oukaci et al. [44] studied the catalyst support in both promoted and non-promoted cobalt catalysts was found to play a major role in influencing the overall hydrocarbon production rate with little or no effect on catalyst selectivity (except for titania) in both the fixed-bed and the slurry bubble column reactor. Zr oxide had a similar effect on the activity of Co/silica. Addition of ZrO$_2$ to the support prior to the impregnation of cobalt probably serves somewhat to hinder the formation of cobalt silicates. ZrO$_2$ was found, thus, to be an excellent F–T synthesis rate promoter for SiO$_2$-supported Co catalysts without any effect, negative or positive, on catalyst

selectivity. However, the long-term protecting effect of the zirconia remains to be determined. It is also important to note the differences observed in the two reaction systems, i.e. fixed-bed versus slurry bubble column reactors.

Moradi et al. [45] studied the effect of zirconia addition at various loading ratios on the performance of 10 wt% Co/SiO2 catalysts for the so-called reaction of Fischer–Tropsch synthesis. The catalysts were prepared through a new pseudo sol–gel method, which permits a uniform distribution of the incorporated components and a low deviation from theoretical composition. By increasing zirconia, Co–SiO2 interaction decreases and is replaced by Co–Zr interaction which favours reduction of the catalysts at lower temperatures. The activity and selectivity toward higher hydrocarbons of the promoted catalysts increase with increasing zirconium loading ratios. No appreciable decrease in activity was observed when all catalysts were employed under H_2/CO at 230 $^{\circ}C$ and 8 bar for 240 h.

2.1.2 As a support modifier

Yadav et al. [46] reported zirconium oxide, or zirconia, when modified with anions such as sulphate ions forms a highly acidic or superacidic catalyst depending on the treatment conditions. This catalyst is found to be well suited for catalyzing reactions of industrial importance, e.g. Fischer–Tropsch reaction. The yield of C_3 was found to decrease with increase in the amount of $S-ZrO_2$, whereas the yields of C_1, C_2, C_5 and C_6 hydrocarbons were negligible. Also, the formation of isoalkanes was found to be substantially more than alkenes. All the above changes were attributed to secondary reactions of primary FTS products over the strongly acidic $S-ZrO_2$. These secondary reactions were found to involve oligomerization-cracking, skeletal isomerization, hydrogen transfer and coking. The calcination temperature of $S-ZrO_2$ had a strong effect on its activity for the secondary reactions.

Rohra et al. [47] studied the effect of adding zirconia to the alumina support on supported cobalt Fischer–Tropsch catalysts. At 5 bar and H_2:CO ratio 9:1 zirconia addition to the support leads to a significant increase in both activity and selectivity to higher hydrocarbons as compared to the unmodified catalysts. Reducibility and cobalt

dispersion on the other hand are not improved by the presence of zirconia compared to the unmodified catalysts. SSITKA measurements have been performed in order to determine the intrinsic activity per active site. At constant temperature, zirconia-modified and unmodified catalysts showed basically the same intrinsic activity. Similar results were obtained with a noble metal (Pt) promoted catalyst. The promoting effect appears to be mainly due to coverage effects rather than a change in the intrinsic activity of the active sites. The turnover frequencies were found to be independent of pressure but strongly temperature dependent. However, the increase in turnover frequency did not account for the entire increase in reaction rate with temperature. This indicates that also the coverage of reactive intermediates increases with increasing temperature.

Jacobs et al. [48] studied TPR and H2 chemisorption with pulse reoxidation were carried out on cobalt Fischer–Tropsch catalysts prepared using different supports (e.g. Al_2O_3, TiO_2, SiO_2, ZrO_2 modified SiO_2, ZrO_2 modified Al_2O_3) employing a variety of promoters, including noble metals and metal cations. Addition of non-reducible metal oxides such as B, La, Zr, and K was found to cause the reduction temperature of Co species to shift to higher temperatures, resulting in a decrease in the percentage reduction. For both Al_2O_3 and SiO_2, modifying the support with Zr was found to enhance the dispersion. Increasing the cobalt loading, therefore the average Co cluster size resulted in improvements to the percentage reduction.

Jongsomjit et al. [30] reported Zr modification of the alumina support had a significant impact on the properties of Co/γ -Al_2O_3 catalysts. The overall catalytic activity during FTS increased significantly (> 65%) upon Zr modification. SSITKA showed that the number of active reaction intermediates (N_M) increased with Zr modification while the intrinsic activity ($1/\tau$M) remained constant. Most of this increase appears to have been due to an increase in reducibility during standard reduction. The increase in reducibility appeared to have been caused by a decrease in the amount of Co-SCF, as seen by Raman spectroscopy. Zr modification may have caused (i) a stabilization of the alumina support by blocking its defect sites, thus blocking Co "aluminate" formation, and/or (ii) a minimization of the impact of water vapour in modifying the surface properties of alumina, thereby decreasing the ease of

Co reaction with the alumina. Thus, in summary, Zr modification increased Co reducibility and, probably, the number of exposed Co sites active for CO hydrogenation. Considering the variation in TOFH but the lack of variation in $1/\tau M$ (a measure of intrinsic activity), it is likely that TOFH is in error due to errors in measuring accurately by H_2 chemisorption the number of reduced Co surface atoms.

2.1.3 As a catalyst support

Maruya et al. [49] investigated the selective formation of isobutene from CO and H_2 over ZrO_2. ZrO_2 catalysts having different fraction of monoclinic phase were prepared by changing pH value in the mother solution at the precipitation of zirconium hydroxide. The rate of isobutene formation increased with an increase in the volumetric fraction of monoclinic phase in ZrO_2, while those of C_1, C_2, C_3, and C_5+ were independent of the fraction. The amounts of adsorbed methoxy and formate species during the reaction and also of the surface sites with strong basicity increased with an increase in the fraction of monoclinic phase. Chemical trapping experiment showed that the amount of surface methoxy species is comparable to that of site with the strong basicity. These findings were explained by both coordinate unsaturation and stronger basicity based on the configuration of ZrO_2 group in the monoclinic structure.

Enache et al. [24] reported the thermal treatment, which leads to the best catalytic results, is the direct reduction of the nitrate precursor in the reactor. The effect of the pretreatment is higher in the case of zirconia supported catalyst. The direct reduction of nitrate precursors is even more effective when using a slow-temperature ramping protocol. This phenomenon is explained by the exothermicity of the nitrate reduction. The slower the temperature ramps, the better the heat evacuation, avoiding any increase in cobalt-support interactions or particle agglomeration. The reduction of Co_3O_4 oxide is difficult and leads to an increase of the cubic crystallised cobalt at the expense of amorphous cobalt or hexagonal cobalt with stacking faults. The direct reduction of nitrate precursor increases the quantity of amorphous cobalt or hexagonal cobalt with crystallographic defects, which are active phases in this reaction. At the same time, the direct reduction leads to weaker metal-support interactions than does precalcination of catalysts.

The nitrogen-flow calcination conducts to an intermediate situation. The quantity of crystallised Co_3O_4 is less important than in the case of airflow calcination and it is more reducible.

Enache et al. [23] studied the activity and the selectivity of cobalt catalysts supported on a crystallised and on an amorphous zirconia were compared with cobalt supported on a γ-alumina catalyst. The catalysts supported on zirconium dioxide were found to present a better reducibility of the active phase and also to be capable of hydrogen adsorption via a spillover mechanism. It is proposed that these properties could account for a better catalytic activity and an increase of the chain growth probability ($α$). At the same time, the estimated quantity of crystallised Co_3O_4 obtained after airflow calcination (for the same total cobalt loading) is related with the surface area of the support.

Shinoda et al. [29] investigated the Co/SiO_2 catalysts derived from silica bimodal supports were tested in slurry phase FTS. It showed higher activity and favourable selectivities, due to its improved dispersion of supported cobalt crystalline by bimodal structure, as proved by XRD and TEM, and fastened diffusion efficiency inside catalyst pellet with bimodal structure. Furthermore, besides the spatial effect from bimodal structure as shown in silica–silica bimodal catalyst, significantly enhanced activity was realized using ZrO_2-silica bimodal support, as ZrO_2 inside the large pores of SiO_2 not only formed small pores but also intrinsically promoted FTS.

CHAPTER III

THEORY

Theoretical aspects of the study are briefly described in this chapter, consisting of general features of zirconia and preparation methods, i.e. precipitation, hydrothermal, solvothermal, sol-gel, and the modified Pechini's method. Since two of fundamental reactions, i.e. elimination of 2-propanol and CO hydrogenation were chosen to test the synthesized zirconia as catalysts and catalyst supports respectively, thus details of these processes are also given in this chapter.

3.1 General feature of zirconia

Zirconia exhibits three polymorphs, the monoclinic, tetragonal, and cubic phases. As shown in Figure 2.1, crystal structures of cubic, tetragonal and monoclinic zirconia are shown in Figure 3.2. The monoclinic form is stable up to ~1170°C, at which temperature it transforms into the tetragonal phase, which is stable up to 2370°C [50]. The stabilization of the tetragonal phase below 1100°C is important in the use of zirconia as a catalyst. Above 2370°C, the cubic phase is stable and it exists up to the melting point of 2680°C. Due to the martensitic nature of the transformations, neither the high temperature tetragonal nor cubic phase can be quenched in rapid cooling to room temperature. However, at low temperature, a metastable tetragonal zirconia phase is usually observed when zirconia is prepared by certain methods, for example by precipitation from aqueous salt solution or by thermal decomposition of zirconium salts. This is not the expected behaviour according to the phase diagram of zirconia (i.e., monoclinic phase is the stable phase at low temperatures). The presence of the tetragonal phase at low temperatures can be attributed to several factors such as chemical effects, (the presence of anionic impurities) [51,52] structural similarities between the tetragonal phase and the precursor amorphous phase [52, 53-54] as well as particle size effects based on the lower surface energy in the tetragonal phase compared to the monoclinic phase [52-53,55]. The transformation of the metastable tetragonal form into the monoclinic form is generally complete by 650-700°C.

Crystal system	Unit cell shape
Cubic	$a = b = c,\ \alpha = \beta = \gamma = 90^{\circ}$
Tetragonal	$a = b \neq c,\ \alpha = \beta = \gamma = 90^{\circ}$
Monoclinic	$a \neq b \neq c,\ \alpha = \gamma = 90^{\circ},\ \beta \neq 90^{\circ}$
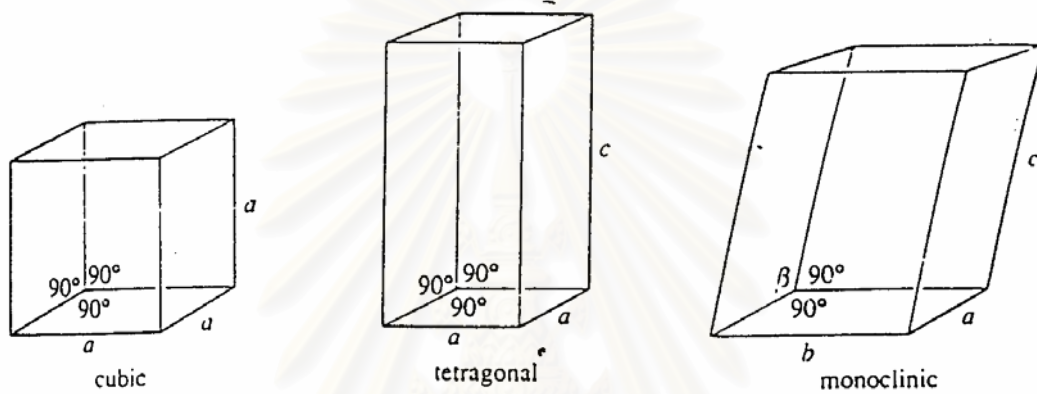
Figure 3.1 The unit cells of the crystal systems. [56]
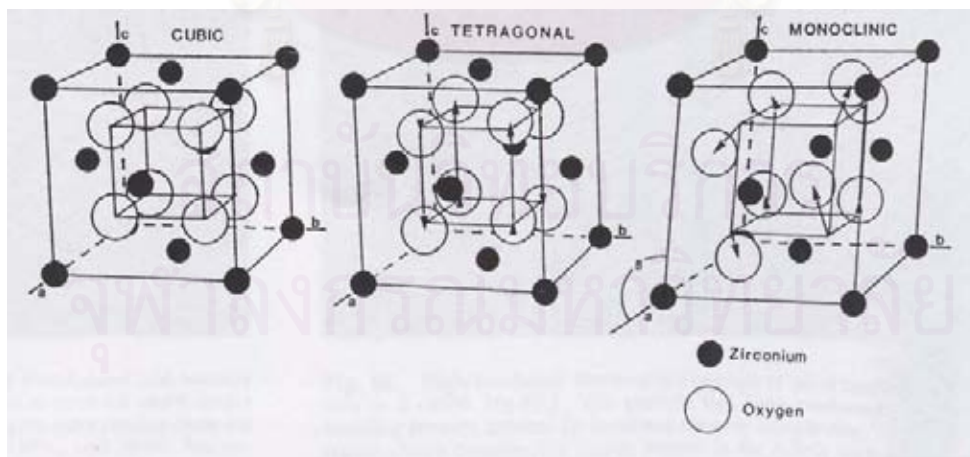
Figure 3.2 Crystal structure of cubic, tetragonal and monoclinic zirconia. [57]

3.2 Preparation of zirconia

The preparation of zirconia has been revised by many researchers as in chapter II and widely reported in both ceramic and catalysis fields. The main conventional synthesis for multicomponent ceramic powders is a solid-state reaction between oxide and/or carbonate powder precursors. Thus, this method requires repeatedly milling cycles and high temperature calcination to approach a point of solid-state reaction. This conventional method causes some disadvantages, i.e. (i) large grain sizes due to high temperature operation, (ii) poor chemical homogeneity, and (iii) undesirable phase formation. Synthesis via chemicals, an alternative route, is attracting much attention because the chemical route is also operated at much lower reaction temperatures to approach the required crystalline points. Moreover, these routes have the potential to improve chemical homogeneities especially on a molecular scale. The interesting chemical routes, investigated intensively worldwide for powder preparation, are described below.

3.2.1 Precipitation method

Precipitation from a saturated solution can be possibly controlled for a brief period and the solution needs to be concentrated to a supersaturation condition either by rising temperature and/or increasing concentration or pH. Chuah et al. has reported one precipitation methods described as the following [25]. Zirconia was prepared by adding a solution of zirconium chloride to a well-stirred precipitating solution (e.g. NH_4OH, KOH, or NaOH) at room temperature to control a pH condition approximately equalling to 11. The resulting precipitate was repeatedly rinsed using distilled water to remove chloride ions. Cleaned precipitate was then dried overnight at $100^{\circ}C$ resulting in amorphous hydrous oxide, and then obtaining the crystalline zirconia after calcination at $500^{\circ}C$. The resulting zirconia was predominantly monoclinic, 84%. After heat treatment at $500^{\circ}C$ for 1 h, the surface area was only 65 m^2/g and decreased further to 40 m^2/g when calcined for 12 h.

3.2.2 Sol-gel method

The sol-gel method is started by preparation of a sol. It is necessary to choose compatible starting materials, i.e. reactant and solvent, to form a fairly nice sol. Sol preparation can be simplified either by (i) immiscible dispersion of insoluble solids (particle size less than 9 nm) in liquid or (ii) reaction of precursor and solvent to form colloid. In the first case, solid oxide or hydroxide dispersion is created by slightly adjusting pH condition of a clear starting solution. The pH condition for this case must be lower than the pH of precipitation condition; otherwise it may cause precipitation of oxide or hydroxide instead of sol formation [58]. In the latter case, metal alkoxide and organic solvent, usually using alcohol, are starting materials. The system consists of 2 reactions, which occur during mixing the starting materials, i.e. (i) hydrolysis and (ii) condensation. Hydrolysis takes place by water contained in alcohol reacting with metal alkoxide. It can result in a few hydroxyl groups surrounding metal ions and condensation of these hydroxyl groups can continuously form a metal hydroxide network becoming a sol and, eventually, a gel after gradually removing solvent. Finally, the amorphous form of metal hydroxide can be obtained, and the crystalline forms will be obtained after calcinations at a certain temperature.

3.2.3 The modified Pechini's method

In 1967, M.P. Pechini [40] prepared resin intermediates of alkaline earth and transition ions and alpha-hydroxycarboxylic acid and polyhydroxyl alcohol were employed as starting materials. The alpha-hydroxycarboxylic acid, such as citric, lactic and glycolic acids, can form polybasic acid chelating with transition ions and esterifying with the polyhydroxyl alcohol during heating. Ignition of the synthesized polymeric resin can cause the removal of organic polymer and results in metal oxide or mixed oxide powder. This method is suitable for compound or mixed oxide preparations because the resulting material also consists of close combination of metal ions, due to good mixing on an ionic scale in the starting solutions. Recently, a few researchers have modified this method using starting material different from Pechini [59-62] (the so-called modified Pechini's method). The details of this method are presented in Chapter IV.

3.2.4 Hydrothermal method

Hydrothermal method produces particle sizes in a range of nano size to single crystals. The hydrothermal system consists of (i) metal precursors, (ii) catalyst and (iii) solvent. A few factors, i.e. high temperature and high pressure caused by aqueous solution, vapours and/or fluids in the process, can affect the starting material to transfer pressure, temperature, and mechanical energy. Solvent can play an important role in dissolving or re-precipitating solid material and distilled water usually is used as solvent, which simultaneously acts as a catalyst. After prolonging a reaction under high temperature and pressure, metal precursor will be changed to forms of hydroxide, oxide, oxyhydroxide and/or salt. This synthesis system apparently exhibits the homogeneity of the particles on molecular or atomic scale [63].

3.2.5 Glycothermal and solvothermal method

Glycothermal and solvothermal methods have been developed for metal oxide synthesis and binary metal oxide by using glycol and organic solvent as the reaction medium, respectively. Instead of distilled water, glycol or other solvents has been introduced to hydrothermal method and this method is so-called glycothermal or solvothermal methods.

3.3 Dehydration of alcohol [65]

Dehydration of alcohols to olefin or ethers can be effected with most solid acid catalysts as well as with solid base catalyst. Usually, solid acids are more active than bases. Among acid catalysts, alumina is the most versatile. In industrial situation, dehydration can be carried out using metal phosphates, metal oxide and cation-exchange resin. In 1965, it was noted by Batta et al. [64] that dehydration increases with the covalent character of the metal-oxygen bond of the catalyst, whereas dehydrogenation is enhanced by increasing the ionic character. Thus, the catalyst can be placed in the following selectivity sequence.

$$WO_3 \quad SiO_2 \quad Al_2O_3 \quad TiO_2 \quad Cr_2O_3 \quad FeO \quad ZnO \quad MgO \quad CaO$$

$\longleftarrow$ ─────────── Dehydration

───────────────── $\longrightarrow$ Dehydrogenation
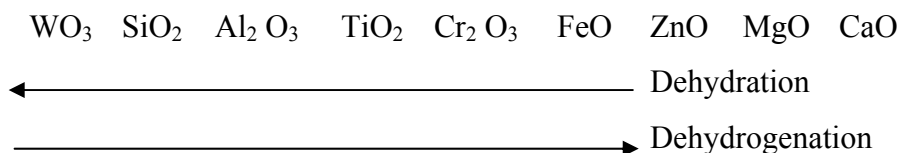
Dehydration over acid catalysts generally yields Saytzeff products, while dehydration over basic oxide such as ThO_2 and ZrO_2 yields Hofmann elimination products. Dehydration over strongly basic catalyst such as MgO and CaO is always accompanied by dehydrogenation. Dehydration is often accompanied by the subsequent isomerization of primary products. It may be avoided by poisoning acid sites with alkali metal ions, ammonia or organic base.

Catalytic dehydration can proceed according to the following types of mechanisms where A and B stand for acidic and basic centres of catalyst, respectively.
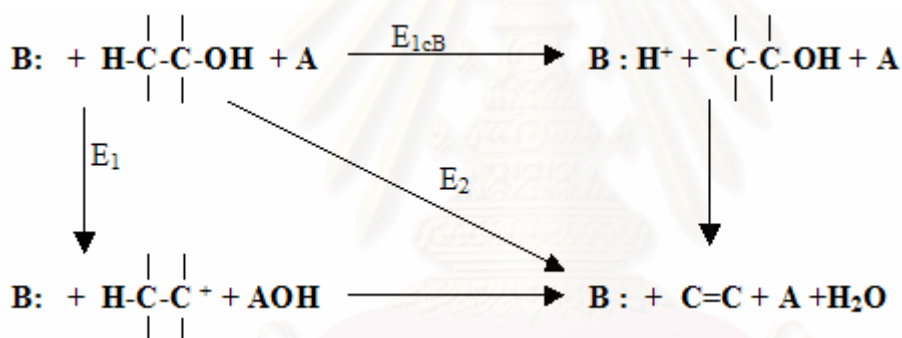
Figure 3.3 Mechanism of dehydration [65]

E_{1cB} mechanism; The first step of dehydration is formation of a carbanion, meaning that a C-H bond is loosened or broken in the first step. This mechanism occurs with strongly basic catalysts such as La_2O_3, ThO_2, and alkaline earth oxides.

E_1 mechanism; The first step of dehydration involves the formation of carbenium ion by abstraction of an OH group. This mechanism occurs with strongly acidic catalysts such as aluminosilicate. The acid centre may be either a Brønsted or Lewis type. In the former case, the carbenium ions may be produced with the intermediacy of oxonium ions.

E_2 mechanism; The elimination of a proton and a hydroxyl group from alcohol are concerted without formation of ionic intermediates. Alumina is a typical E_2 oxide.

The E_2 mechanisms are shown in Figure 3.5 and 3.6. Figure 3.5 exhibits adsorption of 2-propanol over the acid-base concerted bifunctional site and formation of propylene is shown in Figure 3.6.
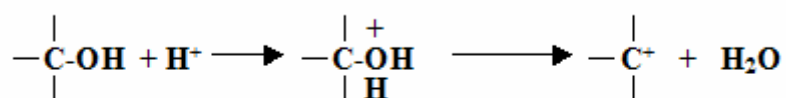
Figure 3.4 Production of carbenium ions by strongly acidic catalyst
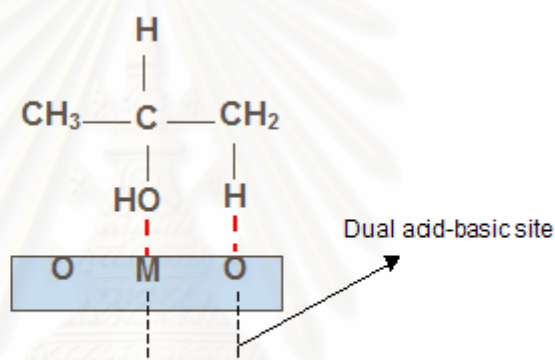
The adsorption of 2-propanol over dual acid-base site (amphoteric site)

Figure 3.5 Scheme of 2-propanol adsorption over dual-base site [65]
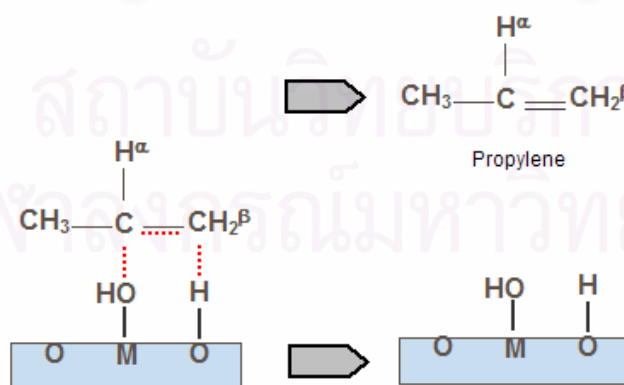
Formation of propylene by eliminating of hydrogen and hydroxyl group on dual acid-base sites

Figure 3.6 Scheme of propylene formation via E_2 mechanism [65]

Nevertheless, Díez et al. [66] recently proposed a mechanism slightly different from E_{1cB} as mentioned by Tanabe et al. [65] for dehydration of 2-propanol. The E_{1cB} could probably occur on acid-base sites of imbalanced strength to form a surface propoxide intermediate as shown in Figure 3.7. The most acidic hydrogen of alcohol is attacked by strong base site (the surface oxygen); in contrast, the Lewis acid site (the surface cation) attacks the oxygen of alcohol resulting in rupture of hydroxyl groups.
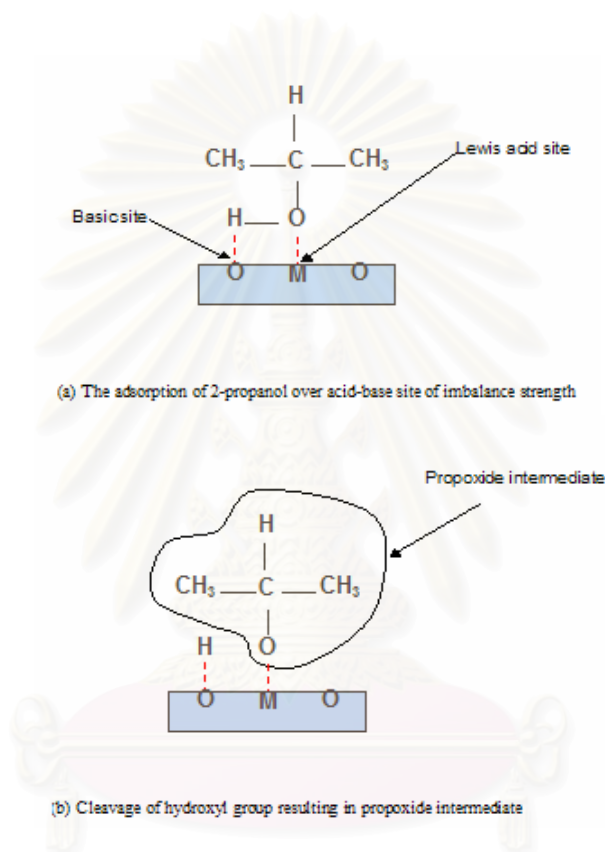
Figure 3.7 Scheme of rupture of hydroxyl group proposed by Díez et. al. [66]

Two pathways were proposed after forming propoxide on the surface: (a) dehydration of 2-propanol where acetone is a result of abstraction of α-hydrogen in Figure 3.8 and (b) dehydrogenation of 2-propanol producing propylene by detaching β-hydrogen in Figure 3.9. The products of the E_{1cB} mechanism could be either propylene or acetone or both, depending on the strength of the base site as summarized in Figure 3.8 and Figure 3.9. However, the base site detaching β-hydrogen is stronger than the one detaching α-hydrogen. This suggest that the characteristic of oxide surface can be explored by analysing product distribution because each of the products can be caused

by different surface characteristics resulting in different pathways, i.e. E_{1cB}, E_1, and E_2. In this study, the mechanism of Díez et al. has been introduced in order to identify the surface characteristic of the synthesized oxide by referring to production distribution

Figure of acetone formation

Formation of acetone by attacking α Hydrogen
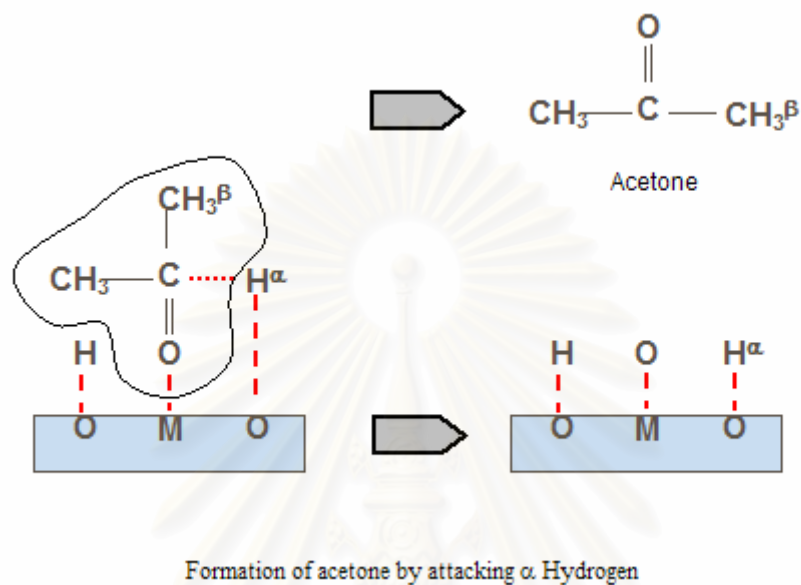
Figure 3.8 Scheme of acetone formation via E_{1cB} mechanism [66]

Formation of propylene by attacking β hydrogen
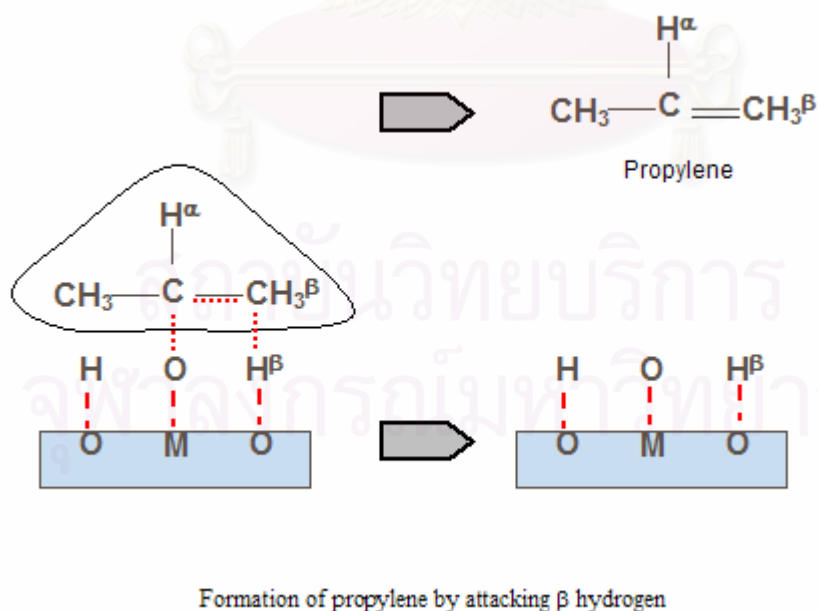
Figure 3.9 Scheme of propylene formation via E_{1cB} mechanism [66]

3.4 Fischer-Tropsch synthesis (FTS)

Fischer-Tropsch synthesis (FTS), the production of liquid hydrocarbons from synthesis gas (CO and H_2), is a promising, developing route for environmentally sound production of chemicals and fuels from coal and natural gas. During the past decades, FTS has been developed continuously by many researchers, although the rise and fall in research intensity on this process has been highly related to the demands for liquid fuels and relative economics. This synthesis is basically the reductive polymerisation (oligomerisation) of carbon monoxide by hydrogen to form organic products containing mainly hydrocarbons and some oxygenated products in lesser amounts. The main reactions of FTS are:

$$CO + 3H_2 \longrightarrow CH_4 + H_2O \qquad (1)$$

$$nCO + 2nH_2 \longrightarrow (1/n)\ C_nH_{2n} + H_2O \qquad (2)$$

$$CO + H_2O \longrightarrow CO_2 + H_2 \qquad (3)$$

$$2CO \longrightarrow C + CO_2 \qquad (4)$$
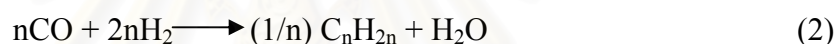
Equation (1) is the formation of methane, equation (2) is the synthesis of hydrocarbons higher than methane, equation (3) is the water-gas shift reaction, and equation (4) is the Boudouard reaction which results in deposition of carbon. Normally, catalysts used for FTS are group VIII metals. By nature, the hydrogenation activity increases in order of $Fe < Co < Ni < Ru$. Ru is the most active. Ni forms predominantly methane, while Co yields much higher ratios of paraffins to olefins and much less oxygenated products such as alcohols and aldehydes than Fe does.

Commercially, entrained bed reactors or slurry bubble column reactors are used in FTS since they can remove heat from this exothermic synthesis, allowing better temperature control. The current main goal in FTS is to obtain high molecular weight, straight chain hydrocarbons. However, methane and other light hydrocarbons are always present as less desirable products from the synthesis. According to the

Anderson-Schulz-Flory (ASF) product distribution, typically 10 to 20% of products from the synthesis are usually light hydrocarbon (C_1-C_4). These light alkanes have low boiling points and exist in the gas phase at room temperature, which is inconvenient for transportation. Many attempts have been made to minimize these by-products and increase the yield of long chain liquid hydrocarbons by improving chain growth probability. It would be more efficient to be able to convert these less desirable products into more useful forms, rather than re-reforming them into syngas and recycling them [67]. Depending upon the type of catalyst used, promoters, reaction conditions (pressure, temperature and H_2/CO ratios), and type of reactors, the distribution of the molecular weight of the hydrocarbon products can be noticeably varied.

3.5 Co-based FTS catalysts

Supported cobalt (Co) catalysts are the preferred catalysts for the synthesis of heavy hydrocarbons from natural gas based syngas (CO and H_2) because of their high Fischer-Tropsch (FT) activity, high selectivity for linear hydrocarbons, and low activity for the water gas shift reaction. It is known that reduced cobalt metal, rather than its oxides or carbides, is the most active phase for CO hydrogenation. Investigations have been carried out to determine the nature of cobalt species on various supports such as alumina, silica, titania, magnesia, carbon, and zeolites.

CHAPTER IV

EXPERIMENTAL

The catalyst preparation, characterization techniques and catalytic testing are described in this chapter. Overall techniques of the modified Pechini method [40] used to prepare support and its starting chemicals are apparently shown as a part of catalyst preparation. After calcinations at $600^{\circ}C$, solid samples were loaded by approximate 8% cobalt metal and employed as supported cobalt catalysts. Physicochemical properties of synthesized solid samples and catalyst samples were investigated by means of BET surface area, X-ray diffraction (XRD), Scanning Electron Microscopy (SEM), Transmission Electron Microscopy (TEM), CO_2 temperature programmed desorption (CO_2-TPD), NH_3 temperature programmed desorption (NH_3-TPD), H_2 chemisorption and temperature programmed reduction (TPR). All of the characterization methods are described in the second part. The catalytic activities over alumina-zirconia, pure alumina and pure zirconia surfaces were tested by dehydration of 2-propanol explained as a procedure mentioned by Robert et al. in 4.3.1.[59]. Finally, CO hydrogenation was used to evaluate the performance of cobalt catalyst as described in 4.3.2.

4.1 Catalysts preparation

4.1.1 Starting Materials of the modified Pechini's method

The modified Pechini's method is a method modified from the method discovered by M.P. Pechini in 1967. The starting materials of the modified method are different from the conventional one and it has been introduced to the Pechini's method by a few authors [68-70]. All of the chemicals used are reported as follows.

1. Zirconyl nitrate hydrate [$ZrO(NO_3)_2 \cdot xH_2O$] for R&D use only was employed as a precursor of zirconium oxide available from Aldrich Chemical Company, Inc.

2. Aluminium nitrate nonhydrate [$Al(NO_3)_3 \cdot 9H_2O$] for R&D use only was employed as a precursor of alumina available from Aldrich Chemical Company, Inc.

3. Yttrium nitrate hexahydrate [$Y(NO_3)_3 \cdot 6H_2O$] 99.99 wt% was used as yttria source available from Aldrich Chemical Company, Inc.

4. Tetraethyl orthosilicate [$Si(OC_2H_5)_4$] 98 wt% was used as silica source available from Aldrich Chemical Company, Inc.

5. Citric acid or CA, [$HOC(COOH)(CH_2COOH)_2 \cdot H_2O$], 99.0-102.0 wt% used as chelating agent to prevent precipitation of hydroxyl salt is available from UNIVAR, Australia.

6. Ethylene glycol [CH_2OHCH_2OH] used as polymerising agent to form polymeric ester is available from UNILAB, Australia

7. 35 wt% Nitric acid aqueous solutions diluted by distilled water from 70wt% of Nitric acid solution available from UNILAB, Australia was used to adjust pH condition of the precursor solution.

4.1.2 The modified Pechini's method

The preparation started with zirconyl nitrate hydrate 10.17 gram dissolved in distilled water (150 ml) and citric acid aqueous solution (prepared by citric acid 44.1 gram dissolved in distilled water 100 ml). The pH condition of citric aqueous solution was adjusted to be lowered ca. 1 by adding 10 ml of 35wt% nitric acid aqueous solution to avoid precipitation during mixing. The modified citrate solution was mixed with the zirconyl nitrate solution to form citrate complexes.

For production of alumina-zirconia mixed oxides, aluminium nitrate aqueous solution was prepared at different concentrations and added to the citrate complexes solution in order to form 0.5, 1, 25, 40 and 75mole% of alumina in zirconia solid powder after calcinations. The molar ratio of [metal:CA] reported by Pechini equals to 1:7. In addition, the pH condition of ethylene glycol was also adjusted to be lowered ca. 1 before mixing with the resulting solution. Ethylene glycol was used at a molar

ratio of EG/CA=30:7. The mixed solution was heated to 70°C and held at that temperature for 3 days until the volume of the solution was decreased by 1/4 of the starting solutions. The nitric acid groups were decomposed at the boiling conditions as observed from brownish exhaust gases when the solution was heated to 100°C. Polymerisation involved by esterification of hydroxyl groups and carboxylic groups from ethylene glycol and citrate molecules, respectively. The solution became a transparent gel when the temperature approached 120°C spontaneously. The gel was calcined at 600°C for 6 hours in dynamic air to remove the organic materials, resulting in spongy white powder. In case of Y- and Si- modified zirconia, the preparation was done as mentioned above by using yttrium nitrate or tetraethyl orthosilicate instead of aluminium nitrate.

4.1.3 Cobalt loading

The Co/ZrO$_2$ catalysts were prepared by the incipient wetness impregnation of the supports with aqueous solution of cobalt nitrate hexahydrate [Co(NO$_3$)$_2$·6H$_2$O] available from Aldrich Chemical Company, Inc. Cobalt loading was approximately 8% by weight of catalyst. The samples were dried at 110°C for 1 day. The catalysts were calcined in air at 300 °C for 2 h.

4.2 Catalyst Characterization

4.2.1 Surface area measurement by nitrogen physisorption

The surface area of all supports and catalysts were determined by means of BET single point and multi points. Nitrogen adsorption and desorption was used for single point method as described below. Multi point measurements were carried out using a Micromeritics ASAP 2020. Prior to starting experimental, all samples were heated to 300°C for 3 hrs.

Single point method

The single point method was carried out using a Pyrex U-tube with sample dried 0.3 gram connected to a reaction rig. Ultra high purity nitrogen and helium gases supported by Thai Industrial Gases Public Company Limited were used at a molar ratio of N_2/He, 3:7 flowing through dried sample with total gas flow rate 30 ml/min. Nitrogen gas physisorption occurred during dipping Pyrex U-tube into liquefied nitrogen. When physical adsorption-desorption equilibrium is approached, the surface is entirely covered by nitrogen molecules. It was approximate within 20 minutes from experimental experience. Then, desorption was carried out by increasing the temperature of the Pyrex U-tube and desorption of nitrogen was measured using a GOW-MAC thermal conductivity detector (TCD). An area of nitrogen desorption profile was integrated and a calculation of surface area is shown in Appendix A.

Table 4.1 Operating condition of gas chromatograph (GOW-MAC) for BET single point method

Model	Operating Condition
Detector type	TCD
Column	Blank column
Carrier gas	UHP Helium
Carrier gas flow rate (ml/min)	30
Detector temperature (^{o}C)	80
Detector current (mA)	80

4.2.2 X-ray Diffraction (XRD) Analysis

Phase identification and crystallite size of all samples were investigated by X-ray diffraction (Siemens D5000) using Ni filter CuK_α radiation with computer software Diffract ZT version 3.3 programmes for full control of the XRD analyser. The refraction or diffraction of X-ray was monitored at various angles from 20° to 80° with respect to primary beam. Crystallite size was calculated from the Scherrer's

equation using the most apparent diffraction peak of X-ray patterns exhibited in Appendix B.

4.2.3 Investigation of morphology by SEM

Scanning Electron Microscopy Model JSM-5410LV at the Scientific and Technological Research Equipment Centre, Chulalongkorn University (STREC) was employed to observe granule morphology.

4.2.4 Investigation of sample particles by TEM

Sample particle and its agglomerating behaviour were investigated by Transmission Electron Microscopy (TEM) JEOL JEM1220 operated at 80 kV available from Kasetsart University Research and Development Institute.

Figure 4.1 X-Ray Diffraction (Siemens D5000)

4.2.5 CO₂ Temperature programmed desorption (CO₂ TPD)

The number of basic sites is generally measured by means of CO_2 Temperature Programmed Desorption. The strength of basic sites can be also identified by this method. The experiment was conducted using a rig connected to a packed-bed reactor. Samples were pre-treated at $400^{o}C$ for 1 hour in He and then saturated with CO_2 (99.99%) at $35^{o}C$ for 3 hours. To remove CO_2 physical adsorption, Helium gas was flooded into the reactor after saturation. Desorption of CO_2 was carried out by heating at $10^{o}C/min$ to $400^{o}C$, and measured using a GOW-MAC thermal conductivity detector (TCD). The calculation of the amount of CO_2 is presented in Appendix C.

Table 4.2 Operating condition of gas chromatograph (GOW-MAC) for CO₂-TPD

Model	Operating Condition
Detector type	TCD
Column	Blank column
Carrier gas	UHP Helium
Carrier gas flow rate (ml/min)	30
Detector temperature (^{o}C)	80
Detector current (Ma)	80

4.2.6 NH₃ Temperature programmed desorption (NH₃ TPD)

TPD of NH_3 (Micromeritics Autochem 2910) was used to characterize the acid sites. Samples were pre-treated in He at $400^{o}C$ for 1 hour and saturated with $10\%NH_3/He$ at $100^{o}C$ for 2 hours. Adsorbed NH_3 was removed by flowing He (10 ml/min) while heating at $10^{o}C/min$ to $400^{o}C$ and detected by TCD. The calculation of the amount of NH_3 was done and reported by Chemsorp TP*x* Software.

4.2.7 Hydrogen Chemisorption

Micromeritic Chemisorption 2750, available at the Analysis Centre of Department of Chemical Engineering, Faculty of Engineering, Chulalongkorn University was employed to perform pulse hydrogen chemisorption at $100^{o}C$ over the

reduced catalysts to determine the amount of metallic cobalt. The procedure was carried out as described by Reuel and Bartholomew (1984) [71]. Prior to chemisorption, reduction of the catalysts was done at $350^{o}C$ for 3 hours with a heating rate of $1^{o}C/min$ and then the catalyst was cooled to $100^{o}C$ in hydrogen. Afterward, ultra high purity nitrogen gas was flushed into the reduced catalyst for removal of physically and/or weakly chemically adsorbed hydrogen molecules at $100^{o}C$. Chemisorption was performed by pulse injection of $100\mu L$ hydrogen gas until approaching equilibrium. The amount of hydrogen adsorption was calculated as shown in Appendix D and a picture of Micromeritic Chemisorption 2750 is shown in Figure 4.2.

Figure 4.2 Micromeritic Chemisorption 2750

4.2.8 Temperature Programmed Reduction (TPR)

The TPR profiles of supported cobalt catalysts were obtained by temperature-programmed reduction using an in-house system. Approximately, 200 mg of dry catalyst was packed in a stainless steel reactor connected to a reaction rig and then the TPR was performed using $3\%H_2/Ar$ as reducing agent at a temperature ramp of $5^{o}C/min$ from 35 to $800^{o}C$. The signal of effluent gas was measured using a GOW-MAC thermal conductivity detector (TCD). Reducibility was calculated using an integration area of TPR profiles calibrated by hydrogen consumption of 200-mg bulk

Co_3O_4, assumed to totally reduce to Co^0. The calculation is exhibited in Appendix E. To safely operate a GOW-MAC, removal of water vapour from the effluent gas during reduction needed to be trapped at dried ice temperature.

Table 4.3 Operating condition of gas chromatograph (GOW-MAC) for TPR

Model	Operating Condition
Detector type	TCD
Carrier gas	$3\%H_2/Ar$
Carrier gas flow rate (ml/min)	30
Detector temperature (^oC)	80
Detector current (mA)	80
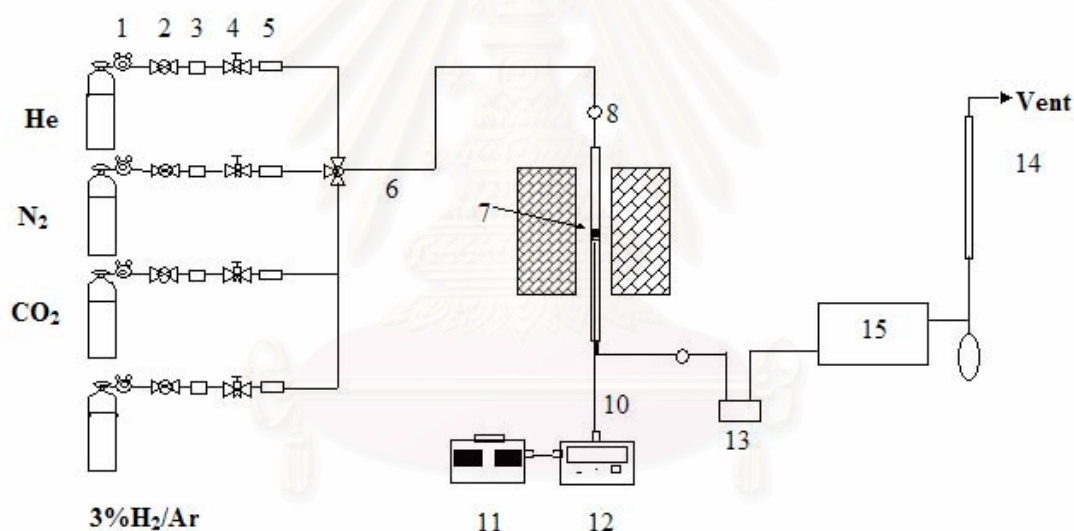
1. Pressure Regulator	6. 3-way Valve	11. Variable Voltage Transformer
2. On-Off Value	7.Catalyst Bed	12. Temperature Controller
3. Gas Filter	8. Sampling point	13. BET cell or cold trap for TPR
4. Metering Valve	9. Furnace	14. Bubble Flow Meter
5. Back Pressure	10. Thermocouple	15. Gas Chromatograph

Figure 4.3 Flow diagram of Multi systems; BET Single Point, CO_2-TPD, and TPR

4.3 Catalyst Evaluation

In this study, the synthesized oxides (i.e. the mixed oxides, alumina and zirconia) were used on catalysts and catalyst supports. (a) To characterize surface of the oxides, 2-propanol was used as probe molecules for elimination reaction i.e. dehydration and dehydrogenation explained in section 4.3.1 and (b) an application for cobalt catalyst support, CO hydrogenation was carried out as explained in section 4.3.2.

4.3.1 Dehydration of 2-propanol

Catalyst testing was carried out at atmospheric pressure in a quartz fixed-bed reactor. The catalyst sample was treated in air at $400^{o}C$ for 1 hour prior to the reaction to remove adsorbed H_2O and CO_2. Helium gas was flooded into pre-treated samples to remove excess oxygen gas for 20 min. Reaction of 2-propanol was carried out at 150, 200 and $250^{o}C$ as in [72,73]. Helium (~12 ml/min) was bubbled through 2-propanol at fixed temperature (~50°C) to give a concentration of 12-mol% 2-propanol in He flowing through 100 mg of catalyst. Typical space velocities (WHSV) were in the range of 20-100 hour^{-1}. Reaction products were analysed using a Shimadzu GC-14A gas chromatograph with a flame ionisation detector and a column containing 15%-Carbowax 1000 supported on Chromosorb W. The operating condition was summarized in Table 4.4. Measurements were taken every 20 min until a steady state was reached, typically after about 2 hours. The reaction products were propylene, acetone and diisopropyl ether.

Table 4.4 Operating condition of gas chromatograph

Model	Operating Condition
Detector type	FID
Packed column	15%-Carbowax 1000 supported on Chromosorb W
Carrier gas	UHP Nitrogen
Carrier gas flow rate (ml/min)	12 ml/min
Detector temperature (^{o}C)	170
Injector temperature (^{o}C)	170
Column temperature (^{o}C)	60
Analysed substances	2-propanol, propylene, acetone, diisopropyl ether

4.3.2 CO hydrogenation

CO hydrogenation was carried out in a fixed-bed stainless steel reactor at 220^oC and 1 atm total pressure. A flow rate of $CO/H_2/Ar$ 4/40/16 ml/min was used. Typically, 0.10 g of the catalyst was reduced *in situ* in flowing hydrogen (30 ml/min) at 350^oC for 2 h prior to reaction. The effluent gases were taken at 20 min and 1 h interval and were analysed by gas chromatograph (Shimadzu GC-8A (Molecular sieve 5A) and GC-14B (VZ-10) operated at conditions in Table 4.5). In all cases, the reaction approached steady state within 6 h.

Table 4.5 Operating condition of gas chromatographs

Model	GC-8A	GC-14B
Detector type	TCD	FID
Packed column	Molecular Sieve 5A	VZ-10
Carrier gas	UHP Helium	UHP Nitrogen
Carrier gas flow rate (ml/min)	30 ml/min	50 ml/min
Detector temperature (^{o}C)	100	100
Injector temperature (^{o}C)	100	150
Column temperature (^{o}C)	50	70
Analysed substances	CO and CH_4	C_1, C_2, C_3, C_4 and C_4+

1. Pressure Regulator
2. On-Off Value
3. Gas Filter
4. Metering Valve
5. Back Pressure
6. 3-way Valve

7. Catalyst Bed
8. Sampling point
9. Furnace
10. Thermocouple
11. Variable Voltage Transformer
12. Temperature Controller

13. Heating Line
14. Bubble Flow Meter
15. Gas Chromatograph
16. Saturator
17. Heating Line

Figure 4.4 Systematic diagram for testing 2-propanol dehydration
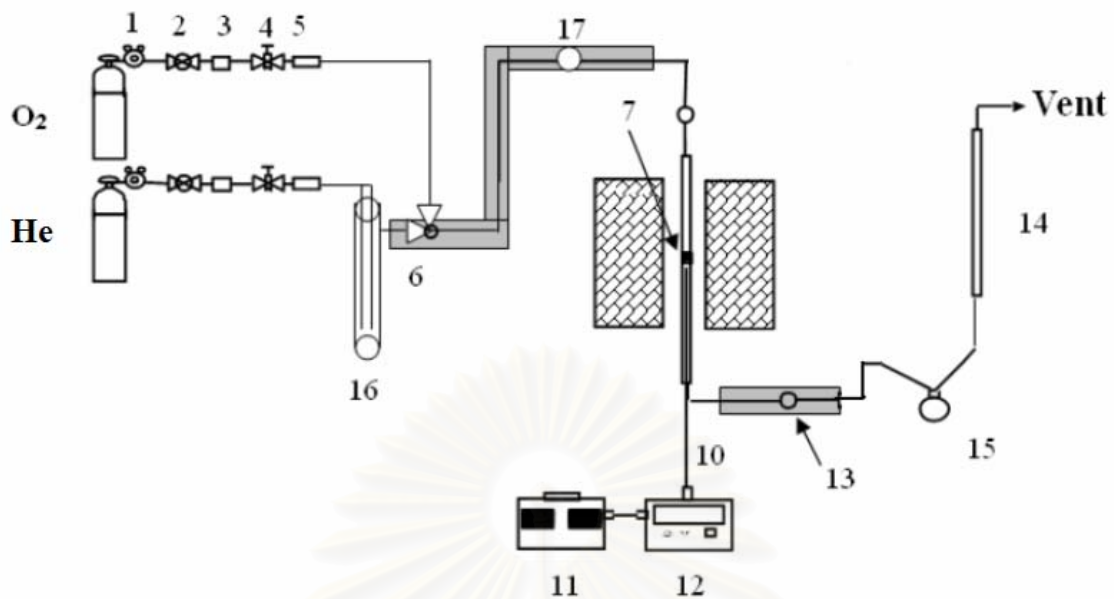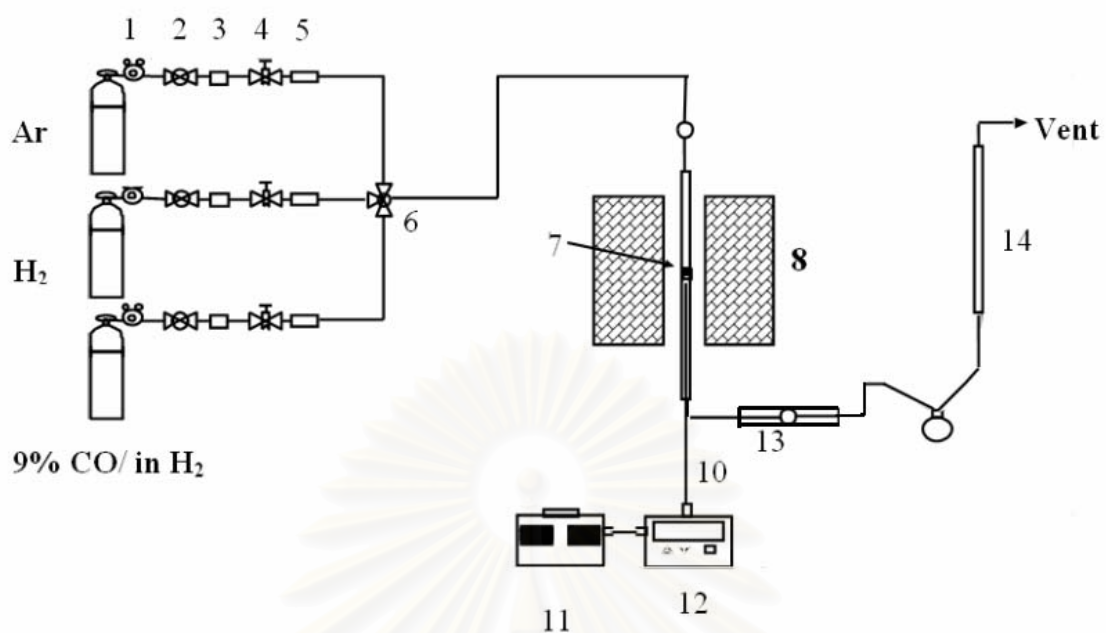
1. Pressure Regulator   7.Catalyst Bed   13. Heating Line

2. On-Off Value   8. Sampling point   14. Bubble Flow Meter

3. Gas Filter   9. Furnace

4. Metering Valve   10. Thermocouple

5. Back Pressure   11. Variable Voltage Transformer

6. 3-way Valve   12. Temperature Controller

Figure 4.5 Systematic diagram for testing CO hydrogenation

CHAPTER V

RESULTS AND DISCUSSION

This chapter is divided into three parts. The first part shows the effect of alumina content (25-75% by mole) on the surface characteristics and the catalytic activity for the elimination of 2-propanol over the alumina-zirconia mixed oxides as compared to pure tetragonal zirconia and pure amorphous alumina.

In the second part, zirconia, alumina, and alumina-zirconia oxides were employed as Co catalyst supports for CO hydrogenation. The influence of low to high alumina content (0.5, 1, 25, 40 and 75% by mole) in zirconia supports was investigated. The zirconia with low alumina content supported catalyst was found to be more active than the pure alumina and pure zirconia supported catalysts.

It is likely that the zirconia with addition of small amount of the second metals (alumina) allowed good dispersion of the cobalt metallic active phase despite no significant change in surface area. In order to prove this suggestion, zirconia with a low content of other elements, (silica and yttria), was employed as a Co catalysts support and compared with alumina-modified zirconia in the third part of this chapter.

5.1 Characteristics and Catalytic Properties of Alumina-Zirconia Mixed Oxide Prepared by the Modified Pechini's Method

5.1.1 Effect of alumina content on the physicochemical properties

5.1.1.1 BET surface areas of alumina-zirconia mixed oxide

The BET surface areas and BJH pore size distributions of the mixed oxides solid powders after calcination for 6 hours at 600°C are given in Table 5.1. The surface areas increased with alumina content. For 40-75% by mole of alumina in the oxides, zirconia was probably present in an alumina matrix and the oxides possessed the high surface area of alumina. For pure zirconia, most of the pores were macro-sized (>50 nm), while the mixed oxides had pore volumes more evenly distributed between micro-, meso- and macropores. Pure alumina had most of its pore volume in

the meso and macro range. The macropore zirconia system may occur after removal of polymerising material as has been subject for sol-gel derived zirconia that appeared to be formed from polymeric unit of hydrolysed zirconium precursors [74].

Table 5.1 Surface areas and pore size distribution of zirconia, alumina and the mixed oxides

Powder Sample	BET Surface Area (g/m^2)	BJH Pore Size Distribution (%)		
		Micro <2nm	Meso 2-50nm	Macro >50nm
Zirconia	56	6.2	24.1	69.7
Al25-ZrO$_2$	70	26.4	43.8	29.7
Al40-ZrO$_2$	182	24.5	33.9	41.7
Al75-ZrO$_2$	228	34.2	30.5	35.4
Alumina	319	13.6	44.7	41.7

5.1.1.2 Phase Identification from XRD results

Crystal phases of the mixed oxides were identified by X-ray diffraction. Figure 5.1 shows the XRD patterns of pure zirconia, Al25-ZrO$_2$, Al40-ZrO$_2$, Al75-ZrO$_2$ and pure alumina after calcination at 1000°C. The identified crystal structures and crystallite sizes after ignition at 600°C and calcination at 800°C and 1000°C (calculated using Scherrer's equation) are summarized in Table 5.2. Calcination of zirconia at 600°C and above gave mostly the tetragonal phase, with the monoclinic phase becoming dominant at 1000°C. Alumina was amorphous after calcination at 600°C and changed from θ to α between 800°C and 1000°C. In the mixed oxide sample, no alumina XRD peaks could be detected at any temperature. The sample calcined at 600°C was completely amorphous while only tetragonal zirconia peaks were detected even at 1000°C.

In all cases, the crystallite sizes increased with increasing calcination temperature. It is suggested that under these preparation conditions, well dispersed alumina and zirconia influences the orientation of alumina and zirconia crystal

structures in the mixed oxide. Using this method, tetragonal phase of pure zirconia were obtained after calcination at 600°C. The tetragonal phase zirconia is thermodynamically stable at a temperature above 1170°C [75]. However, removal of combustible organic materials at 600°C during preparation could result in sufficient energy to arrange the zirconia structure in the tetragonal form [55].

Table 5.2 Crystal structure and size of zirconia crystals in zirconia, alumina and the mixed oxides

Sample	Crystal Structure (Crystal size, nm)		
	Calcination Temperature		
	600°C	800°C	1000°C
Zirconia	T(13)	T(26)	M(31),T
Al25-ZrO$_2$	A	T(13)	T(28)
Al40-ZrO$_2$	A	T(14)	T(19)
Al75-ZrO$_2$	A	A	T(13)
Alumina	A	θ	α

Symbols A, M and T indicate amorphous, monoclinic and tetragonal phases of zirconia (or pure alumina) respectively.

Symbols θ and α indicate theta and alpha phases of alumina respectively.
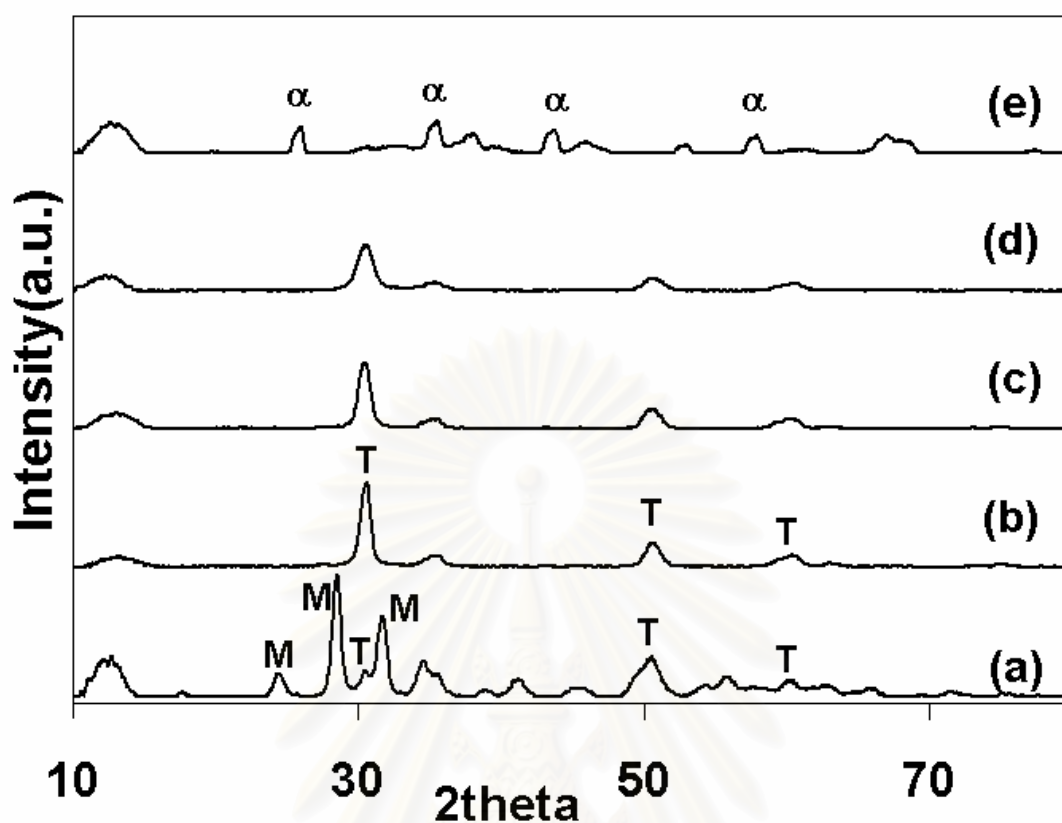
Figure 5.1 X-ray diffraction pattern of the oxide calcined at 1000 ^{o}C, (a) amorphous Al_2O_3, (b) Al25-ZrO_2, (c) Al40-ZrO_2, (d) Al75-ZrO_2, and (e) tetragonal ZrO_2

5.1.1.3 CO_2 temperature-programmed desorption

Basicity of the catalysts was measured by CO_2 temperature programmed desorption up to 400°C. Figure 5.2 shows the CO_2 TPD profiles of all the catalyst samples. In all cases, a single desorption peak was observed around 100-115°C. The CO_2 desorption temperature of pure zirconia and pure alumina were found to be slightly lower than that of the mixed oxides. The amounts of CO_2 desorbed from the mixed oxides, pure alumina and pure zirconia were calculated by integrating the areas of CO_2 TPD profiles and are reported in Table 4.3. The amount of CO_2 desorption was taken as a measure of the amount of basic sites because the electron affinity of CO_2 molecule results in acceptance of electrons from surface to form carbonate species [76]. It should be noted that the number of basic sites increased with increasing alumina content, but pure amorphous alumina exhibited the lowest basicity despite its

relatively high surface area. It is possible that the interaction between the CO_2 probe molecules and zirconia or mixed oxides surfaces might be physical adsorption in accordance with a result of Y. Li et al. [77] who showed that desorption of CO_2 physical bonding on zirconia occurrs at around 100°C. Desorption temperatures might be higher after atomically mixing zirconia with alumina, due to the interaction between aluminium, oxygen and zirconium ions in the mixed oxide increasing the physical strength of the bond between surface oxygen and the CO_2 probe molecule.
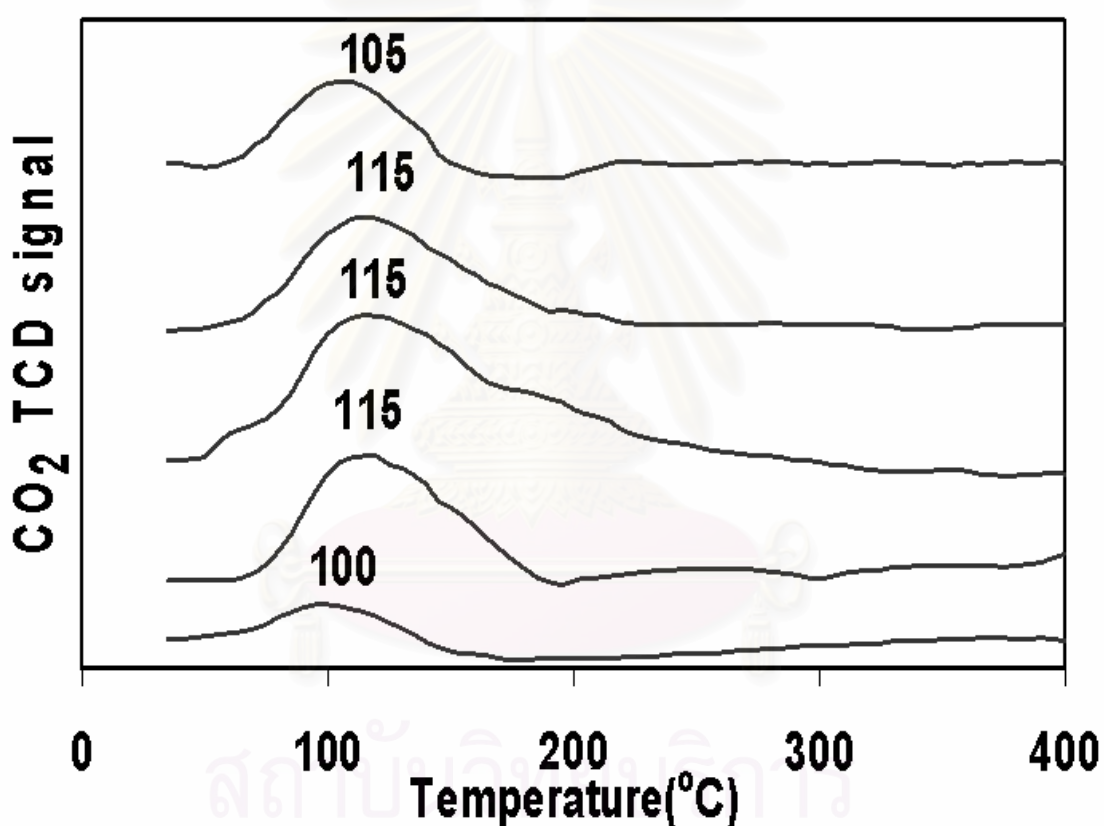
Figure 5.2 The CO_2 Temperature programmed desorption profile of (a) amorphous Al_2O_3, (b) Al25-ZrO_2, (c) Al40-ZrO_2, (d) Al75-ZrO_2, and (e) tetragonal ZrO_2 (carried out from 30-400°C with 10°C/min)

Table 5.3 Quantities of CO_2 and NH_3 desorbed from zirconia, alumina and the mixed oxides

Sample	CO_2 desorbed ($\mu mol/g$)	NH_3 desorbed ($\mu mol/g$)
ZrO_2	172	202
Al25-ZrO_2	279	478
Al40-ZrO_2	632	752
Al75-ZrO_2	485	830
Al_2O_3	146	69

5.1.1.4 NH_3 temperature programmed desorption

Acidity of the catalysts was measured by NH_3-TPD. The NH_3 TPD profiles for all the catalysts are shown in Figure 5.3. None of the materials tested showed distinct NH_3 desorption peaks up to 400°C. The broad desorption peaks below 200°C occurred at slightly higher temperatures for two of the mixed oxides as composed to pure alumina or zirconia. This suggests that the acid strength of those mixed oxides is slightly greater than the pure oxides. Table 5.3 also shows the amounts of NH_3 desorbed from each sample, but as seen from Figure 5.3-values are expected to be approximate.

5.1.1.5 SEM micrograph results

Morphologies of alumina, zirconia, and alumina-zirconia mixed oxide are shown in Figure 5.4. All samples possessed irregular shape particles and their sizes were in the range of 10-100 μm. For pure zirconia, particle sizes were obviously larger than the crystallite size calculated from X-ray broadening peak reported in Table 5.2. The growth of large particles may be caused by agglomeration of very fine zirconia particles, resulting in densification of powder and a very low surface area. For amorphous alumina and the mixed oxides (with a higher surface areas), it is suggested that their primary particles are loosely agglomerated.
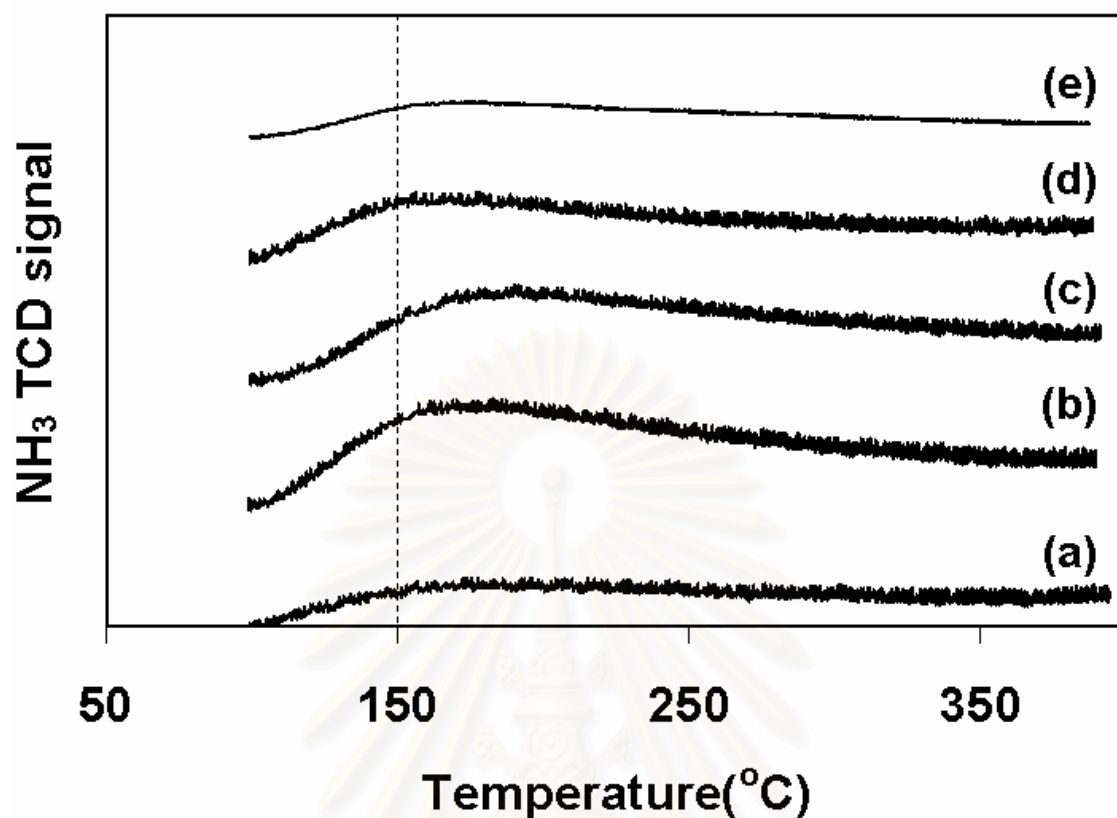
Figure 5.3 The NH$_3$ Temperature programmed desorption profile of (a) amorphous Al$_2$O$_3$, (b) Al25-ZrO$_2$, (c) Al40-ZrO$_2$, (d) Al75-ZrO$_2$, and (e) tetragonal ZrO$_2$

5.1.2 Effect of alumina content on testing of the probe reaction

5.1.2.1 Elimination of 2-propanol

The catalytic activities of the mixed oxides were tested in the elimination reactions of 2-propanol at 150, 200, and 250°C. The results are given in Table 5.4. At 150°C, the elimination product was almost entirely acetone for all catalysts. At 200°C, the product distribution depended on the catalyst composition. Catalysts high in alumina content produced mainly acetone, while those high in zirconia produced large amounts of propylene. Traces of diisopropyl ether appeared at this temperature. At higher temperature (250°C) the product distribution changed again, to favour propylene production over all materials. Catalysts high in alumina also produced significant amounts of diisopropyl ether at this temperature. It should be noted that

alumina activated in oxygen could exhibit dehydrogenation activity that may exceed considerably the dehydration selectivity [78]. The effect of oxygen pretreatment was not observed in this study (no oxidation reaction) since one would expect changes in selectivity to acetone with increasing reaction time due to consumption of oxygen covering the catalyst surface. The calculations of oxygen needed to oxidize total amount of 2-propanol are shown in Appendix I and reports in Table 5.4. As can be seen in Table 5.4, amount of oxygen involving total oxidation of 2-propanol are much larger than amount of oxygen covering surface of testing samples. It suggests that acetone formation can be partly caused by oxidation; however, most of acetone can occur via other pathways.

Table 5.4 Amount of oxygen needed to entirely oxidize 2-propanol 0.06 mole/min : (A) compared to amount of oxygen covering surface of the samples

Sample	Surface area (cm^3/g)	Amount of oxygen covering sample surface (mole): (B)	Ratio of A/B
Zirconia	56	2.12×10^{-9}	2.83×10^{7}
Al75-ZrO$_2$	70	2.99×10^{-9}	2.01×10^{7}
Al40-ZrO$_2$	182	7.75×10^{-9}	7.75×10^{6}
Al25-ZrO$_2$	228	9.70×10^{-9}	6.18×10^{6}
Alumina	319	12.77×10^{-9}	4.69×10^{6}

The calculations are shown in Appendix I

It is known that the reaction pathways of 2-propanol elimination forming dehydration and dehydrogenation products occur on different nature and strength of acid-base sites [64]. Different mechanisms have been derived based on individual transition states including E_1, E_2, and E_{1cB} [65]. E_1 mechanism requires strong acidic catalysts to form carbenium ions by abstraction of OH-group as shown in chapter III. The carbenium ions are rearranged via isomerization and abstracted hydrogen resulting in different kind of alkenes [65].

In this study, the NH_3 temperature programmed desorption results exhibited a single peak below 200°C suggesting that the acidic strength was probably insufficient to abstract OH groups. The E_1 mechanism then can be excluded.

For the E_2 mechanism, reaction is suggested to occur on dual acid-base sites simultaneously to eliminate a proton and a hydroxyl group to produce the main product alkene as shown in Figure 5.8. For the E_{1cB} mechanism, strong basic sites are required in order to firstly detach β hydrogen and then eliminate hydroxyl group [65].

Recently, Díez et. al. [65,66] proposed a mechanism slightly different from the E_{1cB} mechanism in which reaction takes place via acid-base sites of imbalanced strength. Adsorptions of OH groups occur on weak acid-base sites to form a surface propoxide intermediate as shown in Figure 5.5(a) and 5.5(b). The most acidic hydrogen of alcohol is attacked by the strong base site (the surface oxygen); in contrast, the Lewis acid site (the surface cation) attacks the oxygen of alcohol resulting in rupture of hydroxyl groups.

Two pathways were proposed after forming propoxide on the surface: (a) dehydration of 2-propanol where acetone is a result of abstraction α-hydrogen as shown in Figure 5.6 and (b) dehydrogenation of 2-propanol producing propylene by detaching β-hydrogen as shown in Figure 5.7. The products of the E_{1cB} mechanism could be either propylene or acetone or both-depending on the strength of base site as summarized in Figure 5.9. However, the base site detaching β-hydrogen is stronger than that detaching α-hydrogen. Waugh et al. [79] found that the activation energy of α-hydrogen abstraction is lower than the activation energy of β-hydrogen abstraction.

Table 5.5 Catalyst activity and selectivity during elimination of 2-propanol

Sample	T=150 °C				T=200 °C				T=250 °C			
	%Conversion*	S_P**	S_A** (%)	S_{DIP}+	%Conversion	S_P	S_A (%)	S_{DIP}	%Conversion	S_P	S_A (%)	S_{DIP}
Alumina	3.5	2.0	98.0	0.0	9.8	1.6	98.1	0.3	36.6	66.3	24.1	9.5
Al75-ZrO$_2$	5.5	1.3	98.7	0.0	2.5	6.3	92.6	1.1	6.9	66.6	28.7	4.6
Al40-ZrO$_2$	0.3	10.2	89.8	0.0	1.0	7.7	92.3	0.0	10.7	48.3	48.8	2.9
Al25-ZrO$_2$	2.2	2.0	98.0	0.0	1.3	27.5	71.7	0.8	7.5	64.3	34.5	1.2
Zirconia	1.0	8.9	91.1	0.0	4.4	89.2	10.2	0.6	7.5	75.2	24.5	0.3

(The reaction was carried out at WHSV 90 h⁻, inlet = 12% propanol in He gas, total flow rate = 30 cm^3/min, weight of the catalyst = 0.1 gram)

2-Propanol conversion (%)

$$= \frac{100 \times (\text{mole of propylene} + \text{mole of acetone} + 2 \times \text{mole of DIP})_{product}}{(\text{Mole of 2-propanol} + \text{mole of propylene} + \text{mole of acetone} + 2 \times \text{mole of DIP})_{product}}$$

**%Selectivity of P or A* $= \dfrac{\text{Mole of P or A in product}}{(\text{Mole of propylene} + \text{mole of acetone} + 2 \times \text{mole of DIP})_{product}}$

+%Selectivity of DIP $= \dfrac{2 \times \text{Mole of DIP}}{(\text{Mole of propylene} + \text{mole of acetone} + 2 \times \text{mole of DIP})_{product}}$
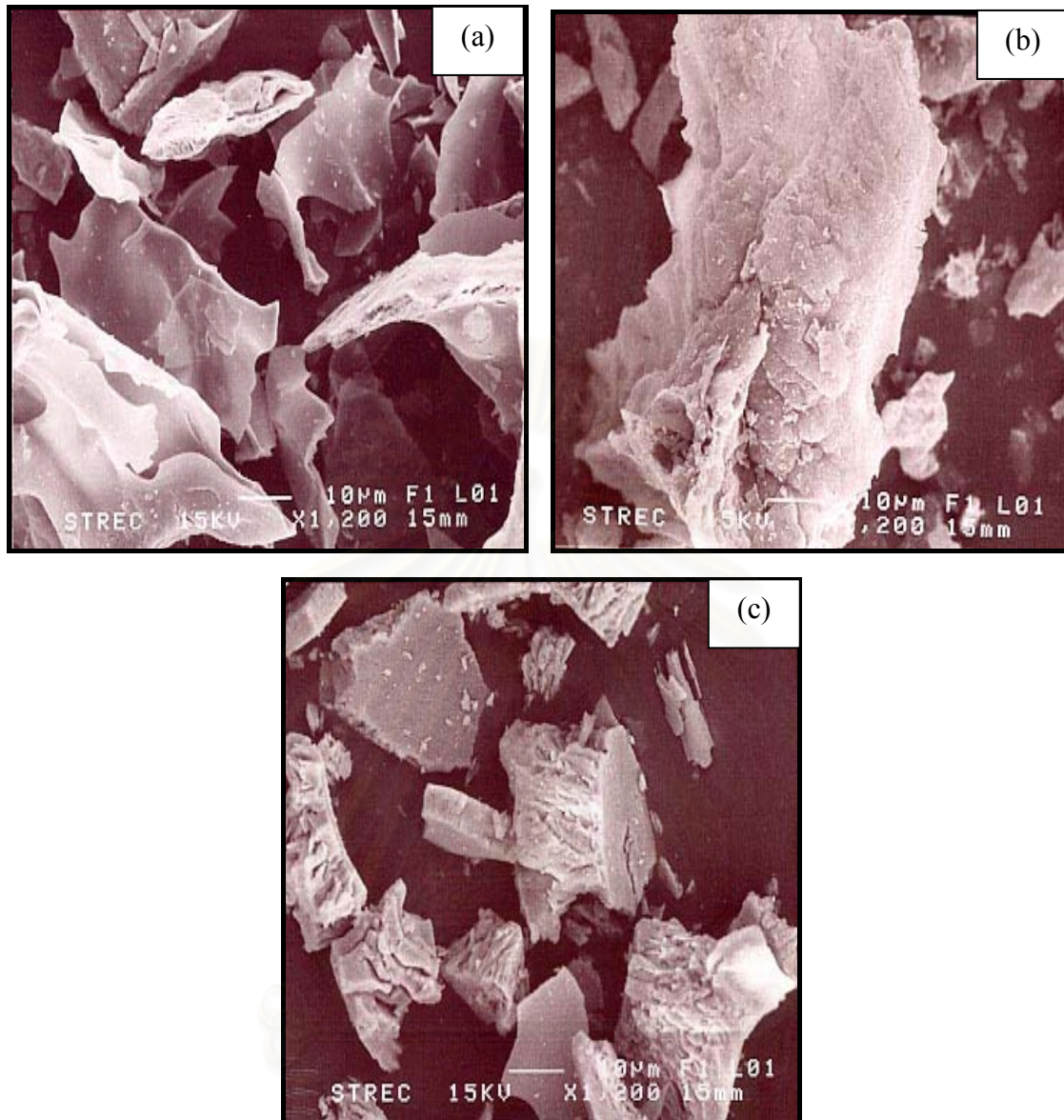
Figure 5.4 SEM micrographs of (a) Al25-ZrO$_2$, (b) pure alumina, and (c) pure zirconia
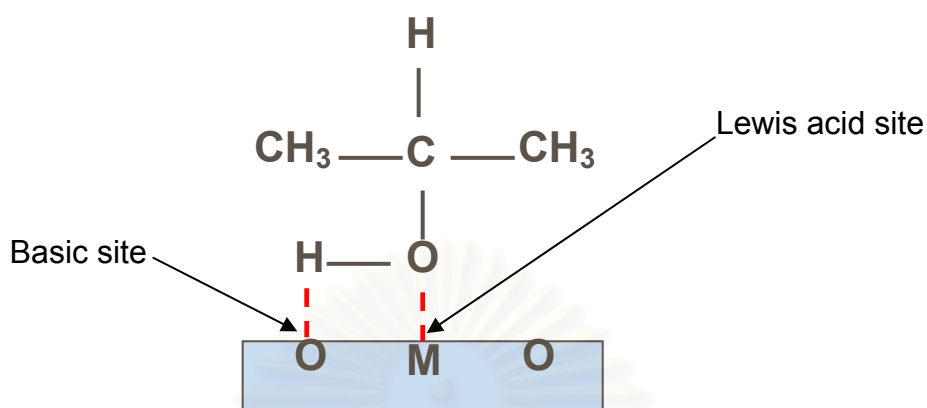
(a) The adsorption of 2-propanol over acid-base sites
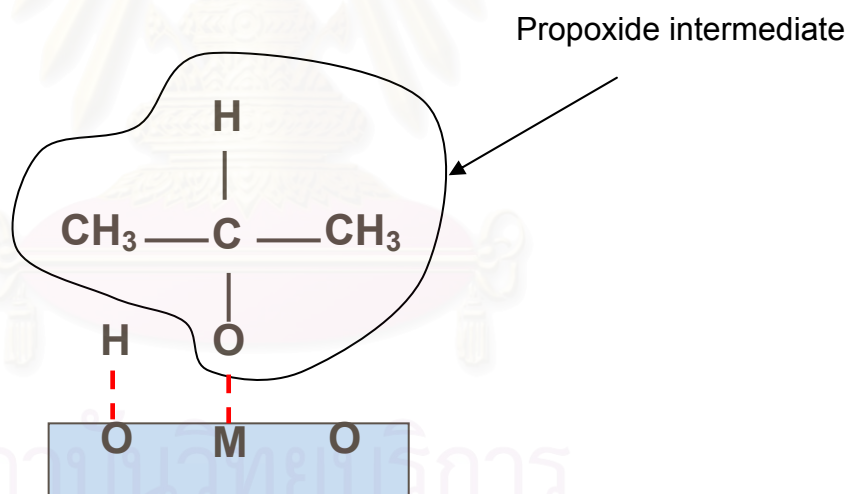
(b) Cleavage of hydroxyl group resulting in propoxide intermediate (mechanism E_{1cB})

Figure 5.5 Scheme of rupture of a hydroxyl group proposed by Díez et. al.[66]
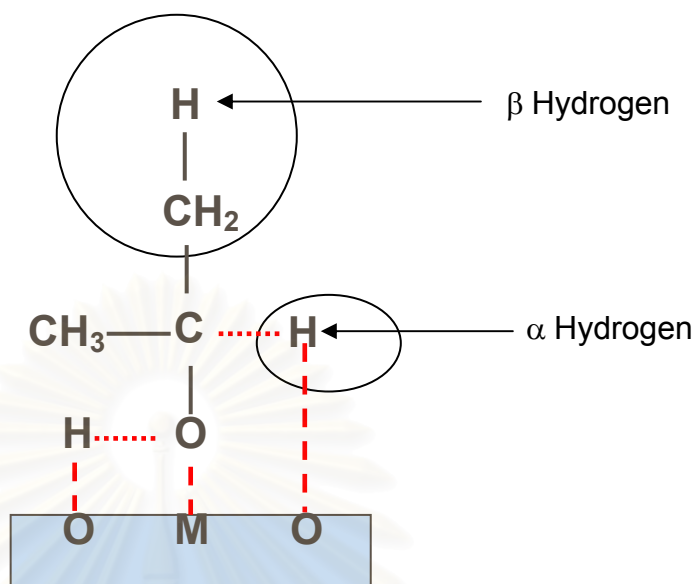
(a) Elimination of α Hydrogen
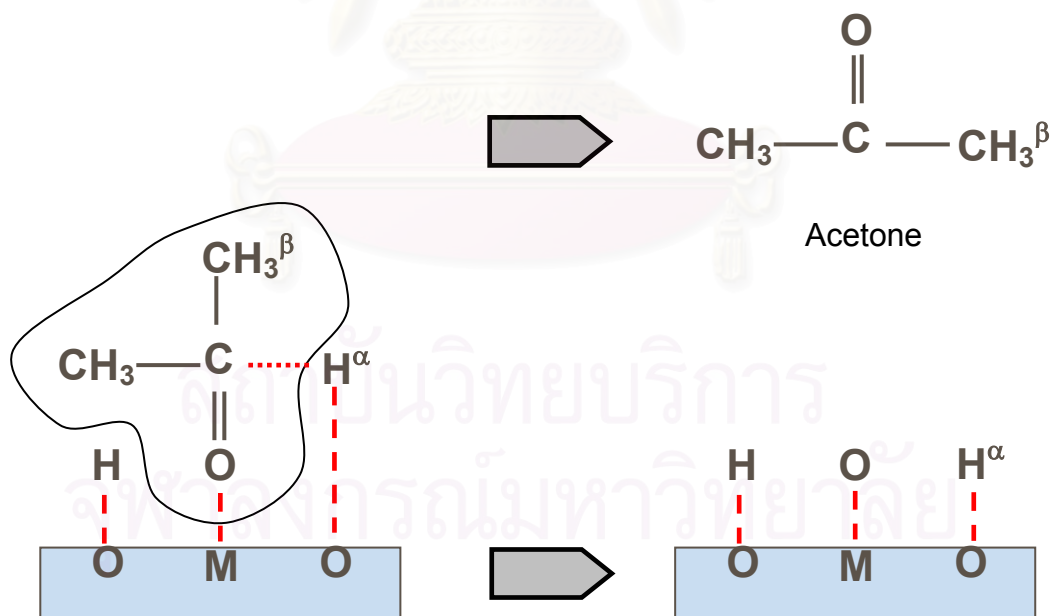
(b) Formation of acetone by attacking α Hydrogen

Figure 5.6 Scheme of acetone formation proposed by Díez et. al. [66]

(a) Elimination of β Hydrogen

(b) Formation of propylene by attacking β hydrogen
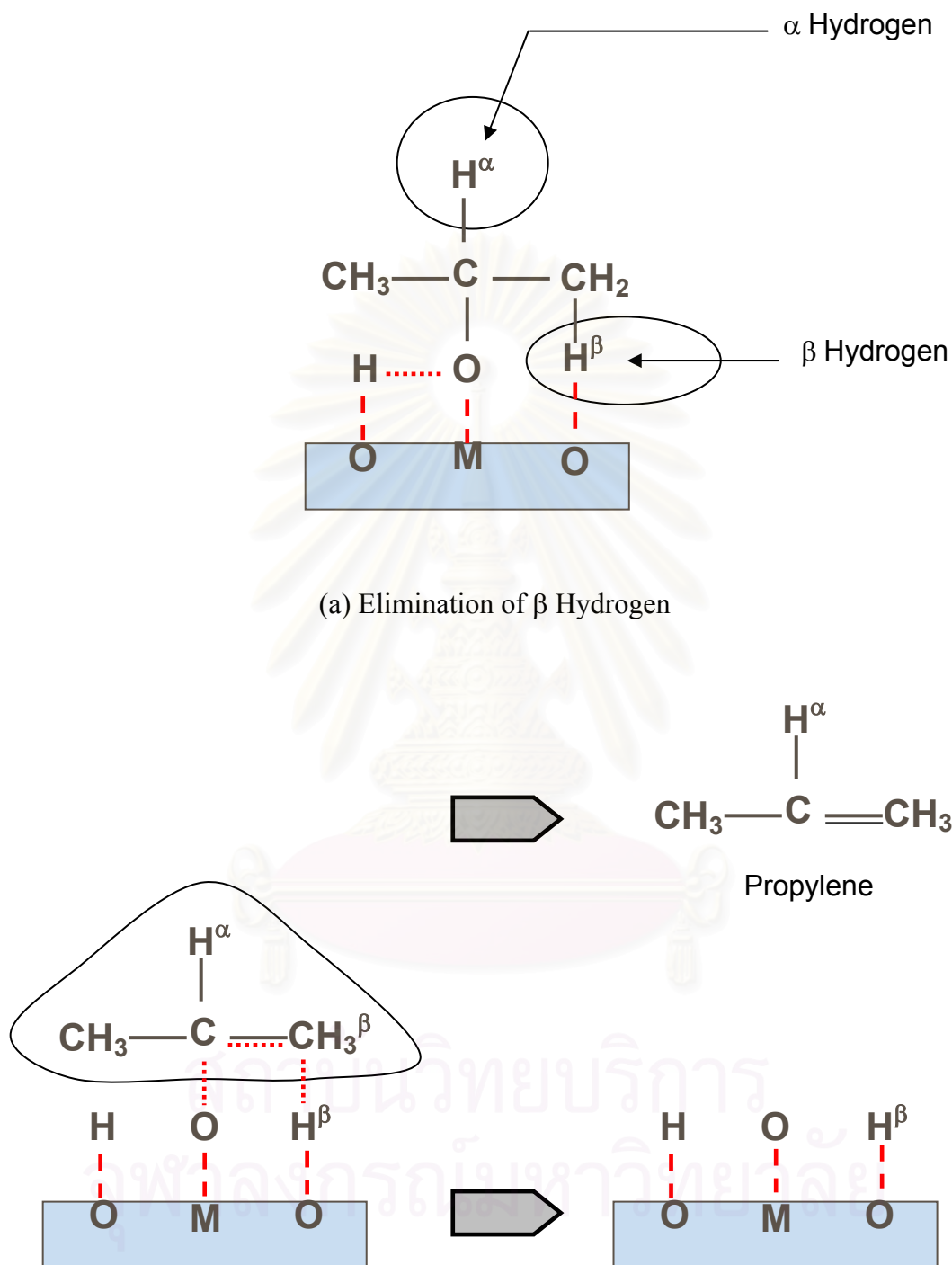
Figure 5.7 Scheme of propylene formation proposed by Díez et. al. [66]
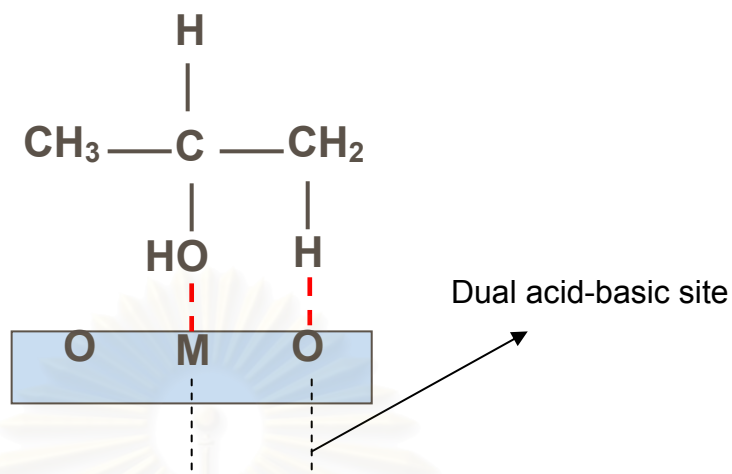
(a) The adsorption of 2-propanol over dual acid-base site (amphoteric site)
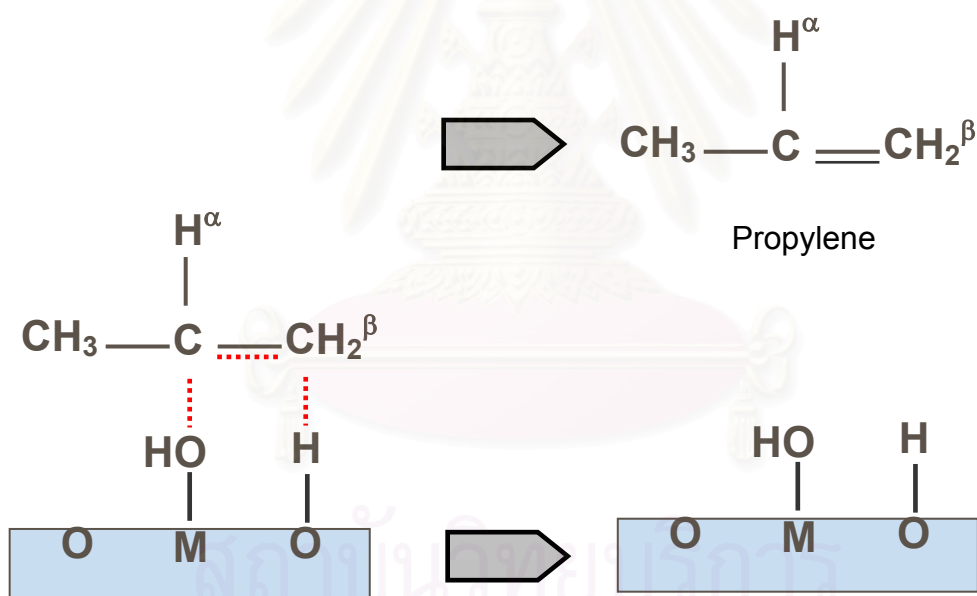
(b) Formation of propylene by eliminating of hydrogen and hydroxyl group on dual acid-base sites

Figure 5.8 Scheme of propylene formation via the E_2 proposed by Tanabe et. al.[65]

Elimination of 2-propanol
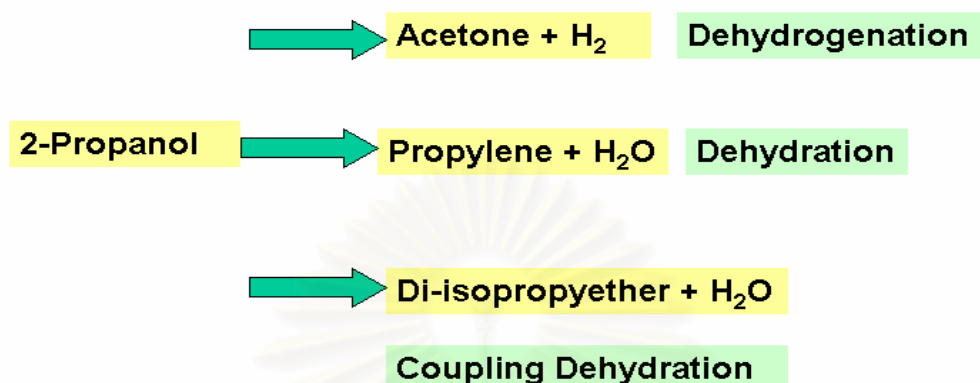
Figure 5.9 Reaction pathway of elimination of 2-propanol proposed by Díez et al.
[66,73]

Generally, elimination of 2-propanol on alumina produces propylene as the main product via the E_2 mechanism due to the amphoteric properties of alumina [63,80]. Dominuguez et al. [72] showed that γ-alumina gave propylene with selectivity more than 80% over a range of reaction temperature of 180-240°C. However, in this study we observed that most (more than 90%) of the propanol elimination products over the Pechini alumina were acetone. The disordered structure of the Pechini amorphous alumina could result in an imbalanced strength of acid-base sites and the reaction pathway might occur via the E_{1cB} route proposed by Díez et al. The weak physically adsorbing CO_2 site of alumina, shown by the low temperature CO_2 desorption peak in Figure 5.2, could bring about abstraction of α-hydrogen to result mainly in acetone formation. This might be representative of very poor basicity of alumina.

Similarly to the pure alumina, the Pechini alumina-zirconia mixed oxides converted propanol acetone with more than 70% selectivity at 150 and 200°C as exhibited in Table 5.5. Increasing zirconia content in the mixed oxides resulted in a slight decrease in acetone and an increase in propylene selectivity at 200°C. The propylene formation may be ascribed to zirconia and the E_{1cB} mechanism appeared to

dominate over the alumina-zirconia mixed oxides. Although the CO_2 desorption peaks of the mixed oxides shifted towards $115^{\circ}C$, the strength of basicity would not be very effective for the abstraction of β-hydrogen. Increasing propylene selectivity over the alumina-zirconia mixed oxides was probably affected by the dual acid-base property of zirconia via the E_2 mechanism. This is in a good agreement with the work reported by Tanabe et al. [1], in which 2-propanol elimination on zirconia catalysts involved acid-base site bifunctional catalysis. The orientation of these sites plays an importance role in governing the reaction [18]. However, the orientation of alumina-zirconia mixed oxides structure would be undisciplined resulting in a decrease in acid-base bifunctionality. Therefore, the E_2 mechanism would not dominate over the alumina-zirconia mixed oxides.

Conversion of propanol propylene over tetragonal zirconia was observed with more than 80% selectivity at $200^{\circ}C$. The well-ordered structure of tetragonal zirconia exhibited high selectivity of propylene via the dominant E_2 mechanism (Figure 5.8). In contrast, partly imperfect crystals of tetragonal zirconia could result in imbalanced acid-base site leading to acetone formation via the E_{1cB} mechanism.

It should be noted that the alumina-zirconia mixed oxides produced by the modified Pechini method resulted from a combination of aluminium and zirconium atoms. Due to the good dispersion of aluminium and zirconium ions, the mixed oxides were only amorphous. Apparently, the interaction between Al, Zr, and O in the mixed oxides resulted in higher physical strength CO_2 adsorption. The modified acidity was, however, ambiguous because all the catalyst samples exhibited low acidity. The imbalance strength of acid-base site due to the imperfect crystal structure of all the catalysts resulted in higher acetone formation via the E_{1cB} mechanism. However, 90% propylene selectivity was obtained on pure zirconia prepared by the modified Pechini's method and $200^{\circ}C$ reaction temperature.

Alumina-zirconia mixed oxides were also employed as Co catalyst supports and tested for CO hydrogenation. As known, high-surface-area support may contribute good dispersion of metal active sites and it was supposed that catalytic activity of mixed oxide supported Co catalysts would be improved by the increasing mole% of alumina, due to the significantly increased support surface area. However, the effect of support surface area can be neglected with modification of zirconia with very low mole% Al, which resulted in no significant difference in surface area. Thus, zirconia

with 0.5 and 1 mole% Al was prepared and used as a Co catalyst support in order to compare with pure zirconia support. The characteristics and catalytic activity was reported and discussed as follows.

5.2 Characterization and catalytic activity of alumina-zirconia mixed oxide supported Co catalysts

5.2.1 Effect of alumina content on the properties of alumina-zirconia mixed oxides

The XRD spectra of the alumina-zirconia mixed oxide powders in a range of alumina content 0.5-75mole% are shown in Figure 5.10. It was found that pure zirconia and zirconia samples prepared with 0.5-1mole%Al content exhibited the pure tetragonal phase of zirconia whereas the sample prepared with higher alumina content (25-100mole%) were completely amorphous. It is suggested that the orientation of alumina and zirconia structures were affected by good dispersion of alumina and zirconia mixed oxides under these preparation conditions.

In general, tetragonal phase zirconia is thermodynamically stable at temperatures above $1170^{o}C$ [75]. However, according to the work reported by Garvie et al. [55], the energy from combustion of the polymeric material during calcination at $600^{o}C$ was probably sufficient to arrange the crystal structure in tetragonal form with crystal size less than its critical size. The crystallite sizes calculated from the Scherrer's equation using in 202 diffraction peaks of tetragonal material and the BET surface areas of the same samples are reported in Table 5.6.

The average crystallite sizes of the zirconia and the Al-modified zirconia were approximately 6-7 nm. The BET surface areas of support samples were found to be ca. 50-300 m^{2}/g. It has been reported that introducing a small amount of alumina (<5%) into zirconia can stabilize the porous structure of the zirconia [81]. A significant increase in BET surface areas was observed for the alumina-zirconia mixed oxides prepared with high alumina contents. Under these preparation conditions (40-75mole % Al), zirconia was possibly introduced into alumina matrix to give insignificantly highs surface areas.
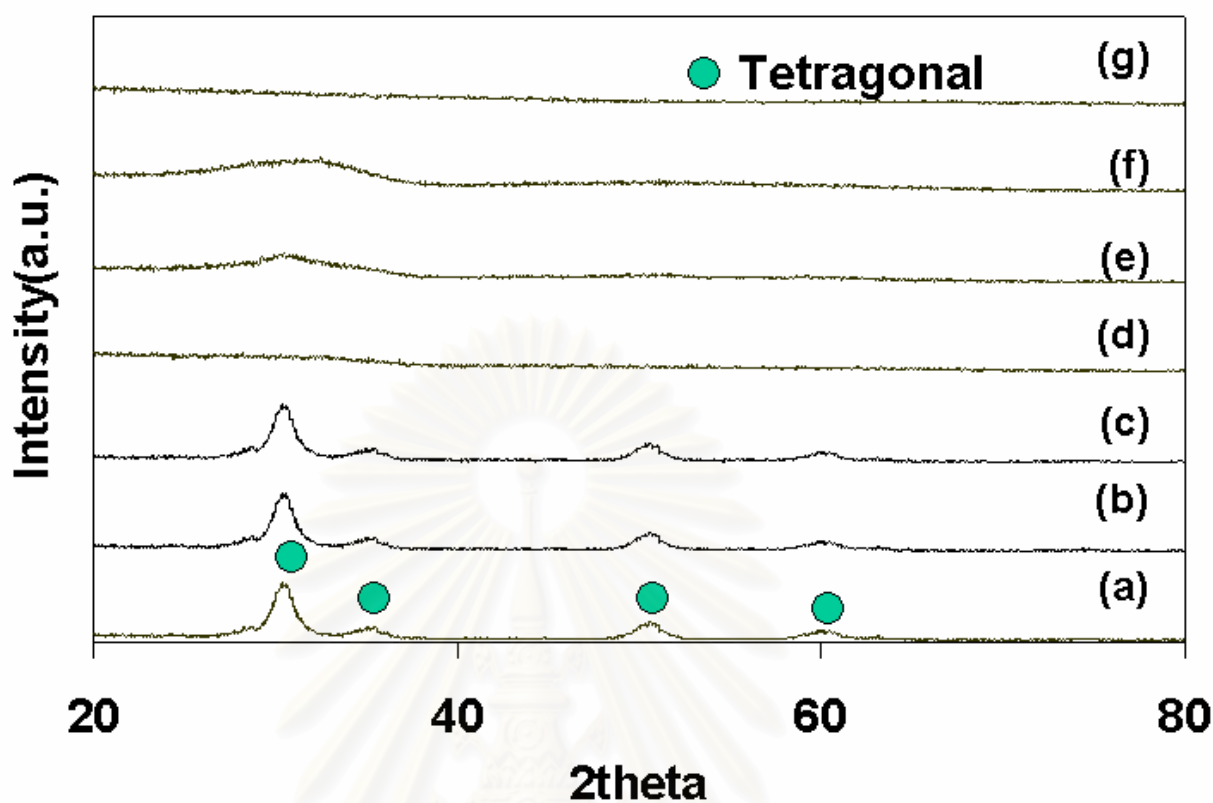
Figure 5.10 The XRD pattern of the supports, (a) ZrO_2, (b) $Al0.5-ZrO_2$, (c) $Al1-ZrO_2$, (d) $Al25-ZrO_2$, (e) $Al40-ZrO_2$, (f) $Al75-ZrO_2$, and (g) Al_2O_3

Table 5.6 Physical properties of alumina-zirconia mixed oxide supports

Supports	BET surface area of support (m^2/g)	Crystal size[a] (nm)	Phase Identification of Zirconia (from XRD)
ZrO_2	56	6	Tetragonal
$Al0.5-ZrO_2$	68	6	Tetragonal
$Al1-ZrO_2$	65	7	Tetragonal
$Al25-ZrO_2$	70	-	Amorphous
$Al40-ZrO_2$	182	-	Amorphous
$Al75-ZrO_2$	228	-	Amorphous
Al_2O_3	319	-	-

[a] calculated from XRD broadening peak at 2θ ca. 30.8^o

5.2.1 The physicochemical properties and performances of alumina-zirconia mixed oxide supported cobalt catalysts

5.2.1.1 X-Ray Diffraction Analysis

The X-ray diffraction patterns of Co/Alx-ZrO$_2$ (x = mole% of alumina), Co/Al$_2$O$_3$, and Co/ZrO$_2$ catalysts are shown in Figure 5.11. The XRD characteristic peak of Co$_3$O$_4$ at 2θ of ca. 36.8^o was observed for all the catalyst samples except Co/Al40-ZrO$_2$ and Co/Al75-ZrO$_2$. The crystallite size of cobalt oxide on those supports was probably below the limit of XRD detectability (3-5nm) and/or cobalt did not form Co$_3$O$_4$ crystallites on Co/Al40-ZrO$_2$ and Co/Al75-ZrO$_2$ but existed in an amorphous form [82]. The average crystallite sizes of Co$_3$O$_4$ derived from X-ray line broadening using Scherrer's equation were 8-19 nm and increased with increasing amount of alumina.
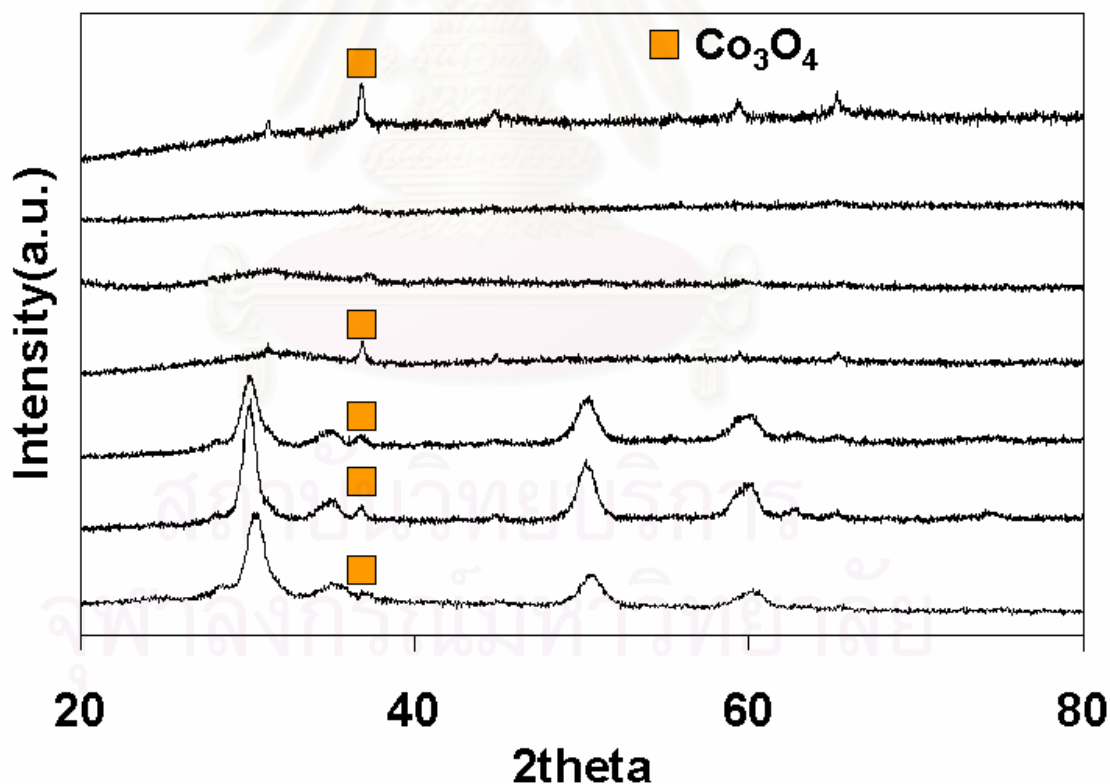
Figure 5.11 The XRD patterns the catalysts, (a) 10%Co/ZrO$_2$, (b) 10%Co/Al0.5-ZrO$_2$, (c) 10%Co/Al1-ZrO$_2$, (d) 10%Co/Al25-ZrO$_2$, (e) 10%Co/Al40-ZrO$_2$, (f) 10%Co/Al75-ZrO$_2$ and (g) 10%Co/Al$_2$O$_3$

5.2.1.2 Catalytic characteristics and BET surface areas

The BET surface areas, the reducibility, the amount of H_2 chemisorption, and %cobalt dispersion are reported in Table 5.7. Surface areas of the supported cobalt catalysts were found to be slightly less than that of the original supports, and cobalt appears to have been deposited in some the pores of the support. The impact of high surface area of alumina on the BET surface areas of the mixed oxide supported Co catalysts were observed only for Co/Al40-ZrO$_2$ and Co/Al75-ZrO$_2$: at low alumina contents (<25mole%), the modification of zirconia properties was not due to the changes in BET surface areas. It was found that H_2 chemisorption and %Co dispersion of these low alumina content oxide supported Co catalysts were higher than those of Co/ZrO$_2$ and Co/Al$_2$O$_3$. The surface properties of zirconia were probably modified by the alumina resulting in larger amount of active surface cobalt measured by H_2 chemisorption. Surprisingly, for the higher alumina contents (Co/Al40-ZrO$_2$ and Co/Al75-ZrO$_2$), they exhibited low H_2 chemisorption and Co dispersion despite their relatively high surface areas.

The interaction of cobalt oxide species and the supports was further investigated by means of temperature-programmed reduction (TPR).

Table 5.7 Catalytic characteristics and BET surface area of the mixed oxide supported Co catalysts

Sample	BET surface area of the catalyst (m^2/g)	Hydrogen Chemisorption (molecules/g cat) $\times 10^{18}$	%Reducibility[a]	Crystal size of Co_3O_4 (nm)[b]	%Co dispersion[c]
Co/ZrO$_2$	34	8.3	47	8	34
Co/Al0.5-ZrO$_2$	41	10.3	36	11	56
Co/Al1-ZrO$_2$	39	10.3	38	10	53
Co/Al25-ZrO$_2$	42	10.3	37	19	55
Co/Al40-ZrO$_2$	109	3.2	17	n.d.[*]	37
Co/Al75-ZrO$_2$	137	1.5	12	n.d.[*]	25
Co/Al$_2$O$_3$	191	8.5	48	19	35

[a] calculated from

$$\% \ Reducibility = \frac{Amount \ of \ H_2 \ uptake \ to \ reduce \ 1 \ g \ of \ catalyst \times 100}{Amount \ of \ theoretical \ H_2 \ uptake \ to \ reduce \ Co_3O_4 \ to \ Co^0 \ for \ 1 \ g \ of \ catalyst}$$

[b] calculated from XRD broadening peak at 2θ ca. 36.8^o

[*] n.d. = not detected

[c] %Co dispersion

$$= \frac{Amount \ of \ Co \ equivalent \ to \ H_2 \ adsorption \ on \ catalyst \ after \ reduction \ (H_2:Co=1:2) \times 100}{Total \ amount \ of \ Cobalt \ active \ sites \ expected \ to \ exist \ after \ reduction}$$

5.2.1.3 Temperature programmed reduction (TPR) and reducibility

TPR profiles of all the catalysts are shown in Figure 5.12. Reduction of cobalt in the oxide form (Co_3O_4 or CoO to Co^0) involves a two-step reduction: first reduction of Co_3O_4 to CoO and then the subsequent reduction of CoO to Co^0 [83, 84]. A wide range of variables such as metal particle size and metal-support interaction has an influence on the reduction behaviour of cobalt catalysts, resulting in the observation of different locations of the TPR peaks [85, 86]. It was found that for the Co catalyst supported on the mixed oxides with low alumina content (<25%), the reduction peaks below 400°C shifted slightly to low temperatures, whereas the Al40-ZrO_2 and Al75-ZrO_2 supported catalysts exhibited only a single reduction peak at temperature higher than 400°C. The higher reduction peak may be attributed to formation of nonreducible phases, i.e. cobalt–aluminate [85, 86] and cobalt- zirconate [24, 25].

The reducibilities of all the alumina-zirconia mixed oxide supported catalysts during TPR (30-800°C) were found to be lower than those of Co/ZrO_2 and Co/Al_2O_3. It is suggested that the surface properties of the mixed oxide supported catalysts were different from those of the pure oxide. Furthermore, it was found that Co/Al40-ZrO_2 and Co/Al75-ZrO_2 exhibited distinctly low reducibilities (12-17%). From the XRD results, the samples were amorphous and no XRD peaks for Co_3O_4 were found on these samples. It is likely that amorphous forms of alumina and zirconia caused formation of cobalt-aluminate and/or cobalt-zirconate by combining unreduced cobalt oxides with amorphous alumina and/or amorphous zirconia [24, 25].

It should, however, be noted that the reducibility of pure amorphous alumina supported Co catalyst was similar to that of the tetragonal zirconia supported catalysts. Although, cobalt aluminate compounds can be formed on the amorphous alumina surface as suggested for Al40-ZrO_2 and Al75-ZrO_2 supported catalysts, some large cobalt oxide crystallites were found on amorphous alumina and higher reducibility was obtained.
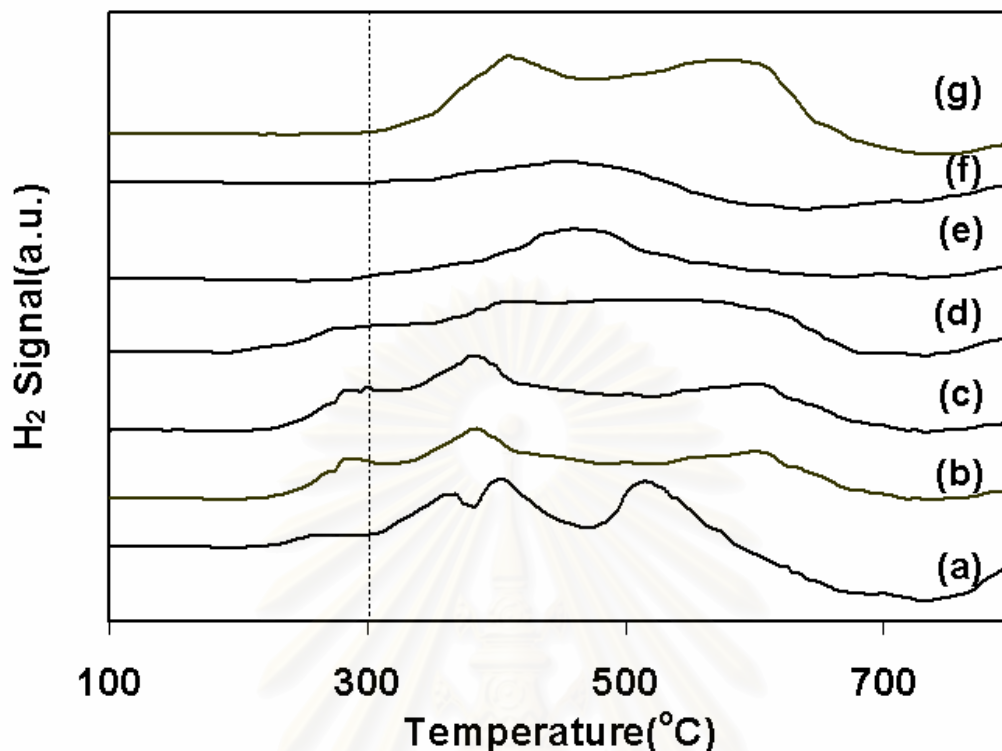
Figure 5.12 Influence of alumina-zirconia support on the reduction behaviour of the cobalt catalysts, (a) 10%Co/ZrO$_2$, (b) 10%Co/Al0.5-ZrO$_2$, (c) 10%Co/Al1-ZrO$_2$, (d) 10%Co/Al25-ZrO$_2$, (e) 10%Co/Al40-ZrO$_2$, (f) 10%Co/Al75-ZrO$_2$ and (g) 10%Co/Al$_2$O$_3$

5.2.1.4 Catalytic activity and product selectivity

The catalytic activity and product selectivity of all the catalysts for CO hydrogenation are given in Table 5.8. Figure 5.13 exhibits typical time-on-stream behaviour. The mixed oxide with 0.5-25mole% Al supported catalysts appears to be more stable than pure alumina or pure zirconia supported catalysts. This suggests that the surface of alumina-zirconia mixed oxides probably inhibits metal active site sintering during CO hydrogenation or that may retard carbon formation which covers metal active sites. Both effects decrease %CO conversion. There was no significant difference in the product selectivities since, under reduction conditions used, all the catalysts exhibited methanation (ca. 95-99%). The conversion and CO hydrogenation

rates of the mixed oxide supported cobalt catalysts prepared with low alumina contents (0.5, 1, and 25mole %) increase by 30% at the steady state compared to those of Co/ZrO$_2$ and Co/Al$_2$O$_3$ even though their reducibilities were slightly lower. The 0.5-25mole% Al-modified zirconia supports may have a positive influence on a phase dispersion of cobalt oxide and active metallic phases derived from the Co$_3$O$_4$ particles.

Enache et al. [24, 25] have proposed a relation of degree of crystallization of Co$_3$O$_4$ particles and types of cobalt active phase after hydrogen reduction, i.e. crystalline metallic cobalt derived from the crystalline Co$_3$O$_4$ particles and poor crystalline metallic cobalt derived from the amorphous Co$_3$O$_4$ particles. The catalyst consisting of poor crystalline metallic cobalt appeared to be more active than the one with more perfect crystalline metallic cobalt. It is possible that the surface properties modified by low amount of alumina resulted in high dispersion of active metallic cobalt phase; hence high CO hydrogenation activities were obtained.

Table 5.8 Rate of CO hydrogenation and product selectivity

Sample	Product Selectivity (%)			Rate of CO hydrogenation (mmole of $-CH_2$-g^{-1}.sec^{-1})^a		TOF (sec^{-1})^b	
	C_1	C_2-C_3	C_4-C_{4+}	Initial	Final	Initial	SS
Co/ZrO$_2$	94.4	4.8	0.7	12.2	10	0.43	0.36
Co/Al0.5-ZrO$_2$	99.3	0.7	0.0	13.3	12.7	0.43	0.39
Co/Al1-ZrO$_2$	98.8	1.1	0.1	13.3	12.2	0.43	0.41
Co/Al25-ZrO$_2$	98.9	1.1	0.0	13.3	12.2	0.38	0.36
Co/Al40-ZrO$_2$	95.4	4.5	0.1	5.0	3.9	0.46	0.36
Co/Al75-ZrO$_2$	96.7	3.3	0.0	2.7	2.2	0.51	0.48
Co/Al$_2$O$_3$	99.3	0.7	0.0	12.2	9.4	0.43	0.34

The reaction was carried out at 220°C, flow rate of CO/H$_2$/Ar 4/40/16 ml/min, WHSV= 4500 h$^-$

^{a} *CO hydrogenation rate =*

$$\text{CO hydrogenation rate} = \frac{[\% \text{ Conversion of CO}/100] \times 60min \times 14g\ CH_2 \times 4(cc/min)}{W(g) \times 22400\ (cc) \times (273+220)/273}$$

^{b}*TOF =*

$$TOF = \frac{\text{Rate of CO hydrogenation (molecules of CO / g catalyst. sec)}}{2\times\ \text{Hydrogen chemisorption(molecules/ g catalyst)}}$$

Reaction condition; T= 220°C, Flow rate of CO/H2/Ar 4/40/16 ml/min, WHSV= 4500 h⁻

Figure 5.13 Typical time-on-stream behaviour of the catalyst samples in the CO-hydrogenation, ◆Co/ZrO$_2$, ■Co/Al$_2$O$_3$, ●Co/Al0.5-ZrO$_2$, ＋Co/Al1-ZrO$_2$, ○Co/Al25-ZrO$_2$, × Co/Al40-ZrO$_2$ and ▲Co/Al75-ZrO$_2$

Alumina-zirconia mixed oxide supports with various mole% of alumina prepared by the modified Pechini's method exhibited interesting properties when employed as Co catalyst supports for CO hydrogenation. For the low alumina contents (0.5-25mole %), alumina modified the surface properties of zirconia leading to high dispersion of cobalt and high performance in the CO hydrogenation reaction. However, for higher alumina contents (40 and 75mole%), the catalysts showed much lower Co dispersion and CO hydrogenation activities probably due to compound formation from cobalt and amorphous alumina/zirconia.

In the third part, tetragonal zirconia with low silica or yttria contents (0.1-2mole %) was also prepared by the modified Pechini's method and employed as the support of a Co catalyst. The CO hydrogenation and characterization of the catalysts were carried out in order to compare these catalysts with alumina modified zirconia

supported catalyst. It was found that Si-modified zirconia exhibited a positive influence on metal dispersion within a range of 1-2mole% Si, whereas 2mole% of yttria in zirconia exhibited slightly high catalytic performance compared to that of pure tetragonal zirconia.

5.3 The influence of Si-modified and Y-modified zirconia on the characteristics and catalytic activity of Co/ZrO₂ for CO hydrogenation

5.3.1 Effect of Si and Y addition on the properties of zirconia

5.3.1.1 X-ray diffraction and BET surface area results

The X-ray diffraction patterns of the zirconia and modified zirconia powders prepared by the modified Pechini's method are shown in Figure 5.14 and 5.15. All the samples exhibited tetragonal crystalline zirconia phase. No other crystal structures were observed. It has been suggested that the energy from combustion of the polymeric materials during calcination at 600°C was sufficient to arrange the crystal structure in the tetragonal form with a crystal size less than its critical size [55]. Addition of Si or Y did not have any effect on XRD patterns of the tetragonal zirconia. The crystallite sizes of tetragonal zirconia calculated from the XRD line broadening using the Scherrer's equation and the BET surface areas are reported in Table 5.9. The average crystallite sizes of the zirconia and the Si- or Y-modified zirconia were approximately 5-7 nm. The BET surface areas of the nanocrystalline zirconia were found to be 85-100 m²/g.

Within experimental error, there was no significant difference in BET surface areas and the crystallite sizes caused by addition of a Si or Y. This is in contrast to the work reported by Alvarez et al. [37] who observed that doping zirconia by 2-5mole% yttria prepared by a sol-gel method resulted in narrower interparticle pores and the formation of denser agglomerates. However, in the present study the amounts of Y and Si addition were probably low (ca. 0.10-1.96%) and no change in BET surface areas was found.

Table 5.9 Crystallite sizes and BET surface areas of Si- and Y-doped zirconia

Sample	Avg. Crystallite size (nm)[a]	BET surface area[b] (m^2/g)
ZrO_2	6.3	90.4
Si0.1-ZrO_2	6.2	95.2
Si0.5-ZrO_2	5.3	83.1
Si1-ZrO_2	5.9	86.4
Si2-ZrO_2	5.2	92.1
Y0.1-ZrO_2	5.9	93.1
Y0.5-ZrO_2	6.1	94.5
Y1-ZrO_2	6.9	92.2
Y2-ZrO_2	5.9	98.4

[a] calculated from X-ray line broadening.

[b] Error of measurements = +/- 10%.
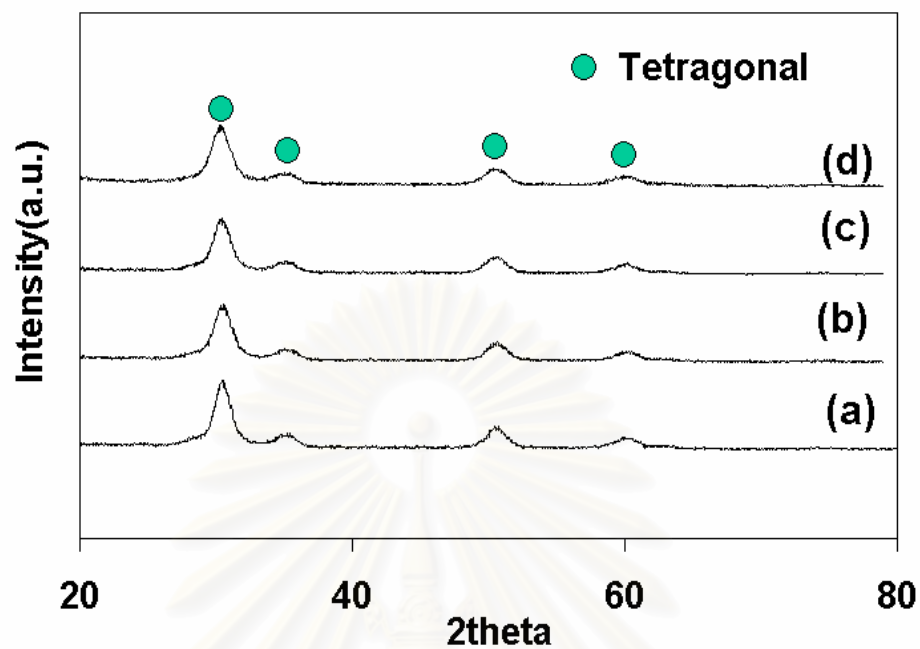
Figure 5.14 The XRD patterns Si-modified zirconia supports, (a) Si0.1-ZrO_2, (b) Si0.5-ZrO_2, (c) Si1-ZrO_2, and (d) Si2-ZrO_2
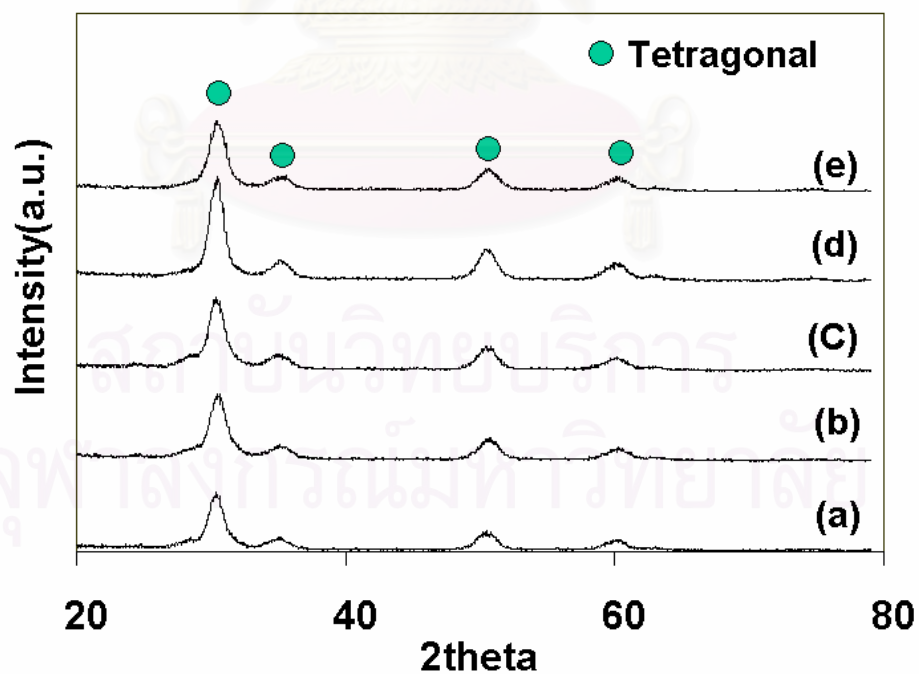
Figure 5.15 The XRD patterns Si-modified zirconia supports, (a) ZrO_2, (b) Y0.1-ZrO2, (c) Y0.5-ZrO2, (d) Y1-ZrO2, and (e) Y2-ZrO2

5.3.1.2 Structure and morphology of Si- and Y-modified alumina

Typical SEM micrographs of zirconia and Si- and Y-modified zirconia samples are shown in Figure 5.16. It was found that both zirconia and modified-zirconia prepared by the modified Pechini's method have irregular long shapes involving of sandwich parallel pores similar to those of sol-gel derived zirconia that appeared to form from polymeric units of hydrolysed zirconium precursors [74]. Pores were in a macro-range. There was no change in the morphology of the zirconia after Si or Y doping.
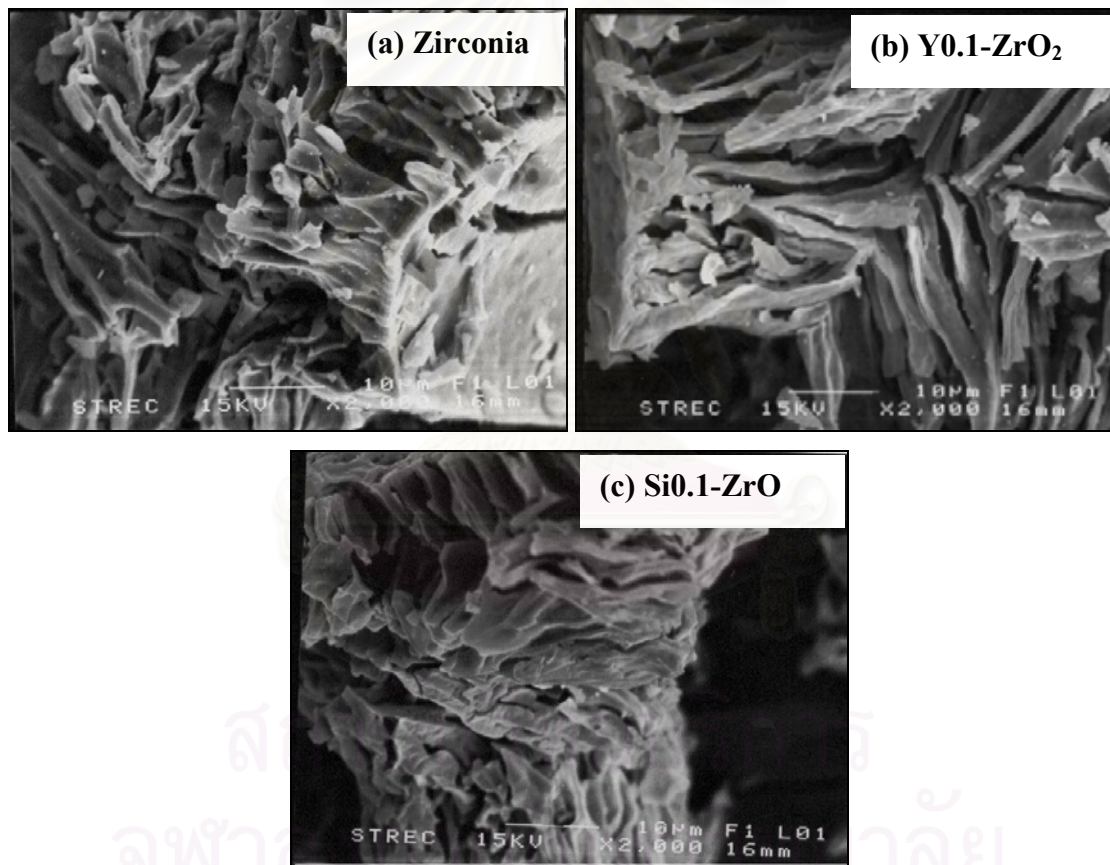
Figure 5.16 SEM micrographs of (a) zirconia, (b) Si0.1-ZrO$_2$, and (c) Y0.1-ZrO$_2$ synthesized via the modified Pechini's method

5.3.2 Characteristics and catalytic properties of the catalysts

    5.3.2.1 X-ray diffraction and BET surface area results

       The X-ray diffraction patterns of the Co/ZrO_2 catalysts are shown in Figure 5.17 and 5.18. After impregnation of 10wt% cobalt, the diffraction peaks of Co_3O_4 were observed at $36.8°2\theta$ for all the catalyst samples. The average crystallite sizes of Co_3O_4 calculated based on X-ray line broadening using Scherrer's equation for Si-modified ZrO_2 supported cobalt catalysts were 20-40 nm. They increased with increasing Si content and were found to be larger than those of Y-modified ZrO_2 supported ones (< 5 nm). The BET surface areas of the various Co/ZrO_2 catalysts and the H_2 chemisorption results are reported in Table 5.10. The BET surface areas of the zirconia supported cobalt catalysts were slightly less than that of the original zirconia supports suggesting that cobalt was deposited in some of the pores of zirconia. There was no significant difference in BET surface areas between all of the Co/ZrO_2 catalysts.

       However, it was found that, at percentages of Si (1-2 mole%) and of Y (2 mole%), the amounts of H_2 chemisorption increased by ca. 10-50% with the Si-modified zirconia (Si 2 mole%) exhibiting the highest cobalt dispersion. The addition of lower amounts of Si or Y did not seem to have a great impact on the amount of surface cobalt measured by H_2 chemisorption.

Table 5.10 Characteristics of various Co/ZrO$_2$ catalysts

Sample	BET Surface area[a] (m^2/g)	H$_2$ chemisorption[b] x10^{18} (molecule H$_2$/g cat.)	%Co dispersion[c]
Co/ZrO$_2$	52.1	5.9	14.4
Co/Si0.1-ZrO$_2$	48.7	5.1	12.5
Co/Si0.5-ZrO$_2$	51.5	5.4	13.3
Co/Si1-ZrO$_2$	50.8	7.0	17.0
Co/Si2-ZrO$_2$	52.4	9.0	21.9
Co/Y0.1-ZrO$_2$	56.2	4.5	11.0
Co/Y0.5-ZrO$_2$	54.3	4.6	11.3
Co/Y1-ZrO$_2$	60.1	5.5	13.5
Co/Y2-ZrO$_2$	53.8	6.4	15.7

[a] *Error of measurements = +/- 10%.*

[b] *Error of measurements = +/- 5%.*

[c]*%Co dispersion*

$$= \frac{Amount\ of\ Co\ equivalent\ to\ H_2\ adsorption\ on\ catalyst\ after\ reduction\ (H_2{:}Co{=}1{:}2)\times100}{Total\ amount\ of\ Cobalt\ active\ sites\ expected\ to\ exist\ after\ reduction}$$
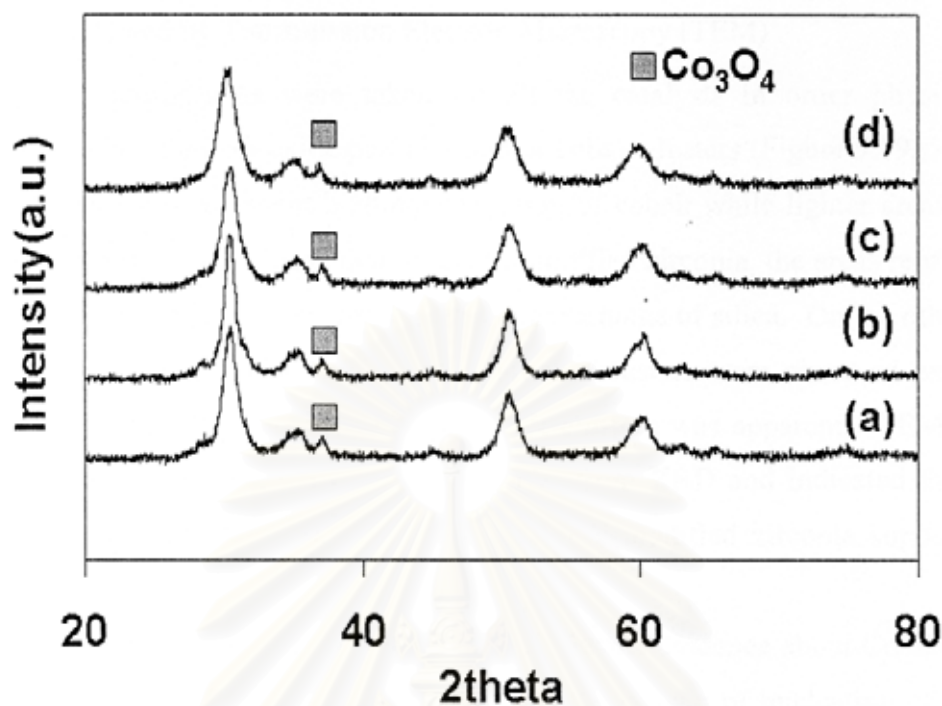
Figure 5.17 X-ray diffraction patterns of the supported catalysts, (a) Co/Si0.1-ZrO₂ (b) Co/Si0.5-ZrO$_2$, (c) Co/Si1-ZrO$_2$, and (d) Co/Si2-ZrO$_2$
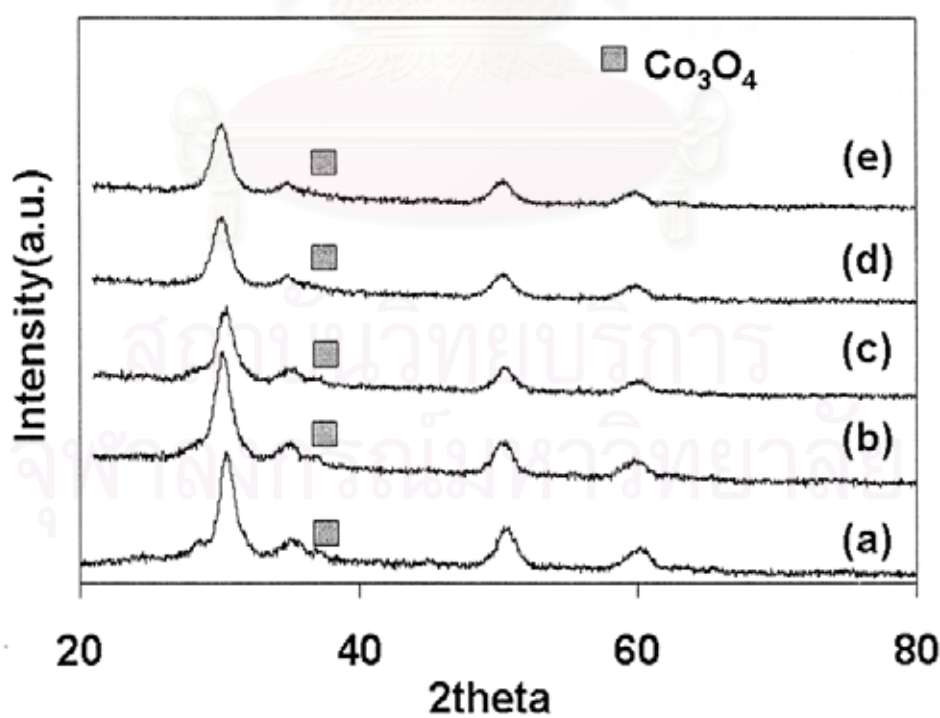
Figure 5.18 X-ray diffraction patterns of the supported catalysts, (a) Co/ZrO$_2$ (b) Co/Y0.1-ZrO$_2$, (c) Co/Y0.5-ZrO$_2$, (d) Co/Y1-ZrO$_2$, and (e) Co/Y2-ZrO$_2$

5.3.2.2 Primary particles of zirconia supports and the areas of active cobalt investigated by Transmission Electron Microscopy (TEM)

TEM micrographs were taken for all the catalysts in order physically to measure the size of cobalt oxide particles and/or cobalt clusters (Figure 5.19, 5.20, and 5.21). Darker spots represent high concentration of cobalt while lighter areas are the zirconia supports. It was found that on the Si-modified zirconia, the areas representing cobalt concentration increased with increasing percentage of silica. On the other hand, on the Y-modified zirconia, small cobalt particles/clusters were observed except for zirconia with 2mole% of Y where large cobalt clusters was apparent. TEM images were found to be in accordance with the results from XRD and indicated that small cobalt oxide particles (< 5 nm) were present on Y-modified zirconia supported Co catalysts.

TEM measurements were able to provide further evidence about Co dispersion. Adding a small amount of Si and Y might alter the growth of nucleation of zirconia crystals [87]. In this study, it was found that primary particles of the nanocrystalline zirconia tend to agglomerate upon Si and Y doping. The effect was, however, more pronounced for modification with silica than with yttria, as seen by agglomeration of zirconia particles for the lower Si/Zr ratios. The results were in good agreement with Alvarez et al. [37] that increasing %Y addition resulted in larger primary particles.
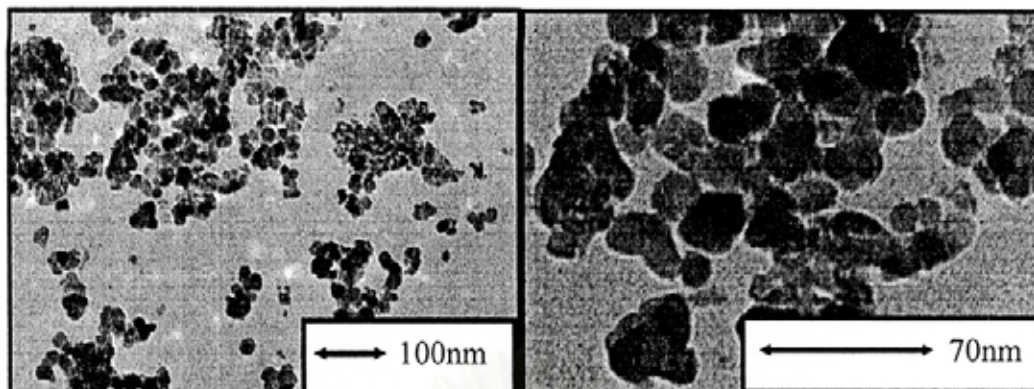
(a) Co/Si0.1-ZrO$_2$
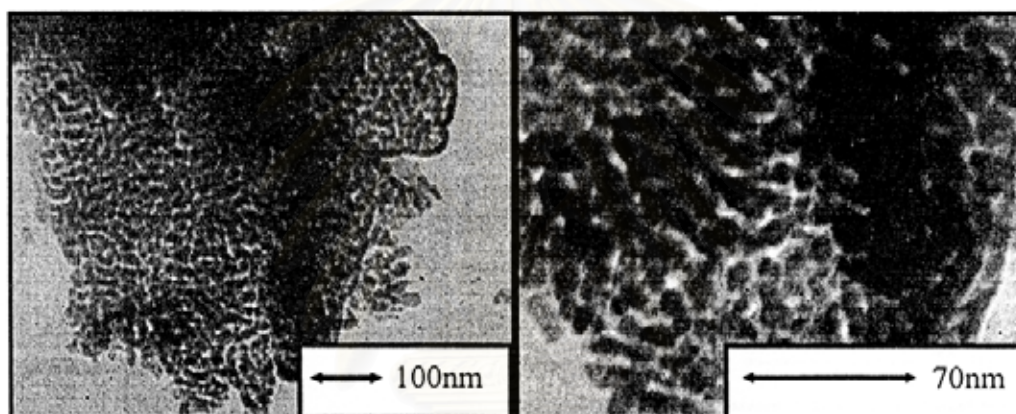
(b) Co/Y0.1-ZrO$_2$

Figure 5.19 TEM micrographs of Si0.1-ZrO2 and Y0.1-ZrO2 supported Co catalysts at different magnifications
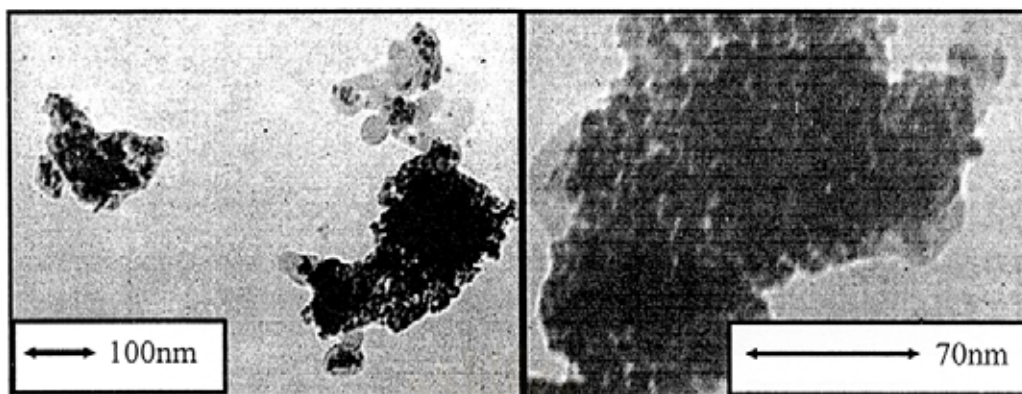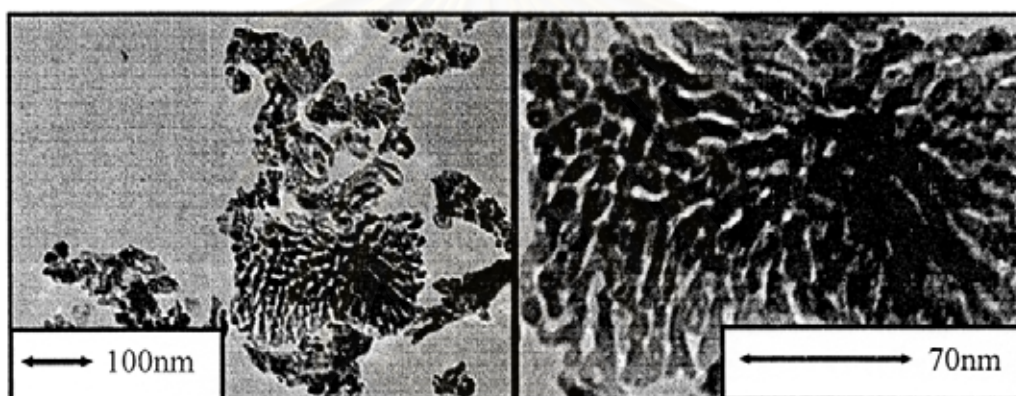
(a) Co/Si1-ZrO$_2$

(b) Co/Y1-ZrO$_2$

Figure 5.20 TEM micrographs of Si1-ZrO$_2$ and Y1-ZrO$_2$ supported Co catalysts at different magnifications
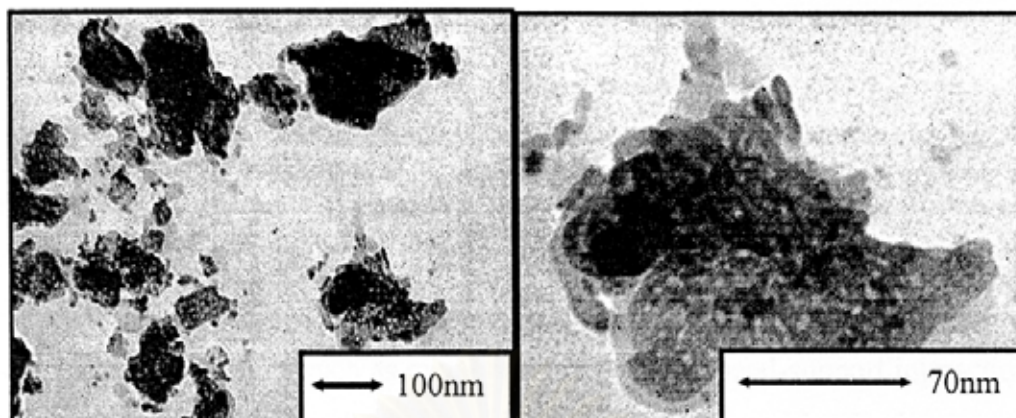
(a) Co/Si2-ZrO$_2$
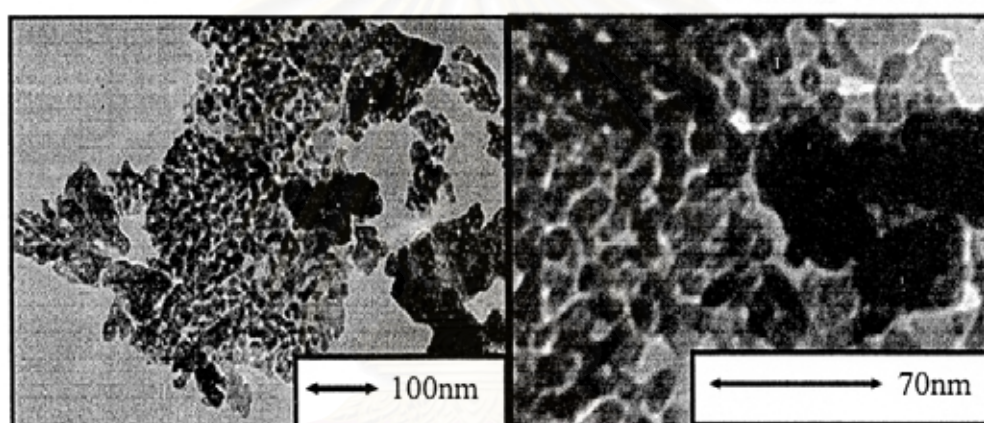
(b) Co/Y2-ZrO$_2$

Figure 5.21 TEM micrographs of Si2-ZrO$_2$ and Y2-ZrO$_2$ supported Co catalysts at different magnifications

5.3.2.2 Temperature programmed reduction

Temperature programmed reduction (TPR) profiles of Si- and Y-modified zirconia supported Co catalysts are shown in Figures 5.22 and 5.23, respectively. TPR is a powerful tool to study the reduction behaviour of the catalysts. Reduction of cobalt in the oxide form (Co_3O_4 or Co_2O_3) to Co^0 involves a two-step reduction: first reduction of Co_3O_4 to CoO and then the subsequent reduction of CoO to Co^0 [83, 84]. A wide range of variables such as metal particle size and metal-support interaction has an influence on the reduction behaviour of cobalt catalysts, resulting in the observation of different locations for the TPR peaks [85]. It was found that for the Si-modified zirconia supported cobalt catalysts reduction peaks below 400°C tended to shift to lower temperatures whereas those of Y-modified ones showed similar TPR profiles.

The reducibilities of the catalysts calculated by integrating areas under the TPR peaks are given in Table 5.11. The reducibilities of all the catalysts were only 30-40%. The low reducibility of the catalysts may be due to formation of a solid solution or of a zirconate phase between unreduced cobalt oxides and zirconia [23].
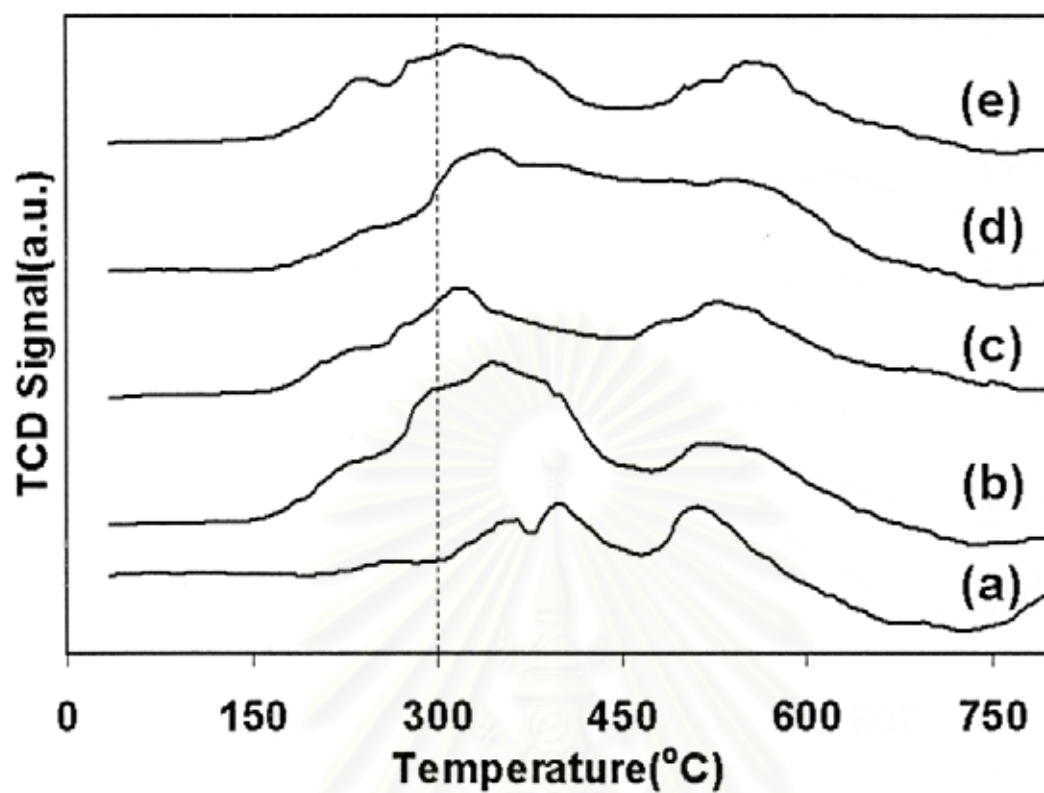
Figure 5.22 Temperature-programmed reduction of the catalyst samples (a) 10%Co/ZrO$_2$, (b) 10%Co/Si0.1-ZrO$_2$, (c) 10%Co/Si0.5-ZrO$_2$, (d) 10%Co/Si1-ZrO$_2$, and (e) 10%Co/Si2-ZrO$_2$
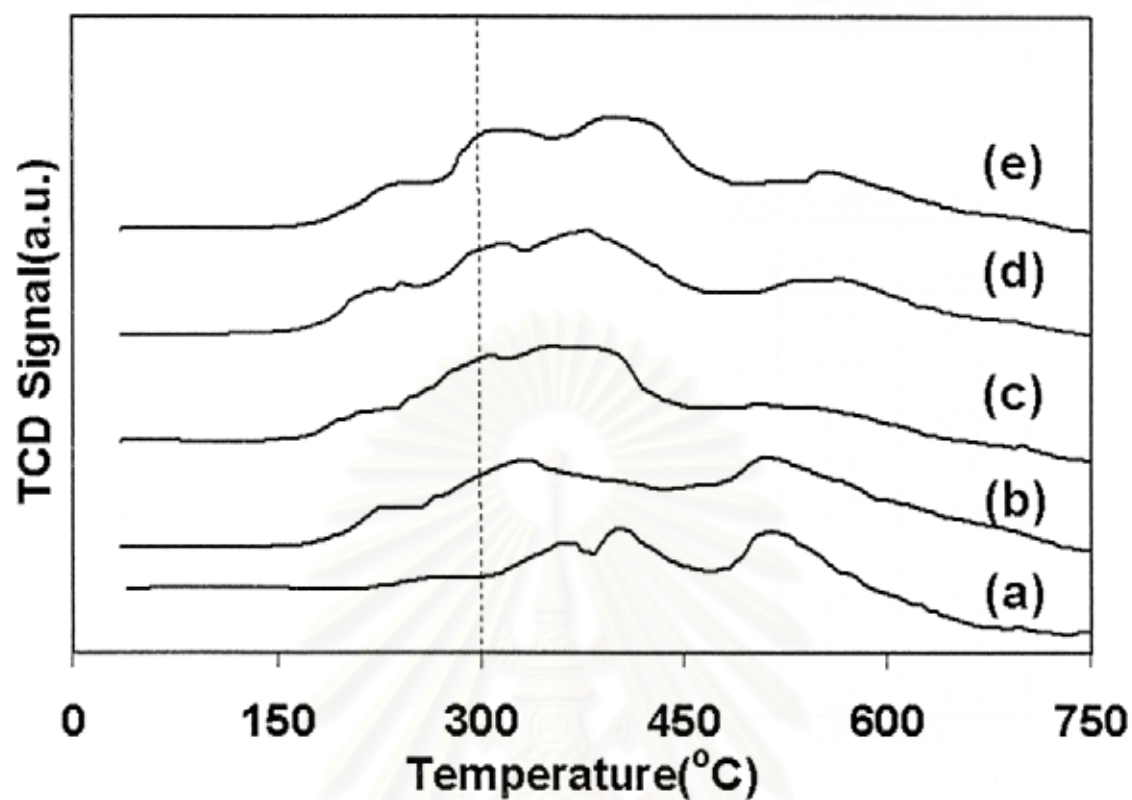
Figure 5.23 Temperature-programmed reduction of the catalyst samples (a) 10%Co/ZrO2, (b) 10%Co/Y0.1-ZrO$_2$, (c) 10%Co/Y0.5-ZrO$_2$, (d) 10%Co/Y1-ZrO$_2$, and (e) 10%Co/Y2-ZrO$_2$

Table 5.11 Catalytic Results in CO hydrogenation ($220^{o}C$, 1 atm, and $H_2/CO =10$)

Catalyst	Reducibility[a] (%)	CO hydrogenation rate[b] ($\mu mol\ CH_2\ g\ cat^{-1}\ s^{-1}$)	Product Selectivity (%)			TOFs[c] (s^{-1})
			C_1	C_2-C_3	C_{4+}	
Co/ZrO$_2$	32	15.4	88.6	9.1	2.3	0.22
Co/Si0.1-ZrO$_2$	39	10.7	86.0	10.8	3.2	0.27
Co/Si0.5-ZrO$_2$	30	10.8	98.0	2.0	0.0	0.72
Co/Si1-ZrO$_2$	34	11.9	98.6	1.4	0.0	0.66
Co/Si2-ZrO$_2$	30	18.8	97.8	2.2	0.1	0.28
Co/Y0.1-ZrO$_2$	31	10.4	97.6	2.3	0.1	0.28
Co/Y0.5-ZrO$_2$	29	16.2	89.3	8.7	2.1	0.26
Co/Y1-ZrO$_2$	29	19.6	91.7	7.1	1.3	0.23
Co/Y2-ZrO$_2$	32	24.1	97.7	2.2	0.1	0.30

Reaction condition at T=220°C, flow rate of CO/H$_2$/Ar 4/40/16 ml/min, WHSV= 4500 h$^-$

[a] *Based on TPR results from 35-800°C.*

[b]*CO hydrogenation rate* $= \dfrac{[\%\ Conversion\ of\ CO/100]\times 60min\times 14g\ CH_2\ \times 4(cc/min)}{W(g)\times 22400\ (cc)\times (273+220)/273}$

[c]*TOF* $= \dfrac{Rate\ of\ CO\ hydrogenation\ (molecules\ of\ CO\ /\ g\ catalyst.\ sec)}{2\times\ Hydrogen\ chemisorption(molecules/\ g\ catalyst)}$

สถาบันวิทยบริการ
จุฬาลงกรณ์มหาวิทยาลัย

5.3.2.3 Catalytic performance of Si- and Y-modified zirconia supported Co catalysts

The catalytic activities of the Co/ZrO_2 catalysts for the CO hydrogenation reaction are also reported in Table 5.11. As expected, the CO hydrogenation rates increased by 30-40% for the Co supported on Si- and Y-modified zirconia with percentage of Si > 0.5 mole% and of Y > 1mole%. A correlation between the amount of active sites and CO hydrogenation activities for various Co/ZrO_2 catalysts is illustrated in Figure 5.24 as a straight line. It should be noted that Si- modified zirconia exhibited a positive influence on catalytic activity which was larger than for Y-modified zirconia. The product selectivities were not significantly different, since all the catalysts exhibited methane selectivities ca. 89-99% (expected product under the reaction conditions used).

Addition of a small amount of Si or Y during the preparation of nanocrystalline tetragonal zirconia accelerated agglomeration of zirconia primary particles. The effect was more pronounced for silica than yttria. However, when used as cobalt catalyst supports, those Si- and Y-modified zirconia supported ones with percentage of Si > 0.5 mole% and of Y >1 mole% exhibited higher H_2 chemisorption and CO hydrogenation activities.
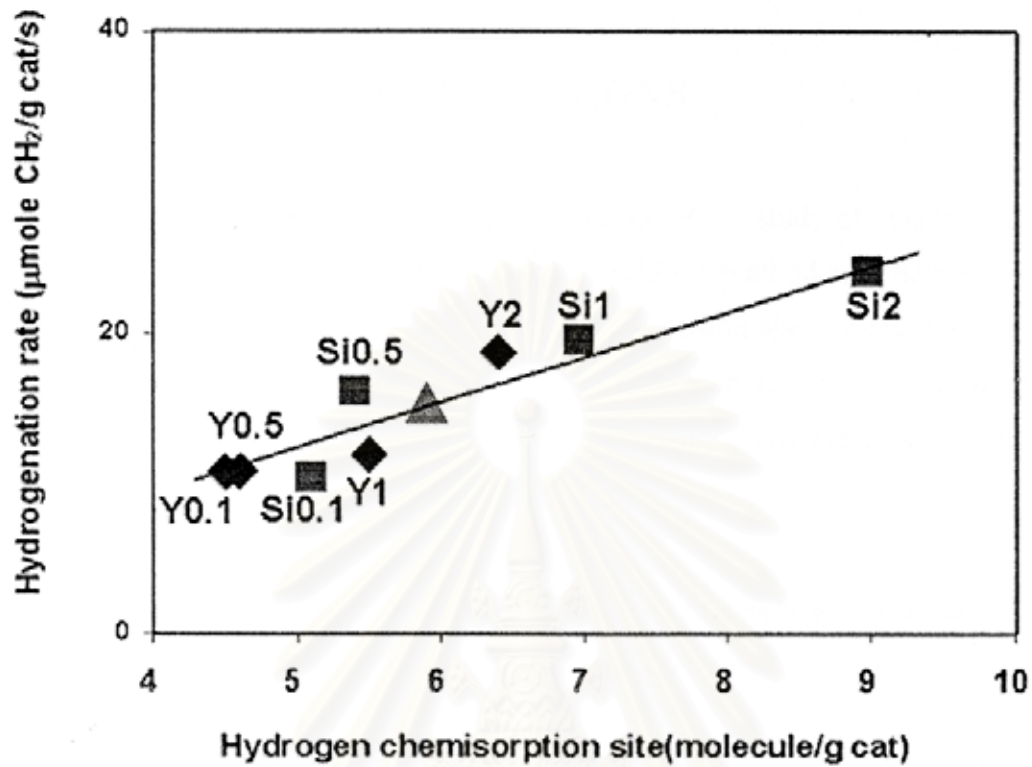
Reaction condition; T=220°C, flow rate of CO/H$_2$/Ar 4/40/16 ml/min, WHSV= 4500 h⁻ and hydrogenation rate based on Table 5.11

Figure 5.24 Correlation of active sites measured by hydrogen chemisorption and CO hydrogenation rates

CHAPTER VI

CONCLUSIONS

This chapter is focused upon the conclusions of the study of characteristics of mixed oxide zirconia prepared by the modified Pechini's method and their application as catalyst and catalyst support. Moreover, this conclusion also summarizes catalytic activity studies of zirconia modified with different elements, i.e. silica and yttria, supported cobalt catalysts. Recommendations for further study are given in the final, part of this section.

6.1 Characteristics of zirconia, alumina, and alumina-zirconia mixed oxide prepared by the modified Pechini's method can be summarized as follows.

1. The alumina-zirconia mixed oxides produced by the modified Pechini's method resulted in combination of aluminium and zirconium atoms. Due to good dispersion of aluminium and zirconium ions, the mixed oxides were presented only in an amorphous form.

2. The interaction between Al, Zr, and O in the mixed oxides resulted in slightly higher physical strength of CO_2 adsorption (description at slightly more than 110^oC). The modified acidity was, however, ambiguous because all the catalyst samples exhibited low acidity. Alumina-zirconia mixed oxide exhibits the more acid and basic sites than pure alumina and pure zirconia.

3. Surface areas of the mixed oxide apparently increase by increasing alumina content. By this preparation condition, surface area of tetragonal zirconia was obtained in a range of 50-90 m^2/g. This is fairly low compared to that of tetragonal zirconia prepared by solvothermal method in our laboratory; however, this preparation method caused a change in surface characteristic because of good dispersion of alumina and zirconia content.

6.2 Application of zirconia, alumina, and alumina-zirconia mixed oxide as catalyst

The surface characteristic of zirconia, alumina, and alumina-zirconia mixed oxides is possibly described from the product distributions of elimination of 2-propanol. Due to amount of oxygen covering surface of testing sample was much lower than oxygen needed to oxidize 2-propanol as calculated in Appendix I. Thus, it suggests that most of 2-propanol converted to acetone via E_{1cB} mechanism. The imbalance strength of acid-base site due to the imperfect crystal structure of all the catalysts resulted in higher acetone formation via the E_{1cB} mechanism. However, 90% propylene selectivity was obtained on pure zirconia prepared by the modified Pechini's method at $200^{o}C$ reaction temperature. At this temperature, propylene selectivity increased with increasing zirconia content.

6.3 Application of zirconia, alumina, and alumina-zirconia mixed oxide as cobalt catalyst supports

Alumina-zirconia mixed oxide supports with various mole% of alumina prepared by the modified Pechini method exhibited interesting properties when employed as Co catalyst supports in CO hydrogenation.

CASE I; Low alumina content (0.5-25mole%)

For the low alumina contents (0.5-25mole%), alumina modified the surface properties of zirconia leading to high dispersion of cobalt and high performance in CO hydrogenation reaction.

CASE II; High alumina content (40-75mole%)

For higher alumina contents (40 and 75mole%), the catalysts showed much lower Co dispersion and CO hydrogenation activities due probably to compounds formation between cobalt and amorphous alumina/zirconia.

6.4 The influence of Si-modified and Y-modified zirconia on the characteristics and catalytic activity of Co/ZrO2 for CO hydrogenation

Addition of a small amount of Si or Y during the preparation of nanocrystalline tetragonal zirconia accelerated agglomeration of zirconia primary particles. The effect was more pronounced for silica than yttria. However, when used as cobalt catalyst supports, those Si- and Y-modified zirconia supported catalysts Si/Zr > 0.005 and Y/Zr > 0.01 exhibited higher H_2 chemisorption and CO hydrogenation activities.

6.5 Comparison of Al-modified, Si-modified and Y-modified zirconia (at 2 mole% of dopant) supported catalyst for CO hydrogenation

It was found that Al-modified and Si-modified zirconia supported catalysts exhibited no different catalytic activities for CO hydrogenation at the initial; however, the difference was found when CO hydrogenation approached steady states. Al-modified zirconia supported catalyst exhibited higher stability than Si-modified zirconia supported catalysts. It suggests that modification of alumina affects surface acidity and retards formation of carbon particles usually occurred during the reaction, caused decrease of catalytic activity. It possibly concludes that modification of the second metal on zirconia supports has an influence on catalytic activity.

6.6 Recommendation for further study

1. The phase stability of Al-modified, Si-modified, and Y-modified zirconia prepared by the modified Pechini's method should be studied.

2. Modification of zirconia by other elements giving rise to phase stability of zirconia, e.g. lanthanum, tin, or tungsten should be studied and should be tested as catalyst and catalyst supports.

3. Alumina-zirconia mixed oxide, prepared by the modified Pechini's method, should be modified using a sulfated solution and the resulting sulfated alumina-zirconia should be applied for other reactions needing strongly acidic sites.

REFERENCES

1. Tanabe, K., Surface and catalytic properties of ZrO_2, <u>Mater Chem. Phys.</u>, 13(1985) 347

2. Tanabe, K., Yamaguchi, T., Acid-base bifunctional catalysis by ZrO_2 and its mixed oxides, <u>Catalysis Today,</u> 20 (1994) 185

3. Tanabe, K., in Imelik, B., et al. (Editors), Catalysis by Acids and Bases, Elsevier, Amsterdam, 1985, 1

4. Tanabe, K., in Tanabe, K., et al. (Editors), Proc. Acid-Base Catalysis, Kodansha-VCH, Tokyo-Weinheim, 1989, 513

5. Tanabe, K., in Phillips, M.J., and Ternan, M., (Editors) Proc. 9th Intern. Congr. Catal., Chem. Inst. Canada, Ottawa, 1988, Ch4.

6. Chisso Corporation (T. Okamoto et al.), Japan Kokai Patent, 49-48614 (1974)

7. Hattori, H., and Wang, G, Proc. 8th Inten. Congr. Catal., Verag Kokai Patent, 85-126242 (1985)

8. Xu, B.-Q., Yamaguchi, T., and Tanabe, K., <u>Chem Lett.</u>, (1988) 281

9. Arata, K., Bledsoe, J.O., and Tanabe, K., <u>Tetrahedal Lett.</u>, 43 (1976); <u>J. Org. Chem.</u>, 43 (1978) 1660

10. Maehashi, T., Maruya, K., Domen, K., Aika, K., and Onishi, T., <u>Chem. Lett.</u>, (1984) 747

11. Caili, S., Junrong, L., Dehua, H., Zhengxing, C., and Qiming, Z., Synthesis of isobutene from synthesis gas over nanosize zirconia catalyst, <u>Applied Catalysis A: General</u>, 202 (2000) 81

12. Tanaka, Y., Imizu, Y., Hattori, H., and Tanabe, K., Proc. 7th Intern. Congr. Catal., Kodansha, Tokyo, B 1254 (1981)

13. Silvia, G. B., Jose, A. N., Maria, C. H., Gloria, M. R., and Marta, I. L., Photocatalytic properties of ZrO2 and Fe/ZrO2 semiconductors prepared by a sol-gel technique, <u>J. Photochemistry and Photobiology A: Chemistry</u>, 129 (1999) 89

14. Yinghong, Y., Xiping, Z., Weiming, H., and Zi, G., Nanosized titania and zirconia as catalysts for hydrolysis of carbon disulfide, <u>Applied Catalysis B: Environmental</u>, 46 (2003) 561.

15. Yamaguchi, T., Sasaki, H., and Tanabe, K., <u>Chem Lett.</u>, (1973) 1017

16. Takahashi, K., Hibi, T., Higashio, Y., and Akai, M., Shokubai (Catalysis), 35 (1993), 12

17. Sumitomo Chemical Co., Ltd., Japan Kokai Patent, 61-130240 (1986)

18. Chokkaram, S., and Davis, B. H., Dehydration of 2-octanol over zirconia catalysts: Influence of crystal structure, sulfate addition and pre-treatment, J. Mol. Catal. A: Chem, 118 (1997) 89

19. Bitter, J. H., Sechan, K., and Lercher, J. A., The state of zirconia supported platinum catalysts for CO_2/CH_4 reforming, J. Catal., 171 (1997) 279

20. Dow,W. P., and Huang, T. J., Effect of oxygen vacancy of yttria-stabilized zirconia support on carbon monoxide oxidation over copper catalyst, J. Catal., 147 (1994) 322.

21. Chuah, G. K., An investigation into the preparation of high surface area zirconia, Catal. Today, 49 (1999) 131

22. Bruce, L., and Mathews, J. F., The Fischer-Tropsch activity of nickel-zirconia, Appl. Catal., 4 (1982) 353

23. Enache, D. I., Roy-Auberger, M., and Revel, R., Differences in the characteristics and catalytic properties of cobalt-based Fischer–Tropsch catalysts supported on zirconia and alumina, Appl. Catal. A: General, 268(2004) 51

24. Enache, D. I., Rebours, B., Roy-Auberger, M., and Revel, R., In SituXRD Study of the Influence of Thermal Treatment on the Characteristics and the Catalytic Properties of Cobalt-Based Fischer–Tropsch Catalysts, J. Catal., 205 (2002) 346

25. Chuah, G. K., and Pong, B.K., The preparation of high-surface-area zirconia - II. Influence of precipitating agent and digestion on the morphology and microstructure of hydrous zirconia, J. Catal., 175 (1998) 80

26. Yashima, M., and Kakihana, M., Hydrothermal synthesis of crystallized nano-particles of rare earth-doped zirconia and hafnia, J. Mater. Res., 61 (1996) 1410

27. Stöcker, C., and Baiker, A., Zirconia aerogels: effect of acid-to-alkoxide ratio, alcoholic solvent and supercritical drying method on structural properties, J. Non-Cryst. Solids, 223 (1998) 165

28. Kongwudthiti, S., Praserthdam, P., Tanakulrungsank, W., and Inoue, M., The influence of Si–O–Zr bonds on the crystal-growth inhibition of zirconia prepared by the glycothermal method, J. Mater. Proc. Tech., 136 (2003) 186

29. Shinoda, M., Zhang, Y., Yoneyama, Y., Hasegawa, K., and Tsubaki, N., New bimodal pore catalysts for Fischer–Tropsch synthesis, Fuel Proc. Tech., In press.

30. Joongsomjit, B., Panpanot, J., and Goodwin Jr., J. G., Effect of zirconia-modified alumina on the properties of Co/γ –Al2O3 catalysts, J. of Catal., 215 (2003) 66

31. Lakshmi, J.L., Jones, T.R.B., Gurgi, M., and Miller, J. M., Synthesis, characterization and activity studies of vanadia catalysts supported on sol–gel derived Al_2O_3–ZrO_2 mixed oxide, J. Mol. Catal. A: Chem, 152 (2000) 99

32. M.-Pineda, M., Castillo, S., López, T., C.-Borboa, R. G., and Novaro, O., Synthesis, characterization and catalytic activity in the reduction of NO by CO on alumina–zirconia sol–gel derived mixed oxides, Appl. Catal. B: Environmental 21 (1999) 79

33. Hao, Y., Li, J., Yang, X., Wang, X., and Lu, L., Mater. Sci. Eng. A 367 (2004) 243

34. Monte, F. D., Larsen, W., and Mackenzie, J. D., Stabilization of tetragonal ZrO_2 in ZrO_2-SiO_2 binary oxides, J. Am. Ceram. Soc., 83 (2000) 1506

35. Yasuda, K., Arai, S., Itoh, M., and Wada, K., J. Mater. Sci., 34 (1999) 3597

36. Ballard, J. D., Davenport, J., Lewis, C., Nelson, W., Doremus, R. H., and Schadler, L. S., J. Thermal Spray Tech., 12 (2003) 34

37. Alvarez, M. R., and Torralvo, M., Textural evolution of zirconia and yttria-doped zirconia on thermal treatment under different conditions, J. Colloids and Surf. A, 113 (1996) 165

38. Loong, C. K., Richardson, J. W., Ozawa, M., and Kimura, M., Crystal structure and short range oxygen defects in La- and Nd-modified ZrO_2, J. Alloys Comp. 207 (1994) 174

39. Devassy, B. M., Shanbhag, G. V., Mirajkar, S. P., Bohringer, W., Flethcher, J., and Halligudi, S. B., *tert*-Butylation of *p*-cresol over WO_x/ZrO_2 solid acid catalysts, J. Mol. Catal. A, 233 (2005) 141

40. Pechini, M.P., US Patent, 11 July (1967) 3,330,697

41. Wen, K.C., Andy, A.W., and Yuan, H.L., Oxygen-induced structure change of zirconia by adding rare earth oxides with solid-state method, J. Alloys Comp., 249 (1997) 251

42. Elisabeth, D., Florence, B., Guihem, D., and Pierre, B., Quantification of chemical pressure in doped nanostructured zirconia ceramics, J. Phy. Chem. B, 107 (2003) 8321

43. Feller, A., Claeys, M., Steen, E.V., Cobalt Cluster Effects in Zirconium Promoted Co/SiO2 Fischer–Tropsch Catalysts, J. of Catal., 185 (1999) 120

44. Oukaci, R., Singleton, A.H., and Goodwin Jr., J., Comparison of patented Co F–T catalysts using fixed-bed and slurry bubble column reactors, Appl. Catal. A: General 186 (1999) 129

45. Moradi, G.R., Basir, M.M., Taeb, A., and Kiennemann, Promotion of Co=SiO2 Fischer–Tropsch catalysts with zirconium, Catal. Comm. 4 (2003) 27

46. Yadav, D.A., and Nair, J.J., Sulfated zirconia and its modified versions as promising catalysts for industrial processes, Microporous and Mesoporous Materials 33 (1999)1

47. Rohra, F., Lindvåga, O.A., Holmenb, A., and Blekkanb, E.A., Fischer–Tropsch synthesis over cobalt catalysts supported on zirconia-modified alumina, Catal. Today 58 (2000) 247

48. Jacobs, G., Das, T.K., Zhang, Y., Li, J. , Racoillet, G., and Davis, B.H. Fischer–Tropsch synthesis: support, loading, and promoter effects on the reducibility of cobalt catalysts, Appl. Catal. A: General 233 (2002) 263

49. Maruya, K., Komiya, T., Hayakawa, T., Lu, L., and Yashima, M., Active sites on ZrO for the formation of isobutene from 2CO and H_2, J. of Mol. Catal. A: Chemical 159 (2000) 97

50. Cormak, A.N., and Parker, S.C., J. Am . Ceram. Soc., 73 (1990) 3220

51. Srinivasan, R., De Angelis, R.J., Ice, G., and Davis, B.H., J. Am. Ceram. Soc., 73 (1990) 3528

52. Tani, E., Yoshimura, M., Somiya, S., Formation of Ultrafine tetragonal ZrO_2 powder under hydrothermal conditions, J. Am. Ceram. Soc., 66 (1983) 11

53. Osendi, M.I., Moya, J.S., Serna, C.J., and Soria, J., Metastability of tetragonal zirconia powders, J. Am. Ceram. Soc., 68 (1985) 135

54. Livage, J. , Doi, K., and Mazieres, C., J. Am. Ceram. Soc., 51 (1968) 349

55. Garvie, R.C., Stabilization of the tetragonal structure in zirconia microcrystals, J. Phys. Chem., 82 (1978) 218

56. West, A. R., Solid State Chemistry and its Application, John Wiley&Sons, Brisbane, 1997

57. Heuer, A.H., Transformation Toughening in ZrO2-containing Ceramics, J. Am. Ceram. Soc., 70 (1987) 689

58. Ertl, G., Knözinger, H., Weitkamp, J., Handbook of Heterogeneous Catalysis (Wiley-VCH, City, 1997)

59. Robert, C.L., Ansart, F., Deloget, C., Gaudon, M., and Rousset, A., Dense yttria stabilized zirconia: sintering and microstructure, Ceramics International, 29 (2003) 151

60. Marcilly, C., Courty, P., and Delmon, B., J. of Am. Ceram. Soc.-Discussion and Notes, 53, 1 (1970) 56

61. Yashima, M., and Kakihana, M., J. Mater. Res., 11, 6 (1996) 1410

62. Kakihana, M., Kato, S., Yashima, M., and Yoshimura, M., Preparation of tetragonal ZrO_2–12 mol% CeO_2 and ZrO_2–6 mol% $YO_{1.5}$ solid solutions at reduced temperature by a simple aqueous solution route using citric acid as a complexant, J. of Alloy and Compounds, 280 (1998) 125

63. Yoshimura, M., and Somiya, S., Hydrothermal synthesis of crystallized nano-particles of rare earth-doped zirconia and hafnia, Master. Chem. Phys., 61 (1999)1

64. Batta, I., Boresok, S., Solymosi, F., and Szabo, Z.G., Proc. 3rd Int. Congr. Catalysis, Amsterdam 1964

65. Tanabe, K., Misono, M., Ono, Y., and Hattori, H., New Solid Acids and Bases, Elsevier, 1989, 260-265

66. Díez, V.K., Apesteguía, C.R., and Di Cosimo, J.I., Acid–base properties and active site requirements for elimination reactions on alkali-promoted MgO catalysts, Catal. Today, 63 (2000) 53

67. Farrauto, R.J., and H.Bartholomew, C., Fundamentals of Industrial Catalytic Processes (1997)

68. Ishii, M., Kakhina, M., Ishii, K., Ikuma, Y., and Yoshimura, M., J. Mat. Res. Soc., 11 No.6 (1996) 1410

69. Kakihana, M., Kato, S., Yashima, M., and Yoshimura, M., Preparation of tetragonal ZrO_2–12 mol% CeO_2 and ZrO_2–6 mol% $YO_{1.5}$ solid solutions at reduced temperature by a simple aqueous solution route using citric acid as a complexant, J. Alloys Comp., 280 (1998) 125

70. Muccillo, E.N.S., Souza, E.C.C., and Muccillo, R., Synthesis of reactive neodymia-doped zirconia powders by the sol–gel technique, J. Alloys Comp. 344 (2002) 175

71. Reuel, R.C., and Bartholomew, C.H., Effects of support and dispersion on the CO hydrogenation activity/selectivity properties of cobalt, J. Catal. 85 (1984) 78

72. Dominguez, J.M., Hernandez, J.L., and Sandoval, G., Surface and catalytic properties of Al_2O_3–ZrO_2 solid solutions prepared by sol–gel methods, Appl. Cata. A: General 197 (2000) 119

73. Díez, V.K., Apesteguía, C.R., and Di Cosimo, J.I., Effect of the chemical composition on the catalytic performance of Mg_yAlO_x catalysts for alcohol elimination reactions, J. Catal. 215 (2003) 220

74. Morris, M. A., and Reidy, H. M., Preparation of ceria–zirconia and yttria–zirconia mixed oxides of unusual pore structures, Ceramics Inter., 31 (2005) 929

75. Mercera, P.D.L., Ommen, J.G. van, Doesburg, E.B.M., Burggraaf, A.J. and Ross, J.R.H., Zirconia as a support for catalysts Influence of additives on the thermal stability of the porous texture of monoclinic zirconia, Appl. Catal. 71 (1991) 363

76. Davydov, A., Molecular Spectroscopy of Oxide Catalyst Surfaces (John Wiley & Sons, England, 2003

77. Li, Y., He, D., Cheng, Z., Zu, C., Le, J., and Zhu, Q., Effect of calcium salts on isosynthesis over ZrO_2 catalysts, J. Mol. Catal. A: Chemical, 175 (2001) 267

78. Davis, B.H., Influence of pre-treatment of alumina on the dehydrogenation: dehydration selectivity of 2-Octanol, J Catal. 26 (1972) 348

79. Waugh, K.C., Bowker, M., Petts, R.W., Vanderwell, H.D., and O'Malley, J., Temperature-programmed desorption studies of alcohol decomposition on ZnO: 1-propanol, 1-butanol and 2-butanol, Appl. Catal., 25 (1986) 121

80. Gervasini, A., Fenyvesi, J., and Auroux, A., Study of the acidic character of modified metal oxide surfaces using the test of isopropanol decomposition, Catal. Lett., 43 (1997) 219

81. Metelkina, O., Hüsing, N., Pongrazt, P., Schubert, U., Effects of the post-synthesis treatment on the structural properties of alumina-doped zirconia, J. Non-Cryst. Solids 285 (2001) 64

82. Kraum, M., Baerns, M., Fischer–Tropsch synthesis: the influence of various cobalt compounds applied in the preparation of supported cobalt catalysts on their performance, <u>Appl. Catal.</u>, 186 (1999) 189

83. Schanke, D., Vada, S., Blekkan, E. A., Hilmen, A., Hoff, A., Holmen, A., Study of Pt-Promoted Cobalt CO Hydrogenation Catalysts, <u>J. Catal.</u>, 156 (1995) 85

84. Zhang, Y., Wei, D., Hammache, S., Goodwin, Jr., J. G., Effect of Water Vapor on the Reduction of Ru-Promoted Co/Al_2O_3, <u>J. Catal.</u>, 188 (1999) 281

85. Panpranot, J., Goodwin, Jr., J. G., and Sayari, A., Synthesis and characteristics of MCM-41 supported CoRu catalysts, <u>Catal. Today</u>, 77 (2002) 269

86. Potoczna-Petru, D., Kepinski, L., Interaction of Co thin films with SiO_2: Effect of Co loading, <u>Catal. Lett.</u>, 73(1), (2001) 43

87. A.R. West, Solid State Chemistry and its applications, John Wiley & Sons (1987) 9

APPENDICES

APPENDIX A

**CALCULATION OF SURFACE AREA BY THE BET SINGLE POINT
METHOD**

From Brunauer-Emmett-Teller (BET) equation:

$$\frac{X}{V(1-X)} = \frac{1}{V_mC} + \frac{(C-1)X}{V_mC} \tag{A.1}$$

Where: X = relative partial pressure of nitrogen, P/P_o

   P_o = saturated vapor pressure of nitrogen (or adsorbed gas) at the experiment
      temperature

   P = equilibrium vapor pressure of nitrogen

   V = volume of gas adsorbed at a pressure P; ml at the STP/ g of sample

   V_m = volume of gas adsorbed at monolayer, ml. at the STP / g of sample

   C = constant

Assume $C \rightarrow \infty$, then

$$\frac{X}{V(1-X)} = \frac{1}{V_mC} + \frac{X}{V_m} \tag{A.2}$$

Hence,

$$V_m = V\left\{1-\frac{P}{P_o}\right\} \quad \text{and} \quad p = \frac{P}{P_o}$$

From the ideal gas law,

$$\frac{P_bV}{273} = \frac{P_tV}{T} \tag{A.3}$$

Where: V = constant volume

P_b = pressure at 0 °C or 273 K

P_t = pressure at t °C

T = 273.15 + t, K

P_t = 1 atm   and thus, $P_b = (273.15 / T)$

Partial pressure of Nitrogen at adsorption temperature (K):

$$P_{N_2} = \frac{[\text{Flow of }(He+N_2) - \text{Flow of He}]}{\text{Flow of }(He+N_2)} \times 1 \text{ atm} \qquad (A.4)$$

$$= \quad 0.3 \times 1 \text{ atm} \times 77/(273+30) = 0.07623 \text{ atm}$$

Saturated vapor pressure of nitrogen gas at 77 K calculated from an equation available in Matheson Gas Data Book 7th Edition,

$$\textbf{Log}_{10}\textbf{P}_o = \textbf{A} + \textbf{B/T} + \textbf{Clog}_{10}\textbf{T} + \textbf{DT} + \textbf{ET}^2 \qquad \textbf{(A.5)}$$

Where; P-mmHg and T-K

A	B	C	D	E
23.8572	-4.7668×10^2	-8.6689	2.0128×10^{-2}	-2.4139×10^{-11}

$\log_{10}P = 23.8572 + (-4.7668 \times 10^2)/77 + (-8.6689)\log_{10}77 + (2.0128 \times 10^{-2})(77) + (-2.4139 \times 10^{-11}(77)^2)$

P_o = 728 mmHg = 0.96 atm

$p = P / P_o = P / 0.96 = 0.076/0.96 = 0.0795$

(The ratio of P/Po at 77 K and room temperature resulted in same values.)

Where: V = constant volume

P_b = pressure at 0 ^{o}C or 273 K

P_t = pressure at t ^{o}C

T = 273.15 + t, K

P_t = 1 atm   and thus, P_b = (273.15 / T)

Partial pressure of Nitrogen at adsorption temperature (K):

$$P_{N_2} = \frac{[\text{Flow of (He+N}_2) - \text{Flow of He}]}{\text{Flow of (He+N}_2)} \times 1 \text{ atm} \qquad (A.4)$$

$$= 0.3 \times 1 \text{ atm} \times 77/ (273+30) = 0.07623 \text{ atm}$$

Saturated vapor pressure of nitrogen gas at 77 K calculated from an equation available in Matheson Gas Data Book 7th Edition,

$$\text{Log}_{10}P_o = A + B/T + C\log_{10}T + DT + ET^2 \qquad (A.5)$$

Where; P-mmHg and T-K

A	B	C	D	E
23.8572	-4.7668 x 10^2	-8.6689	2.0128x10^{-2}	-2.4139x10^{-11}

$$\log_{10}P = 23.8572 + (-4.7668\text{x}10^2)/77 + (-8.6689)\log_{10}77 + (2.0128\text{x}10^{-2})(77) + (-2.4139\text{x}10^{-11}(77)^2)$$

P_o = 728 mmHg = 0.96 atm

p = P / P_o = P / 0.96 = 0.076/0.96 = 0.0795

(The ratio of P/Po at 77 K and room temperature resulted in same values.)

How to measure V

1 ml. / 1 atm at room temperature

S_2
Desorption
of N_2 area

S_1
N_2 calibration area
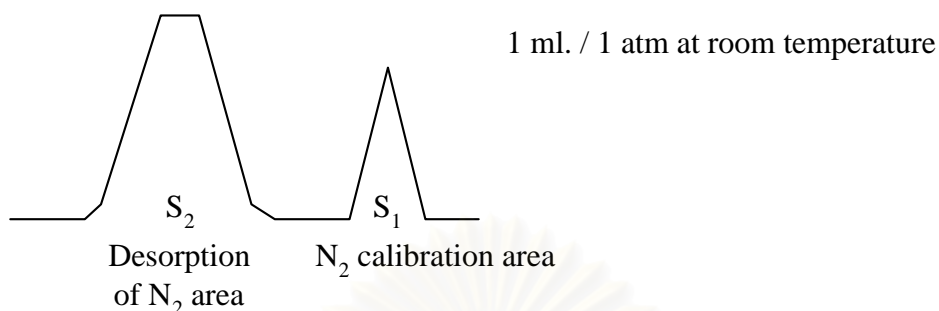
$$V = \frac{S_2}{S_1} \times \frac{1}{W} \times \frac{273.15}{T} \quad \text{ml. / g of catalyst} \qquad (A.6)$$

Where, S_1 = Nitrogen 1 ml/1 atm of room temperature area

S_2 = Desorption of nitrogen area

W = Weight of the sample (g)

T = Room temperature (K)

V = Total volume of nitrogen desorption (cm^3 / g of sample)

Therefore,

$$V_m = \frac{S_2}{S_1} \times \frac{1}{W} \times \frac{273.15}{T} \quad X \ (1\text{-}p)$$

$$V_m = \frac{S_2}{S_1} \times \frac{1}{W} \times \frac{273.15}{T} \quad x \ 0.0795 \qquad (A.7)$$

Surface area of catalyst:

$$S = \frac{N\sigma V_m}{M}$$

Where, N = Avogadro number = 6.02×10^{23} molecule/mole

σ = area occupied by one molecule of adsorbed nitrogen

= 16.2×10^{-20} m^2 per molecule

M = volume of one mole nitrogen = 22410 cm^3/mol

S = Surface area of nitrogen desorption (m^2/ g sample)

$$V_m \quad = \quad \text{Volume of monolayer nitrogen desorption (cm}^3/\text{ g sample)}$$

Then,

$$S \quad = \quad 4.352 \ V_m$$

$$S \quad = \quad \frac{S_2}{S_1} \ \times \ \frac{1}{W} \ \times \ \frac{273.15}{T} \ \times 0.0795 \ \times \ 4.352 \qquad \text{(A.8)}$$

Example: Calculation of BET surface area

Weight of a piece of paper from nitrogen desorption profile (S_2)   *= 6 gram*

Weight of a piece of paper from 1 ml nitrogen injection profile (S_1)   *= 0.1 gram*

Weight of sample   *= 0.3 gram*

Temperature of desorption   *=273+30 K*

$$S \quad = \quad \frac{S_2}{S_1} \ \times \ \frac{1}{W} \ \times \ \frac{273.15}{T} \ \times 0.0795 \ \times \ 4.352$$

S = 6 gram/0.1 gram × 1/0.3 gram × (273/303) × 0.0795 × 4.352

S = 62.0 m²/ g of sample

CALCULATION OF THE CRYSTALLITE SIZE

Calculation of the crystallite size by Debye-Scherrer equation

The crystallite size was calculated from the half-height width of the diffraction peak of XRD pattern using the Debye-Scherrer equation.
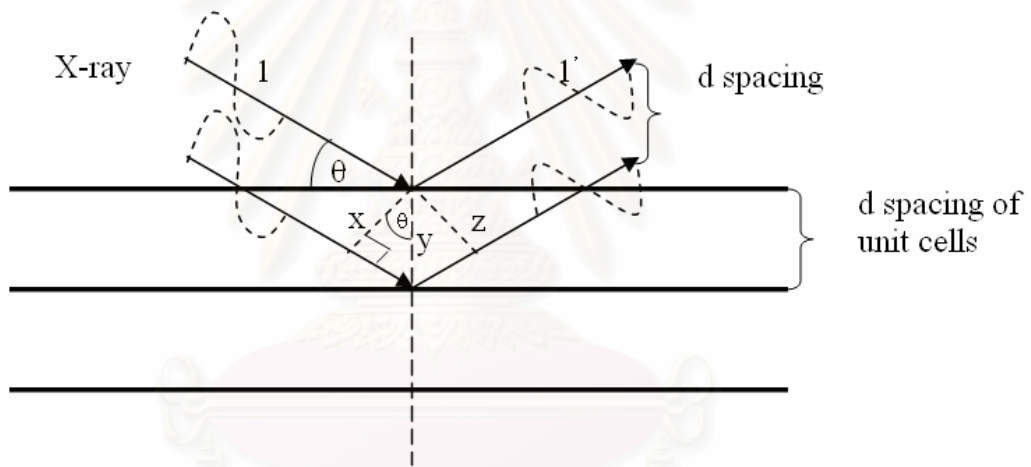
Figure B.1 Derivation of Bragg's Law for X-ray diffraction

$$xy = yz = dsin\theta$$

Thus $\qquad\qquad xyz = 2dsin\ \theta$

But $\qquad\qquad xyz = n\lambda$

Therefore $\qquad\qquad 2dsin\ \theta = n\lambda \qquad\qquad$ *Bragg's Law*

$$d = \frac{n\lambda}{2\ sin\ \theta}$$

The Bragg's Law was derived to B.1

From Scherrer equation:

$$D = \frac{K\lambda}{\beta \cos \theta} \qquad \textbf{(B.1)}$$

Where   D = Crystallite size or a distance between two planes , Å

           K = Crystallite-shape factor = 0.9

           λ = X-ray wavelength, 1.5418 Å for CuKα

           θ = Observed peak angle, degree

           β = X-ray diffraction broadening, radian

The X-ray diffraction broadening (β) is the peak width of powder diffraction free from all broadening due to the experimental equipment. α-Alumina is used as a standard sample to observe the instrumental broadening since its crystallite size is larger than 2000 Å. The X-ray diffraction broadening (β) can be obtained by using Warren's formula.

From Warren's formula:

$$\beta = \sqrt{B_M^2 - B_S^2} \qquad \textbf{(B.2)}$$

Where B_M = the measured peak width in radians at half peak height.

          B_S = the corresponding width of the standard material.

Example: *Calculation of the crystallite size of zirconia*

    The half-height width of 111 diffraction peak   = *1.83^o (from the figure B.1)*

                                                       = *(2πx180)/360*

                                                       = *0.0319 radian*

The corresponding half-height width of peak of α-alumina (from the Bs value

at the 2θ of 30.3° in Figure B.2) = *0.0043 radian*

$$The\ peak\ width,\ \beta = \sqrt{B_M^2 - B_S^2}$$

$$= \sqrt{0.0319^2 - 0.0043^2}$$

$$= 0.0316\ radian$$

B = *0.0316 radian*

2θ = *30.3°*

θ = *15.15°*

λ = *1.5418 Å*

The crystallite size = $\dfrac{0.9x1.5418}{0.0316\cos15.15}$ = *45.49 Å*

= *4.5 nm*
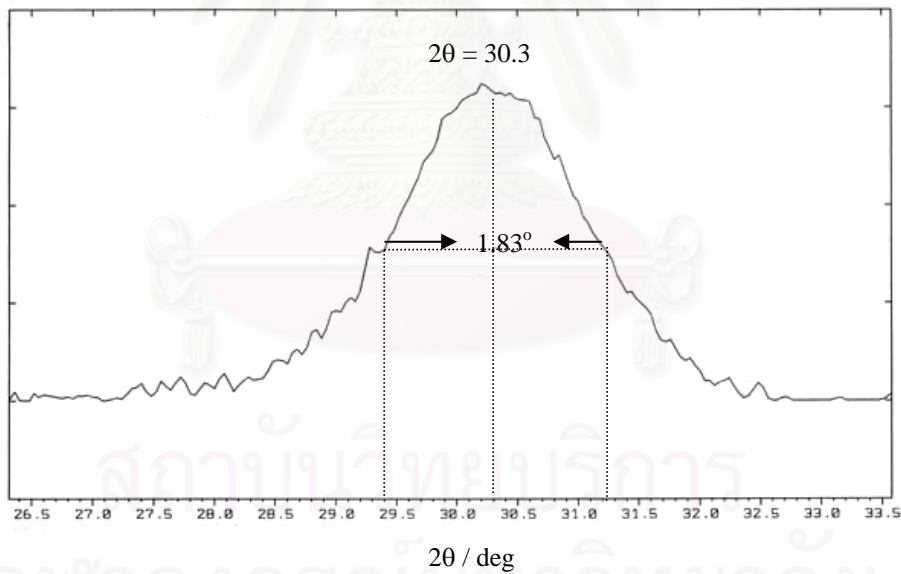
Figure B.1 The 111 diffraction peak of zirconia for calculation of the crystallite size
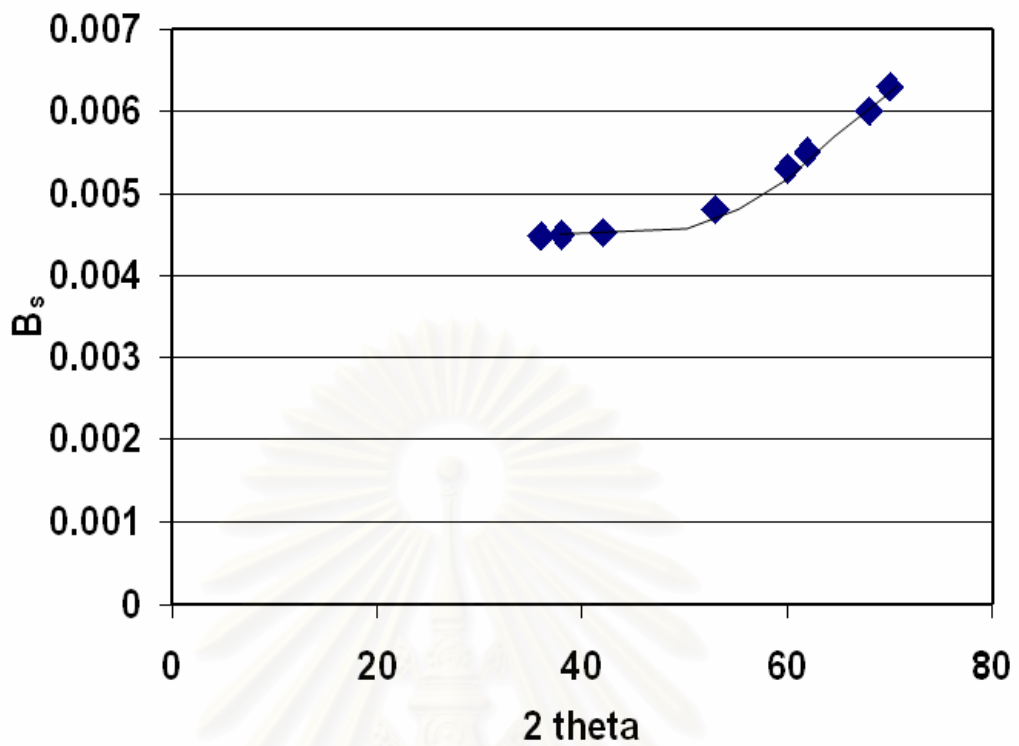
Figure B.2 The plot indicating the value of line broadening due to the equipment. The data were obtained by using α-alumina as a standard

----

APPENDIX C

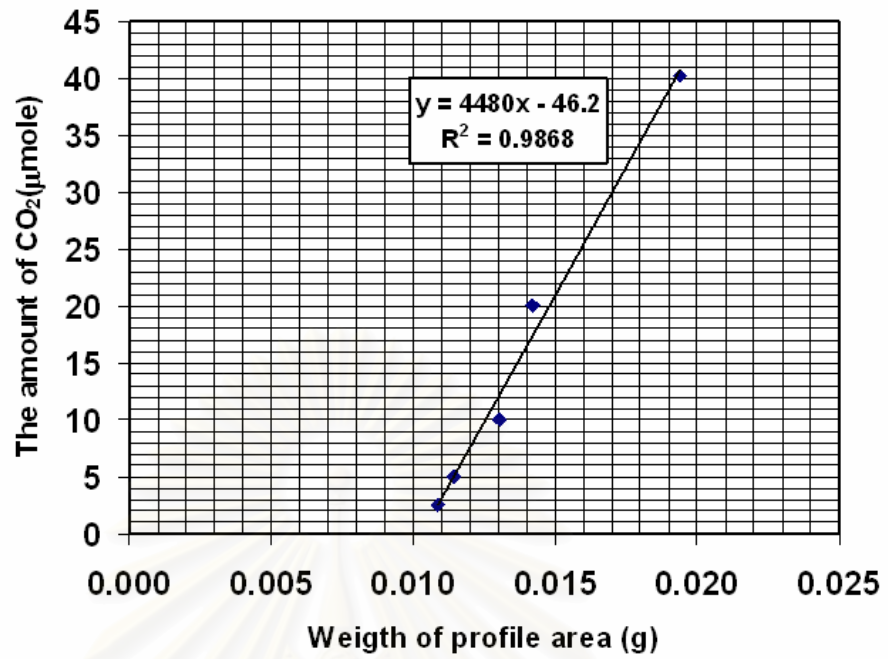## CALCULATION OF THE NUMBER OF CO$_2$ DESORPTION

The amount of CO$_2$ desorption was reported using an area of CO$_2$ temperature programmed desorption profile and calibration curve in Figure C.1. The area was weighed and approximately converted to the amount of CO$_2$. The CO$_2$ measurement was carried out at different volumetric flow rate ratio of CO$_2$ in He and the results were reported in Figure C.1. The signal of different CO$_2$ concentrations in He gas were detected by GAW-MAC TCD and CO$_2$ concentration profiles was recorded by integrator. Due to its broadening, the profile area was unable to be calculated by the integrator; therefore the paper weight of area was employed for calibration curve. Plotting of the profile weights and different amount of CO$_2$ are shown in Figure C.2. Calculations of the amount of CO$_2$ flowing though GC are shown as below.

**Table C.1** Data from the experiment of CO$_2$ in He flowing through reaction rig

Volumetric flow rate of CO$_2$	Volumetric flow rate of He	Volume of CO$_2$(ml) in 6 sec	Weight of area (g)	Amount of CO$_2$ (μmole)
1 ml/ 6 sec	7 ml/ 6 sec	1	0.01940	40.22
0.5 ml/ 6 sec	7.5 ml/ 6 sec	0.5	0.01420	20.11
0.25 ml/ 6 sec	7.75 ml/ 6 sec	0.25	0.01305	10.06
0.125 ml/ 6 sec	7.875 ml/ 6 sec	0.125	0.01143	5.03
0.0625 ml/ 6 sec	7.9375 ml/ 6 sec	0.0625	0.01087	2.51

Figure C.1 The number of CO_2 detected by GAW-MAC TCD and weight of a piece of paper of CO_2 desorption area.
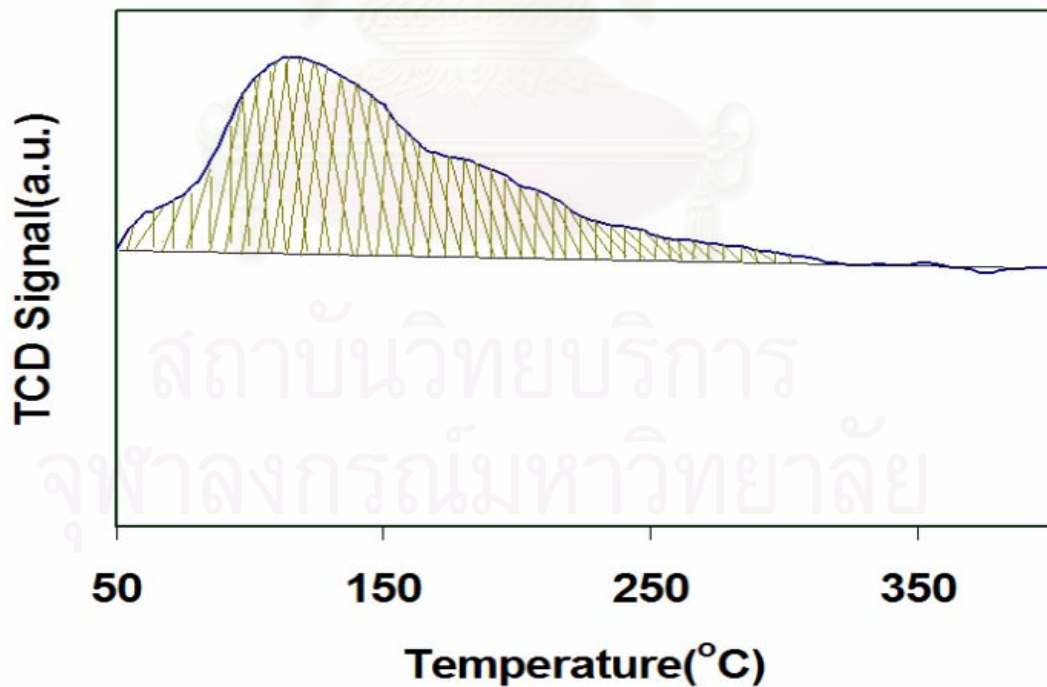
Figure C.2 CO_2 temperature programmed desorption profile of AlZr4060 carried out from 35-400°C with heating rate 10°C/min.

Calculation of CO_2 in He flowing into reaction rig

CO_2 99.99 mole% flowing in helium gas at 80 ml/min equals to 8 ml/ 6 sec

Volumetric flow rate of CO_2/Volumetric flow rate of He = 1:7

Volumetric flow rate of CO_2 = 1 ml/ 6 sec

Volumetric flow rate of He   = 7 ml/ 6 sec

Within 6 sec, we expected to detect a signal of CO_2 1 ml that can convert to 40.22 μmole by ideal gas law (PV=nRT). An area of the profile was weighed approximately 0.019 g. Hence, we can plot a coordinate of (0.019, 40.22) in a Figure C.1. We did more experiment at different conditions. (i.e. volumetric flow rate at different ratio of CO_2/He and data resulted in Figure C.1.)

From Figure C.2, weight of area under temperature programmed desorption profile was converted to the amount of CO_2 by Figure C.1.

.

APPENDIX D

CALCULATION FOR TOTAL H₂ CHEMISORPTION AND DISPERSION

Calculation of the total H_2 chemisorption and metal dispersion of the catalyst, a stoischiometry of $H/Co = 1$, measured by H_2 chemisorption is as follows:

Let the weight of catalyst used	=	0.1	g
Integral area of H_2 peak after adsorption	=	A	unit
Integral area of 45 µl of standard H_2 peak	=	B	unit
Amounts of H_2 adsorbed on catalyst	=	B-A	unit
Concentration of Co (by AAS)	=	8	% wt
Volume of H_2 adsorbed on catalyst	=	$100 \times [(B-A)/B]$	µl
Volume of 1 mole of H_2 at $100^{\circ}C$	=	30.586×10^6	µl
Mole of H_2 adsorbed on catalyst		$[(B-A)/B] \times 100/30.586$	µmole
Total hydrogen chemisorption	=	$[(B-A)/B] \times 100/30.586$	µmole
	=	N µmole	

%Co dispersion

$$= \frac{Amount\ of\ Co\ equivalent\ to\ H_2\ adsorption\ on\ catalyst\ after\ reduction\ (H_2:Co=1:2) \times 100}{Total\ amount\ of\ Co\ expected\ to\ exist\ after\ reduction}$$

|		
Molecular weight of cobalt	=	58.93
Metal dispersion (%)	=	$\dfrac{2 \times H_{2\ tot} \times 100}{No.\ \mu mole\ Co_{tot}}$
	=	$\dfrac{2 \times N \times 100}{No\ \mu mole\ Co_{tot}}$
	=	$\dfrac{2 \times N \times 100}{[(\%reducibility/100 \times 0.08 \times 0.1/58.93) \times 10^6]}$
	=	$\dfrac{200 \times N}{(\%reducibility/100) \times 135.75}$

APPENDIX E

CALCULATION FOR REDUCIBILITY

The major species of the supported cobalt catalysts can be assumed to Co_3O_4. Thus, hydrogen consumption of Co_3O_4 is calculated as follows:

Calculation of the calibration of H$_2$ consumption using cobalt oxide (Co$_3$O$_4$)

Let the weight of Co_3O_4 used	=	0.01 g	
	=	4.153×10^{-5} mole	

From equation of Co_3O_4 reduction;

$$Co_3O_4 \quad + \quad 4H_2 \quad \rightarrow \quad 3Co \quad + \quad 4H_2O \qquad \textbf{(E.1)}$$
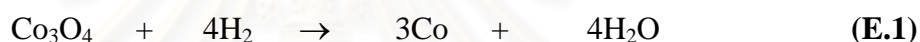
Mole of hydrogen consumption	=	4 Mole of Co_3O_4 consumption		
	=	$4 \times 4.153 \times 10^{-5}$	=	1.661×10^{-4} mole

Integral area of hydrogen used to reduce Co_3O_4 0.01 g = 0.0832 unit

At 100 % reducibility, the amount of hydrogen consumption is 1.661×10^{-4} mole related to the integral area of Co_3O_4 after reduction 0.0832 unit.

Calculation of reducibility of supported cobalt catalyst

% Reducibility = Amount of H$_2$ uptake to reduce 1 g of catalyst $\times$ 100
Amount of theoretical H$_2$ uptake to reduce Co$_3$O$_4$ to Co^0 for 1 g of catalyst

Integral area of the calcined catalyst	=	X	unit
The amount of H_2 consumption	=	$[1.661 \times 10^{-4} \times (X)/0.0832]$	mole
Let the weight of calcined catalyst used	=	W	g
Concentration of Co (by AAS)	=	Y	% wt
Mole of Co	=	$[(W \times Y/100)/58.93]$	mole
Mole of Co_3O_4	=	$[(W \times Y/100)/(3 \times 58.93)]$	mole

Amount of theoretical H_2 uptake $= [(W \times Y/100) \times 4/(3 \times 58.93)]$ mole

Reducibility (%) of supported Co catalyst $= \dfrac{[1.661 \times 10^{-4} \times (X)/0.0832] \times 100}{[(W \times Y/100) \times 4/(3 \times 58.93)]}$

Example for 10%Co on modified Pechini Al$_2$O$_3$

Integral area of the calcined catalyst	$=$	*0.0876*	*unit*
The amount of H_2 consumption	$=[1.661 \times 10^{-4} \times (0.0876)/0.0832]$ mole		
Let the weight of calcined catalyst used	$=$	*0.2*	*g*
Concentration of Co (by AAS)	$=$	*8*	*% wt*
Mole of Co	$=$	*[(0.2×8/100)/58.93]*	*mole*
Mole of Co$_3$O$_4$	$=$	*[(0.2×8/100)/(3×58.93)]*	*mole*
Amount of theoretical H_2 uptake	$=$	*[(0.2×8/100)×4/(3×58.93)]*	*mole*

Reducibility (%) of supported Co catalyst

$$= \dfrac{[1.661 \times 10^{-4} \times (0.0876)/0.0832] \times 100}{[(0.2 \times 8/100) \times 4/(3 \times 58.93)]}$$

$$= 48\ \%$$

CALIBRATION CURVES FOR 2-PROPANOL ELIMINATION
AND %2-PROPANOL CONVERSION AND % SELECTIVITY

The elimination of 2-propanol caused to formation of acetone via dehydrogenation, 2-propylene via dehydration and diisopropylether via coupling reaction. Thus, amount of reactant and products were detected by gas chromatographs Shimadzu model 14A FID with 15%-Carbowax 1000 supported on Chromosorb W. Calibration curves of all chemicals were shown as in Figure F.1-F.4.
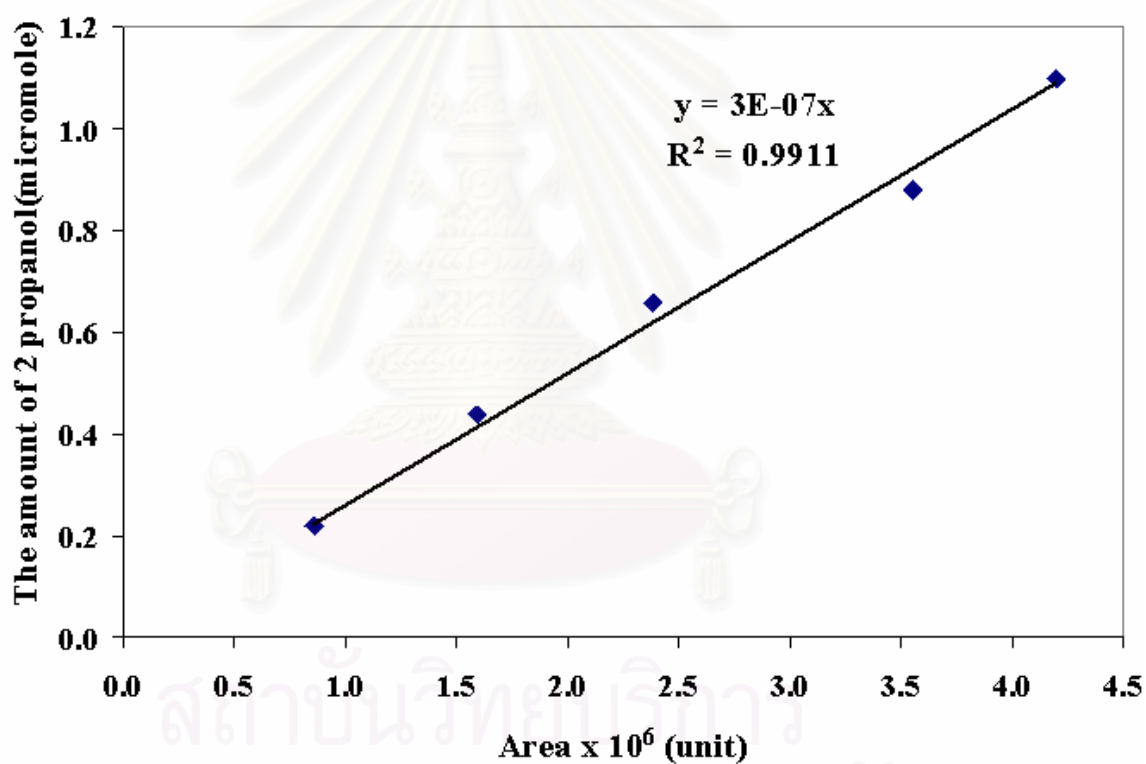

In the figure: $y = 3E\text{-}07x$, $R^2 = 0.9911$. Axes: "The amount of 2 propanol(micromole)" versus "Area x 10^6 (unit)".

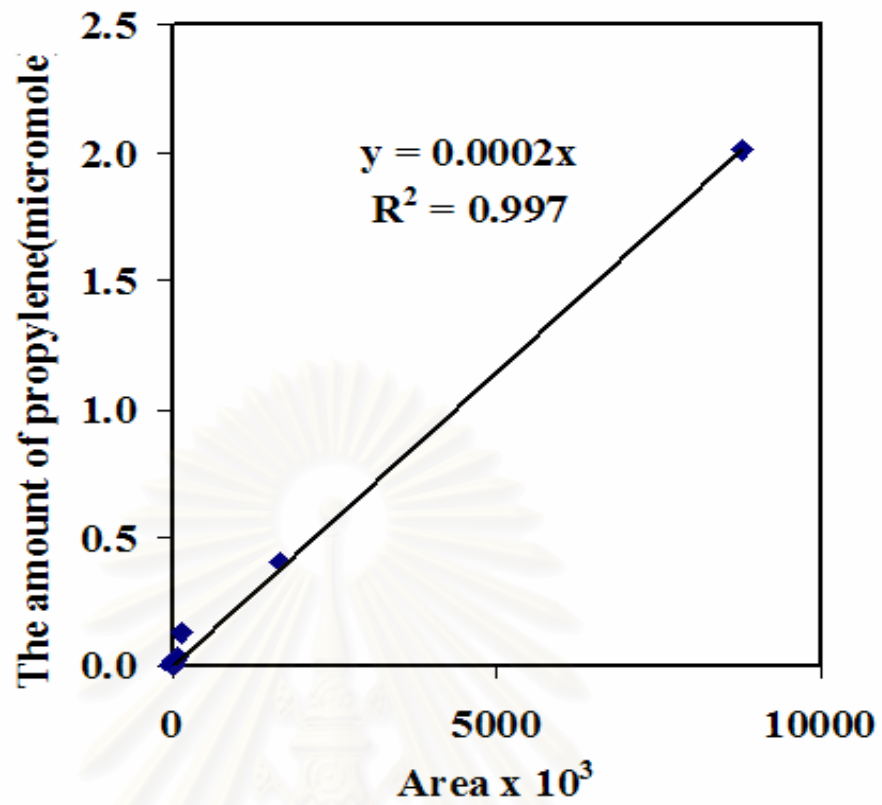**Figure F.1** The calibration curve of 2-propanol

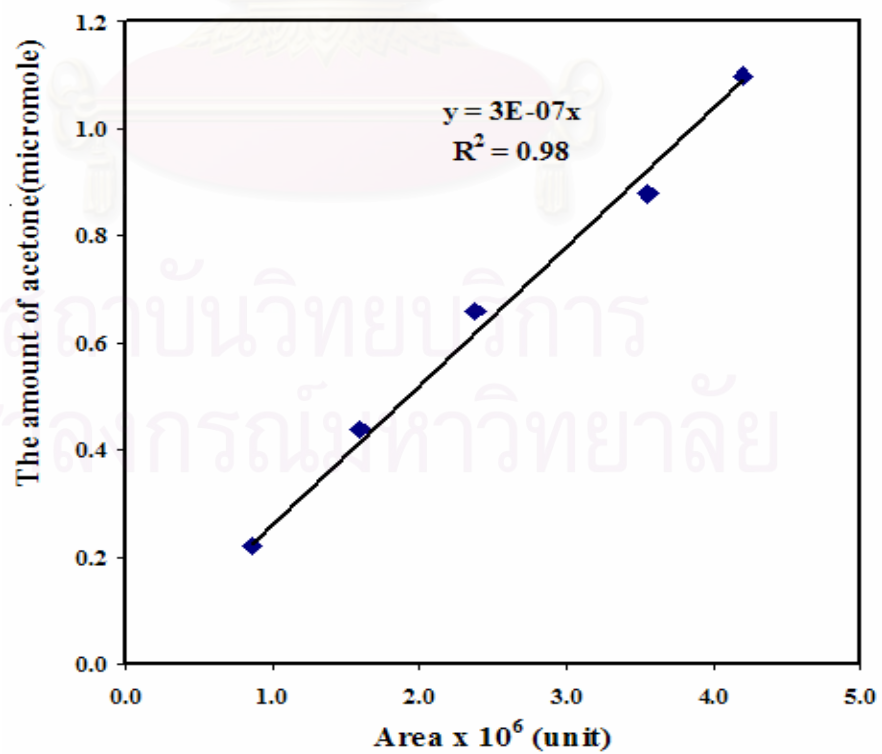**Figure F.2** The calibration curve of propylene

Figure F.3 The calibration curve of acetone

The experiment of elimination of 2-propanol was done by flowing 2-propanol vapor 12mole% in He gas through 0.1 gram of sample with WHSV 90⁻.

Flow rate of carrier gas (He)   =   *30 cm³/min*

The experiment was done at 50 °C of 2-propanol and a percentage of 2-propanol was calculated using Antoine's Equation as follows:

Log₁₀Pₒ = A + B/(T+C)   **(F.1)**

Unit of P_o and T, P_o: KPa, T : 50°C

A	B	C
16.0692	3448	204.09

Log₁₀Pₒ = 16.0692 + 3448/(50+204.09), Pₒ = 12.17 KPa = 0.12 atm

Percentage of 2-propanol in He gas = 0.12/1×100=12%

Flow rate of 2-propanol in He(12mole%) = 0.12 × 30 = 3.6 cm³/min

$$WHSV(h^-) = \frac{\text{flow rate of 2-propanol}(cm^3/min) \times \text{ wt. of the catalyst}(g)}{\text{Volume of the catalyst } (cm^3)} \quad (F.2)$$

$$WHSV(h^-) = 3.6(cm^3/min) \times \frac{0.1064(g)}{0.255357\,(cm^3)} = 1.5\ min^- = 90\ h^-$$

Since, there was no carbon particle observed on surface of tested sample, thus we can calculated a conversion of 2-propanol by following equation;

2-Propanol conversion (%)

$$=\frac{100\times(\text{mole of propylene} + \text{mole of acetone} + 2\times\text{mole of DIP in products})}{\text{Mole of 2-propanol in product} + \text{mole of propylene} + \text{mole of acetone} + 2\times\text{mole of DIP}} \quad (F.3)$$

%Selectivity of B

$$\%Selectivity\ of\ B = \frac{Mole\ of\ B\ in\ product}{Mole\ of\ propylene+mole\ of\ acetone+2\times mole\ of\ DIP} \qquad (F.4)$$

%Selectivity of DIP

$$\%Selectivity\ of\ DIP = \frac{2\times Mole\ of\ DIP}{Mole\ of\ propylene+mole\ of\ acetone+2\times mole\ of\ DIP} \qquad (F.5)$$

Example % 2-propanol Conversion and %Selectivity

Area of reactant and products in output stream;

Time(min)	2-Propanol	Propylene	Acetone	Diisopropylether
20	2344919	193795	26341	5298

Mole of reactant and products in output stream converted by Figure F.1-F.3

Time(min)	2-Propanol	Propylene	Acetone	Diisopropylether
20	0.7035	0.038759	0.0184	0.00106

$$\begin{aligned}
2\text{-Propanol conversion (\%)} &= \frac{(0.038759 +0.0184+2\times0.00106)\times 100}{(0.7035+0.038759 +0.0184+2\times0.00106)} \\
&= 7.8\%
\end{aligned}$$

$$\%Selectivity\ of\ B = \frac{Mole\ of\ B\ in\ product}{Mole\ of\ propylene+mole\ of\ acetone+2\times mole\ of\ DIP}$$

$$\%Selectivity\ of\ propylene = \frac{0.038759\times 100}{(0.038759 +0.0184+2\times0.00106)} = 65.3\%$$

$$\%Selectivity\ of\ acetone = \frac{0.0184\times 100}{(0.038759 +0.0184+2\times0.00106)} = 31.1\%$$

$$\%Selectivity\ of\ DIP = \frac{2\times0.00106\times 100}{(0.038759 +0.0184+2\times0.00106)} = 3.6\%$$

Product Distribution

| Time(min)	% Selectivity of Propylene	% Selectivity of Acetone	% Selectivity of Diisopropylether
20	65.3	31.1	3.6

APPENDIX G

CALIBRATION CURVES FOR CO HYDROGENATION

Gathering data for calibration of reactant and products (i.e. carbon monoxide, methane, ethane, ethylene, propane, propylene and butane) were carried out using by gas chromatographs (Shimadzu model 8A TCD and 14B FID with Molecular Sieve 5A and VZ-10 columns, respectively). Most of CO selectively converted to methane (>90%) and others resulted in C_2-C_4^+. Thus, calibration curve was intensively done for methane and approximately for other products as observed in Figure G3-G9.


(a) Product   (b) Feed
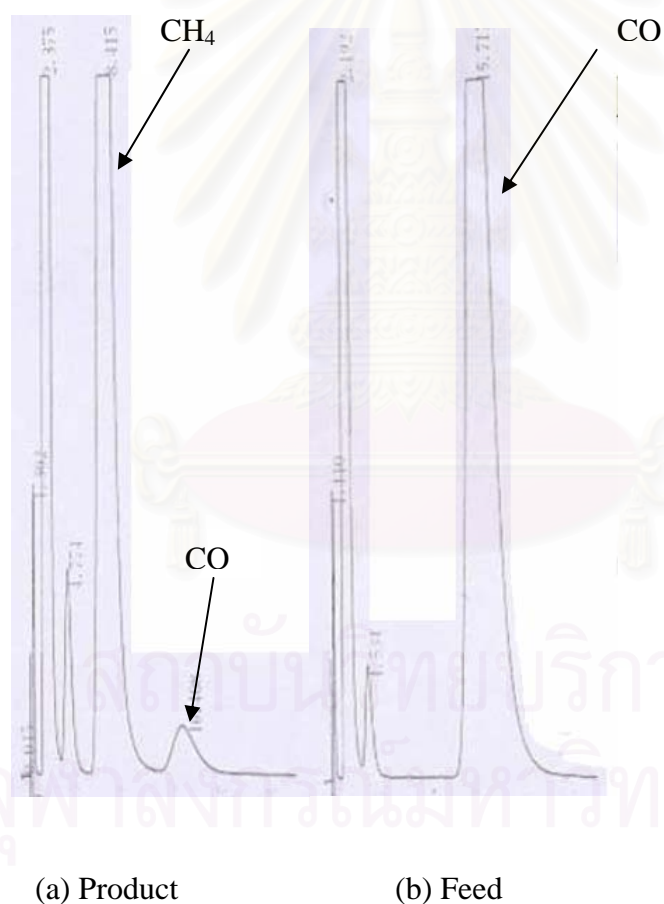
Figure G.1 The chromatograms of feed and product detected by thermal conductivity detector, gas chromatography Shimadzu model 8A (Molecular sieve 5A column)
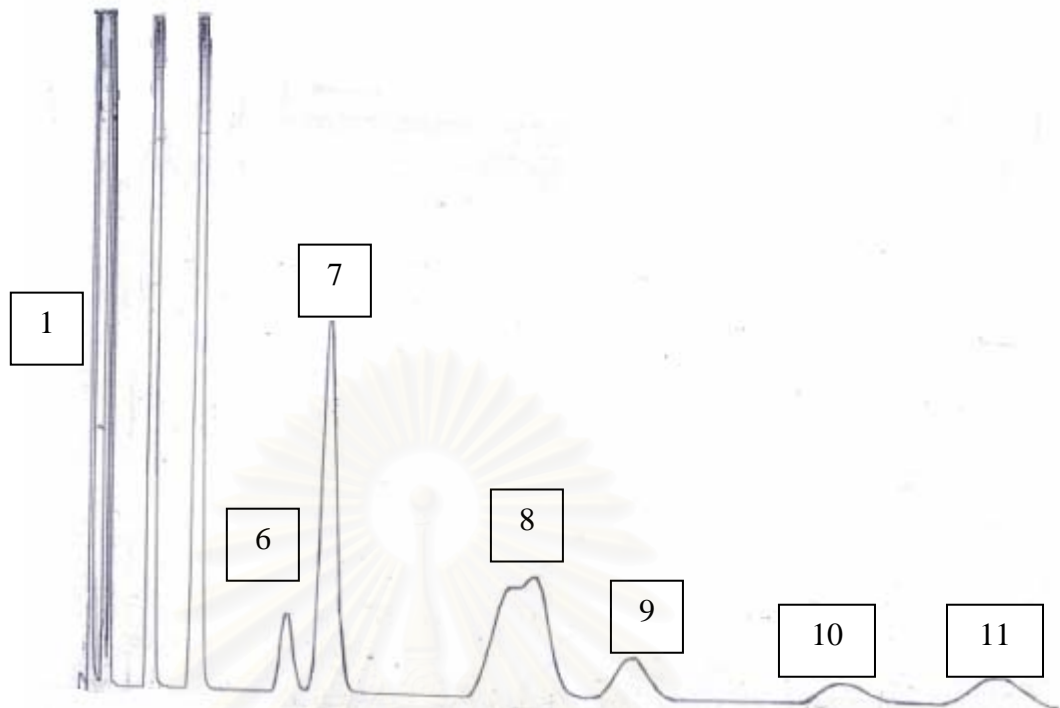
1	CH_4	7	n-C_4H_{10}
2	C_2H_6	8	C_4H_8
3	C_2H_4	9	iso-C_5H_{10}
4	C_3H_6	10	n-C_5H_{10}
5	C_3H_8	11	1,3-C_4H_6
6	iso-C_4H_{10}		

Figure G.2 The chromatograms of feed detected by flame ionization detector, gas chromatography Shimadzu modal 14B (VZ10 column).
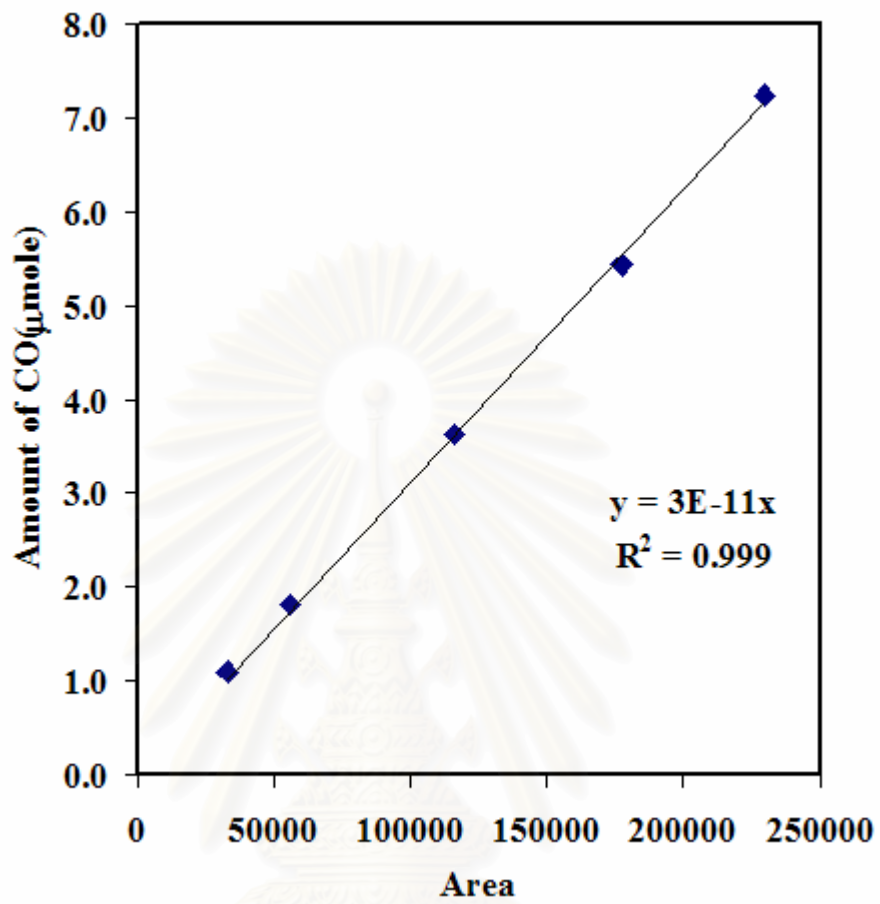
Figure G.3 The calibration curve of CO detected by TCD, gas chromatography

Shimadzu 8A (Molecular Sieve 5A)

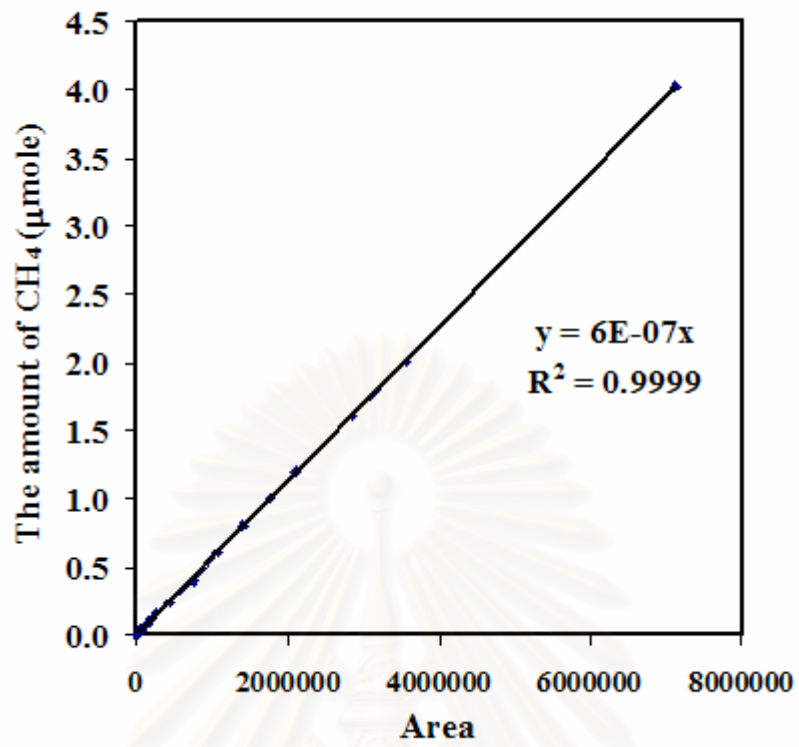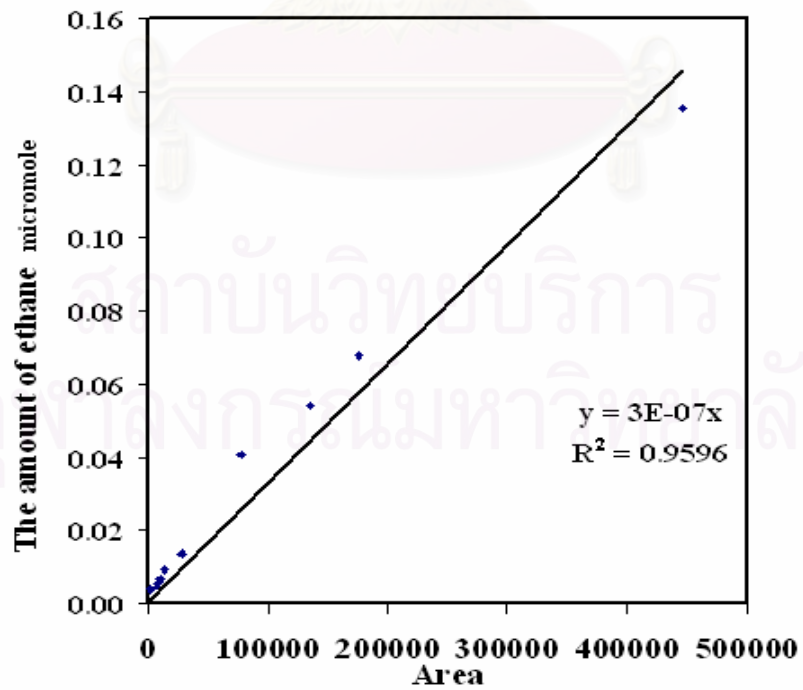**Figure G.4** The calibration curve of methane.

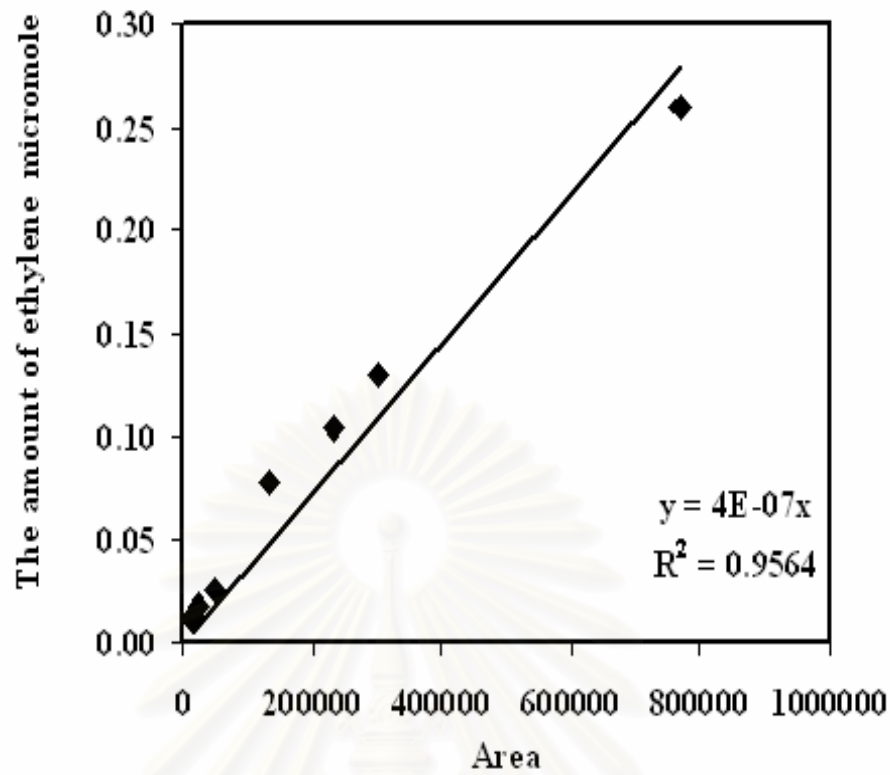**Figure G.5** The calibration curve of ethane.

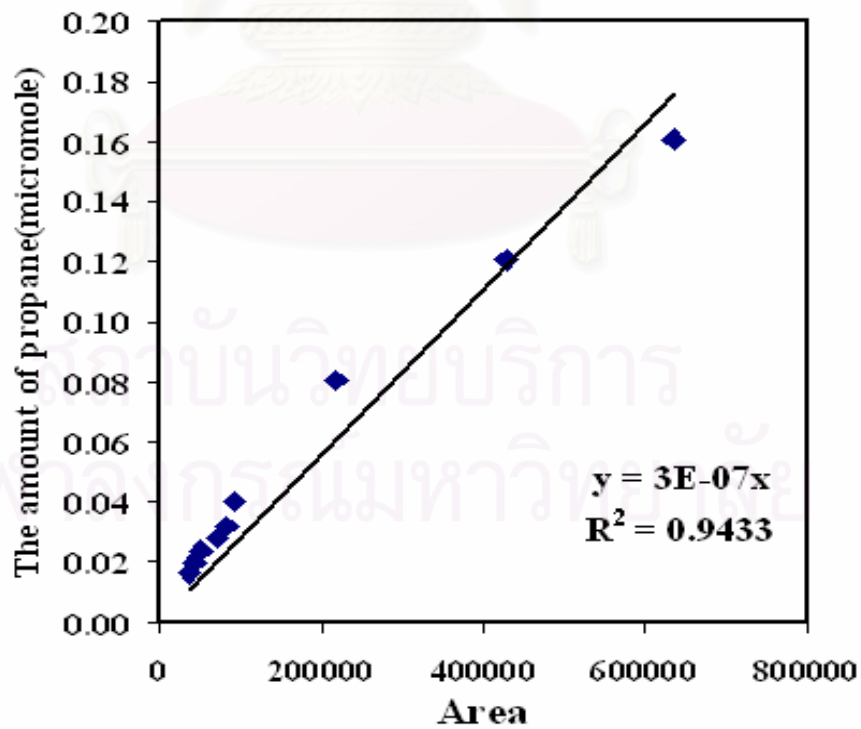**Figure G.6** The calibration curve of ethylene.

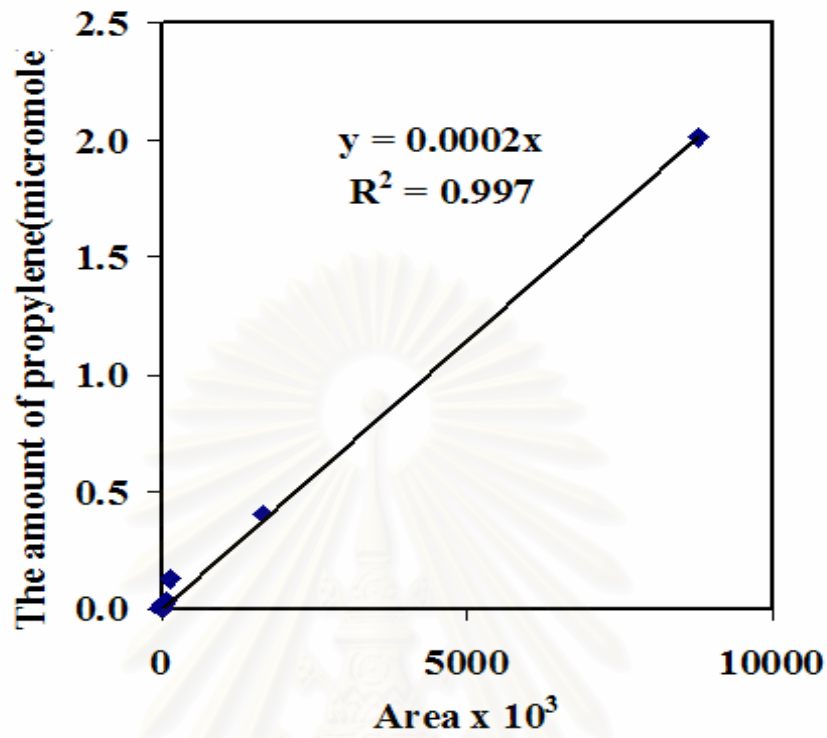**Figure G.7** The calibration curve of propane.
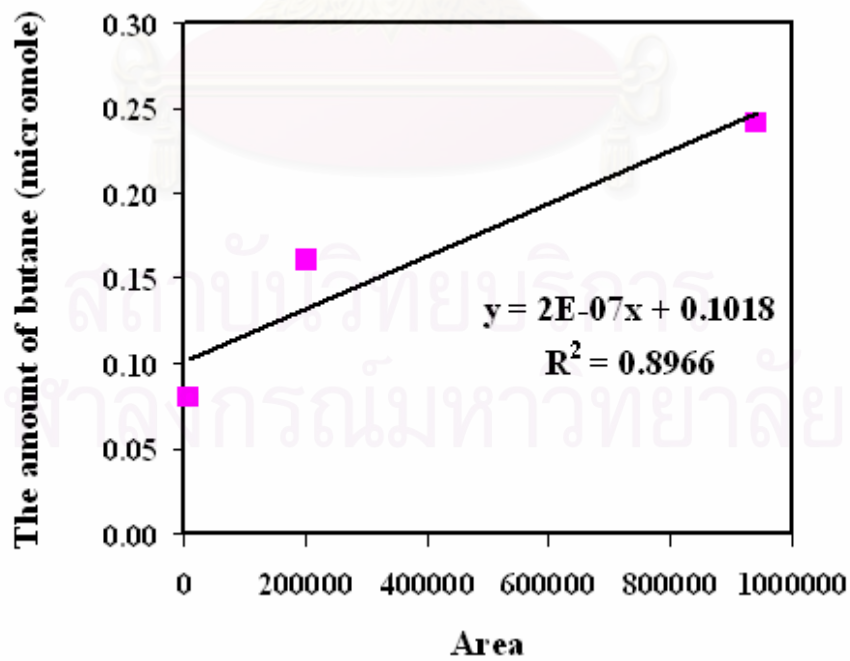
Figure G.8 The Calibration curve of propylene.

Figure G.9 The calibration curve of butane

APPENDIX H

CALCULATION OF CO CONVERSION, REACTION RATE AND SELECTIVITY

The catalyst performance for the CO hydrogenation was evaluated in terms of activity for CO conversion reaction rate and selectivity. Activity of the catalyst performed in term of carbon monoxide conversion and reaction rate. Carbon monoxide conversion is defined as moles of CO converted with respect to CO in feed:

$$CO\ conversion\ (\%) = \frac{100 \times [mole\ of\ CO\ in\ feed - mole\ of\ CO\ in\ product]}{Mole\ of\ CO\ in\ feed} \quad (H.1)$$

$$Mole\ of\ CO = (Area\ of\ CO\ peak\ from\ integrator\ plot\ on\ GC\text{-}8A) \times 3 \times 10^{-11} \quad (H.2)$$

Reaction rate was calculated from CO conversion that is as follows:

Let the weight of catalyst used	=	W	g
Flow rate of CO	=	4	cc/min
Reaction time	=	60	min
Weight of CH_2	=	14	g
Volume of 1 mole of gas at 1 atm	=	22400	cc

Reaction rate (g CH_2/g of catalyst/h) =

$$\frac{[\%\ Conversion\ of\ CO/100] \times 60 \times 14 \times 4}{W \times 22400 \times (273+220)/273} \quad (H.3)$$

Selectivity of product is defined as mole of product (B) formed with respect to mole of CO converted:

Selectivity of B (%) =

$100 \times [mole\ CO\ converted\ to\ B\ /\ mole\ of\ CO\ converted\ to\ product]$ (H.4)

Example *%CO conversion and Reaction rate*

Assumed results; CO input and output detected at 200000 and 150000 units

	Area (Unit)	Amount of CO ($\mu mole$)[*]	%CO Conversion	Reaction rate (g CH_2/g of catalyst/h)
CO input	200000	6	=(6-4.5)/6×100 = 25%	0.207
CO output	150000	4.5		

[*]*Converted by calibration curve in Figure G.3*

Example *Product distribution of CO hydrogenation*

Products (B)	Area of peak (Unit)	Amount of products[*] ($\mu mole$)	CO converted to B ($\mu mole$)	%Selectivity of B
CH_4	1772801	1.418	1.418	88.6
C_2H_6	265817	0.0797	0.1594	5.0
C_2H_4	14581	0.0013	0.0026	0.3
C_3H_8	189728	0.0379	0.1137	2.4
C_3H_6	115638	0.0231	0.0693	1.4
$isoC_4H_{10}$+ $CH_2=C=C H_2$	10296	0.0016	0.0063	0.2
nC_4H_{10}	70391	0.0109	0.0436	0.7
cis-2-C_4H_8+$isoC_5H_{12}$	115132	0.0178	0.0712	0.9
nC_5H_{12}	15029	0.0023	0.0115	0.2
$1,3C_4H_6$	25423	0.0039	0.0156	0.3

[*]*Converted by calibration curve in Figure G.4-G.9*

APPENDIX I

THE AMOUNT OF OXYGEN COVERING CATALYST SURFACE AFTER PRETREATMENT WITH AIR

Since formation of acetone was mostly investigated at reaction temperature 150 and 200°C except for zirconia, we may suggest 2 pathways of acetone formation to identify surface characteristic of the synthesized samples. Acetone can be formed via a mechanism of E_{1cB} resulting in propoxide intermediate, occurred on imbalance acid and base sites. The other pathway is oxidation of 2-propanol to acetone needed oxygen covered surface of the catalyst as reactant. After pretreatment in air, if the amount of oxygen is sufficient to oxidize 2-propanol, acetone should be caused by oxidation and 2-propanol can be converted to propylene over acid-base concerted sites after total oxygen consumption. Thus, calculation of oxygen covering surface of the catalyst was done to considerably define characteristic surface as the following.

I.1 Calculation of amount of 2-propanol in feed flowing through the catalyst 0.1 g

Helium was used as carrier gas at flow rate	*30*	*cm^3/min*
12%mole of 2-propanol in He, flow rate of 2-propanol	*3.6*	*cm^3/min*
MW of 2-propanol=60, molar flow rate of 2-propanol	*0.06*	*mole/min*

Since

$$CH_3CH\,CH_3 \;+\; \tfrac{1}{2}\,O_2 \longrightarrow CH_3C\,CH_3 \;+\; H_2O$$
$$\underset{OH}{|} \qquad\qquad\qquad \underset{O}{\|}$$

Oxygen needed to oxidize 2-propanol is 0.12 mole/min

I.2 Calculation of oxygen covering the catalyst surface

Zirconia

Surface area of zirconia is approximately	*50*	*cm^2/g*
Surface area of zirconia 0.1 g	*0.5*	*cm^2*
Surface area of oxygen 1 molecule	*2.350×10^9*	*cm^2/mole*
Oxygen covering surface of zirconia	*0.5/(2.350×10^9)*	*mole*
	2.12×10^{-9}	*mole*

$$\frac{\text{Mole of oxygen needed to oxidize 2-propanol}}{\text{Mole of oxygen covering zirconia surface}} = \frac{0.06 \text{ mole/min}}{2.12 \times 10^{-9} \text{ mole}} = 2.83 \times 10^{7}$$

Alumina

Surface area of alumina is approximately	*300*	*cm^2/g*
Surface area of alumina 0.1 g	*30*	*cm^2*
Surface area of oxygen 1 molecule	*2.350×10^9*	*$cm^2/mole$*
Oxygen covering surface of alumina	*$30/(2.350 \times 10^9)$*	*mole*
	12.77×10^{-9}	*mole*

$$\frac{\text{Mole of oxygen needed to oxidize 2-propanol}}{\text{Mole of oxygen covering alumina surface}} = \frac{0.06 \text{ mole/min}}{12.77 \times 10^{-9} \text{ mole}} = 4.69 \times 10^{6}$$

It suggests that amount of oxygen covering all 0.1 g samples are insufficient to oxidize 2-propanol. Thus, the majority of acetone occurred via E_{1cB} mechanism and we can suggest that most of samples consist of imbalanced acid and base sites except zirconia mostly composed of acid and base concerted sites.

APPENDIX J

LIST OF PUBICATIONS

1. Patta Soisuwan, Dean C. Chambers, David L. Trimm, Okorn Mekasuwandumrong, Joongjai Panpranot and Piyasan Praserthdam, "Characteristics and Catalytic Properties of Alumina-Zirconia Mixed Oxides Prepared by a Modified Pechini Method", Catalysis Letter, 103 (2005) 63-68

2. Patta Soisuwan, Joongjai Panpranot, David L. Trimm, and Piyasan Praserthdam, "Synthesis, Characterization, and Application of Alumina-Zirconia Mixed Oxides Supported Co Catalyst", submitted Applied Catalysis A: General

3. Patta Soisuwan, Joongjai Panpranot, Piyasan Praserthdam, and David L. Trimm, "Effects of Si- and Y-Modified Nanocrystalline Zirconia on the Properties of Co/ZrO_2 Catalysts", submitted Catalysis Communications

VITAE

Miss Soipatta Soisuwan has her previous name as Patta Soisuwan. She was born on March 27, 1974 in Chonburi, Thailand. She received her Bachelor Degree of Chemical Technology from Faculty of Science, Chulongkorn University and then she continued her study in Faculty of Engineering, Chulalongkorn University and received her Master Degree of Engineering (Chemical Engineering) later 3 years. After her graduation, she had done her job at Burapha University for 4 years and returned to study in Ph.D. program with a scholarship subsidized by the Cooperative Research Network, Thai Ministry of Education in a supervision of Prof. Dr. Piyasan Praserthdam, who gave her an opportunity to investigate a sol-gel preparation method with Prof. Dr. David Trimm at the University of New South Wales, Australia for 12 months. Under a supervision of Prof. David Trimm, she was given a chance to be a trainee student with financial support from CSIRO Petroleum division, Clayton South, Australia. After she finishes her Ph.D. study, she will return to work at Burapha University and she intends to give her study experience benefit for all of her students.